Award Number: W81XWH-11-1-0670

TITLE: Novel Preclinical Testing Strategies for Treatment of Metastatic Pheochromocytoma

PRINCIPAL INVESTIGATOR: Arthur S. Tischler MD

CONTRACTING ORGANIZATION: Tufts Medical Center
Boston MA 02111

REPORT DATE: November 2015

TYPE OF REPORT: Final

PREPARED FOR: U.S. Army Medical Research and Materiel Command
Fort Detrick, Maryland 21702-5012

# REPORT DOCUMENTATION PAGE

*Form Approved*
*OMB No. 0704-0188*



| 1. REPORT DATE | 2. REPORT TYPE | 3. DATES COVERED |
|---|---|---|
| November 2015 | Final | 15 Aug 2011 - 14 Aug 2015 |

**4. TITLE AND SUBTITLE**

Novel Preclinical Testing Strategies for Treatment of Metastatic Pheochromocytoma

**5a. CONTRACT NUMBER**

**5b. GRANT NUMBER**
W81XWH-11-1-0670

**5c. PROGRAM ELEMENT NUMBER**

**6. AUTHOR(S)**
Arthur S. Tischler

E-Mail: atischler@tuftsmedicalcenter.org

**5d. PROJECT NUMBER**

**5e. TASK NUMBER**

**5f. WORK UNIT NUMBER**

**7. PERFORMING ORGANIZATION NAME(S) AND ADDRESS(ES)**

Tufts Medical Center
800 Washington Street
Boston MA. 02111

**8. PERFORMING ORGANIZATION REPORT NUMBER**

**9. SPONSORING / MONITORING AGENCY NAME(S) AND ADDRESS(ES)**

U.S. Army Medical Research and Materiel Command
Fort Detrick, Maryland 21702-5012

**10. SPONSOR/MONITOR'S ACRONYM(S)**

**11. SPONSOR/MONITOR'S REPORT NUMBER(S)**

**12. DISTRIBUTION / AVAILABILITY STATEMENT**

Approved for Public Release; Distribution Unlimited

**13. SUPPLEMENTARY NOTES**

**14. ABSTRACT** Pheochromocytomas (PCC) are catecholamine-producing neuroendocrine tumors. Up to 30% give rise to metastases, for which there is no effective treatment. A major deficiency in current treatment strategies is that they do not account for the fact that metastatic PCCs usually grow very slowly and most of the cells are quiescent at any given time. This project had two overall objectives: to develop treatment paradigms targeting quiescent and replicating PCC cells and to develop new models for-pre-clinical testing. Because there are no human PCC cell lines, mouse pheochromocytoma cell lines developed in our laboratory were used as the principal model for testing of chemotherapeutic drugs and the findings were validated with primary cultures of human PCC. We identified two classes of drugs effective against non-dividing human PCC cells: topoisomerase 1 inhibitors and the mitochondriotoxic agent gamitrinib. New approaches to propagating human PCC cells from primary tumors in cell cultures and xenografts were also tested. Attempts to establish cell lines were unsuccessful. Although there were no overt tumor takes in mice, histologic sections of the implantation sites in a new strain of immunodeficient mice called NSG show long-term cell survival. This provides a new model that can be used for future studies of tumor growth, drug responses and micro-imaging *in vivo*.

**15. SUBJECT TERMS**
Pheochromocytoma, paraganglioma, cell culture, cell line, xenograft, nude mouse, chemotherapy, pre-clinical testing, camptothecin, 5-azacytidine, irinotecan, topoisomerase-1, bioluminescence, imaging, Gamitrinib

| 16. SECURITY CLASSIFICATION OF: | | | 17. LIMITATION OF ABSTRACT | 18. NUMBER OF PAGES | 19a. NAME OF RESPONSIBLE PERSON |
|---|---|---|---|---|---|
| a. REPORT | b. ABSTRACT | c. THIS PAGE | | | USAMRMC |
| Unclassified | Unclassified | Unclassified | Unclassified | 93 | 19b. TELEPHONE NUMBER *(include area code)* |

## Table of Contents

## 1. Introduction

**Purpose and scope of the research effort**.

Pheochromocytomas (PCC) are catecholamine producing neuroendocrine tumors that arise from chromaffin cells in the adrenal medulla or other parts of the peripheral sympathetic nervous system. Extra-adrenal PCCs are arbitrarily classified as paragangliomas (PGLs). For convenience, the two are often referred to collectively as PCC/PGL. These tumors occur sporadically or in hereditary form and are associated with mutations of at least 19 genes. Between 10% and 30% of PCC/PGL give rise to metastases, for which there is currently no effective treatment. Metastasis is particularly likely when tumors harbor mutations of the *SDHB* gene. A major deficiency in current treatment strategies is that they do not account for the fact that, in contrast to many other types of malignant tumor, metastatic PCC/PGLs usually grow very slowly and most of the cells are quiescent at any given time. Mitotic counts and expression of cell cycle markers both in primary tumors and in their metastases are often very low. Treatments that target replicating tumor cells or tumor angiogenesis have therefore met with only limited success. Patients with metastases often die from complications of catecholamine hypersecretion, or from invasive and expansile tumor growth that occur over many years. The need to improve treatment of metastatic PCC/PGLs requires new strategies and valid experimental models for pre-clinical testing of those strategies. Development of models has itself been hampered by failure to establish any human cell lines from the tumors for cell culture or xenograft studies, despite many efforts to establish them and several initially promising reports.
The overall objectives of this project were both to develop treatment paradigms targeting quiescent and replicating tumor cells in PCC/PGL metastases using existing models generated in the PI's laboratory, and to develop new models. Specific Aim 1 used a mouse pheochromocytoma cell line (MPC) *in vitro* as a model to test new approaches to enhance the effectiveness of chemotherapeutic agents by optimizing the combination and timing of their use. Aim 2 used primary cultures of human PCC/PGL cells derived from individual patient's tumors with diverse genetic backgrounds to validate the findings in Aim 1, and Aim 3 tested the ability of drug-administration paradigms developed in specific aims 1 and 2 to kill disseminated PCC *in vivo* using MPC cells as a model in nude mice. Aim 4 tested novel approaches to develop cell lines of human PCC/PGL for cell culture and xenografts, thereby providing a foundation for future studies. Progress was made on all of the specific aims and toward the overall objectives, as summarized in this final report.
.

## 2. Key Words

Pheochromocytoma, paraganglioma, cell culture, cell line, xenograft, nude mouse, chemotherapy, pre-clinical testing, camptothecin, 5-azacytidine, irinotecan, topoisomerase-1, bioluminescence, imaging, Gamitrinib

## 3. Accomplishments Overall Project Summary (15 August 2011- 14 September 2015).

### Major Goals in the Approved SOW

This project was a pre-clinical study aimed to develop new paradigms for treating patients with metastatic pheochromocytoma. The major goals as stated in the SOW were:

Specific Aim 1. To use a mouse pheochromocytoma cell line (MPC) *in vitro* as a model to test new approaches to enhance the effectiveness of chemotherapeutic agents by optimizing the combination and timing of their use. Topoisomerase 1 (TOP1) inhibitors will be used to interfere with mechanisms that maintain DNA integrity during transcription in conjunction with inhibitors of DNA methyltransferase and histone deacetylase (HDAC) that increase transcription, modify neuroendocrine gene expression and reversibly inhibit cell proliferation. Apoptosis, cytotoxicity and survival of MPC cells will be measured.

Specific Aim 2. To validate the findings in Aim 1 using primary cultures of human PCC cells derived from individual patient's tumors with diverse genetic backgrounds.

Specific Aim 3 To test the ability of drug-administration paradigms developed in specific aims 1 and 2 to kill disseminated PCC *in vivo* using MPC cells as a model in nude mice. Tumor growth and responses to drugs will be monitored by biophotonic imaging after tail vein injection of MPC cells into nude mice. Gene expression profiles indicative of responsiveness will be determined and pathway analyses will be performed to direct future drug targeting, which might include additional drugs focused on the same pathways.

Specific Aim 4. To test novel approaches to develop cell lines of human PCC in cell culture and in nude mice, thereby providing a foundation for future studies. The studies for Aim 4 will be conducted in parallel with Aims 2 and 3.

### Summary of Goal Completion in Relation to the Proposed Timetable

**Specific Aim 1** *Development of drug testing paradigms using MPC cell cultures*
100% completed, on schedule

a. Months 1-6: Set up triplex apoptosis/cytotoxicity/survival assay to complete the quantitation of apoptosis and cytotoxicity for prototype drugs already tested on MPC cells in monolayer and 3-dimensional cultures in preliminary data. Define optimal drug combinations and timing.

*Completed on schedule*

b. Months 6-12: Complete testing of additional HDAC and topoisomerase inhibitors as described in project narrative.

*Completed on schedule*

c. Months 12-36: Expand and complete dose-response and time course killing curves for MPC for each paradigm tested, including additional and alternative drugs as described in the project narrative. Define optimal drug combinations and timing.

*Completed on schedule*

**Specific Aim 2** *Validation of drug testing paradigms in primary human cell cultures*
100% completed, on schedule

a. Months 1-6: Continue parallel testing of human PCC for drug sensitivity in preliminary data.

*Completed on schedule*

b. Months 6-12: Complete testing of additional HDAC and topoisomerase inhibitors on human PCC as described in project narrative.

*Completed on schedule*

c. Months 12-36: Expand and complete dose-response and time course killing curves for human PCC for each paradigm tested including additional and alternative drugs as described in the project narrative. Define optimal drug combinations and timing.

*Completed on schedule*

**Specific Aim 3** *In vivo testing of drug-administration paradigms developed in specific aims 1 and 2 using disseminated MPC cells as a model*

70% completed overall

a. Months 1-6: Inject luciferase-expressing MPC cells into nude mice and time the development of pulmonary and hepatic tumors using biophotonic imaging

*Completed on schedule*

b. Months 6-12: Begin *in vivo* cytotoxicity testing using biophotonic imaging.

*Completed on schedule*

c. Months 12-36: Complete *in vivo* cytotoxicity testing using biophotonic imaging to test multidrug paradigms.

*Could not perform these experiments as planned because of unexpected technical issues concerning the bioluminescent cells, equivalent 20% of studies performed using alternate approach*

d. Months 24-36: Conduct and complete gene expression profiling and validation to obtain signatures of drug response.

*Could not perform these experiments because of unexpected technical issues concerning the bioluminescent cells.*

**Specific Aim 4** *Novel approaches to develop cell lines of human PCC for cell culture and xenografts*

80% completed overall, a-d 100% completed on schedule, e & f could not be completed because of negative results in a-d.

a. Begin testing cultures of human PCC for cell proliferation under normoxic and hypoxic conditions. The objective is to test all tumors that become available during the 3-year period of performance, starting with tumors currently on hand.
b. Months 1-2: Inject dissociated human PCC cells from tumors currently on hand into tail veins of nude mice.
c. Months 2-36: Begin to inject additional tumors as they become available. The objective is to inject at least 20 tumors that have already given rise to metastases in afflicted patients or that harbor the genotype associated with highest metastatic potential (*SDHB* mutation).
d. Months 2-36: Observe mice at regular intervals. Euthanize mice that show signs of distress and perform immediate necropsies to remove tumor deposits from lung, liver and other sites.
e. Months 2-36: Perform histological and immunohistochemical analysis of tumor deposits to confirm that they are human PCC takes and not irrelevant endogenous mouse tumors. Freeze viable aliquots of confirmed PCC takes and begin attempts to propagate additional aliquots in cell culture and in serial xenografts *in vivo*.
f. Months 2-36: Propagate any human tumors that grow in *vivo* and *in vitro* in order to establish cell lines. Characterize genotype and phenotype of any human cell lines established. Conduct *in vitro* cytotoxicity testing of any human cell lines established. Compare results to those obtained with MPC cells and primary human tumor cells with the objective of switching from mouse to human model if a valid human model can be developed

**Detailed Activities and Outcomes (15 August 2011- 14 September 2015)**

**Year 1 (15 August 2011- 14 September 2012).**

*Specific Aim 1 Development of drug testing paradigms using MPC cell cultures*

Summary: We completed apoptosis and cytotoxicity assays for prototype drugs tested on MPC cells in studies designed to test the efficacy of topoisomerase 1 (TOP1) inhibition in conjunction with inhibition of DNA methylation by 5-azacytidine (5-aza). TOP1 inhibitors are drugs that interfere with mechanisms that maintain DNA integrity during transcription in both quiescent and dividing cells, while 5-aza is a DNA methylation inhibitor that alters transcription and is therefore mechanistically complementary. We also tested additional drugs representing potential alternative solutions and enhancements of the project.

Task 1. Cytotoxicity/survival/apoptosis assays were set up for use with MPC cells

Four complementary procedures were set up; XTT colorimetric assay (measures cell survival by metabolism of a dye by viable cells), immunoblotting for cleaved poly-ADP-ribose polymerase (indicates apoptosis by showing a cleaved protein band generated by activated caspase 3), staining of cultures with 4'-6-diamidino-2-phenylindole (DAPI, 0.5 uM) (shows nuclear changes characteristic of apoptosis), ApoTox-Glo Triplex Assay (Promega Corporation, Madison WI, simultaneously assesses caspase activation, cytotoxicity and viability).

Task 2 . The effectiveness of TOP1 inhibition against MPC 4/30/PRR cell line was tested using camptothecin, a prototypical TOP1 inhibitor, to obtain proof of principle.

Cells in monolayer cultures were tested with a range of camptothecin concentrations from 0.01 to 10 uM using XTT, PARP cleavage and DAPI stains as read-outs.

Results:

- XTT Results showed approximately 20% survival in the presence of 1 uM camptothecin at 7 days and no survival at 7 days in the presence of 10 uM camptothecin.
- PARP blots and DAPI stains confirmed the presence of ongoing apoptotic death over a 2-week period of testing.
- These results were used as the basis for task 3 (See Figs 1-3 as described below)

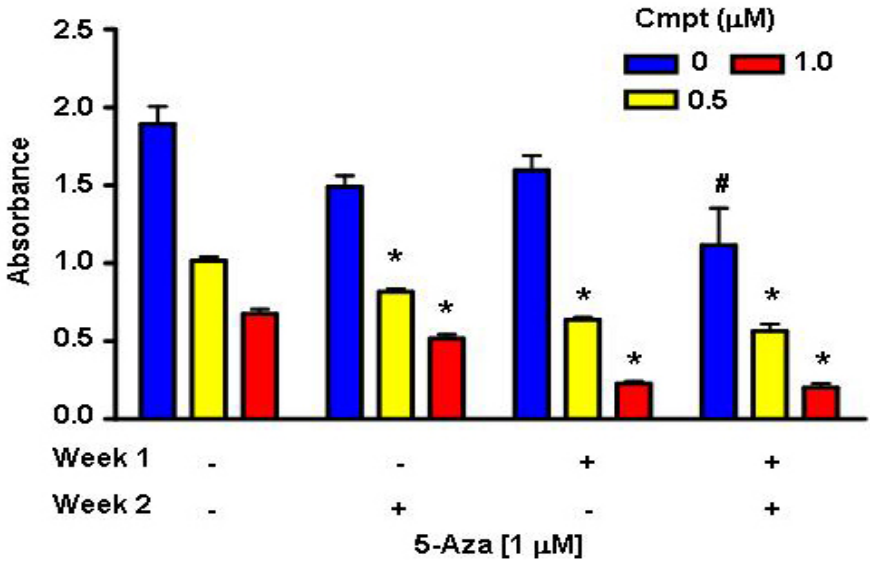


**Fig 1.** Cytotoxicity of camptothecin against MPC cells is increased by short-term concomitant exposure to a sub-toxic concentration of 5-azacytidine (1 uM). Captions under bars indicate whether 5-aza was present during the first week and/or second week of a 2-week experiment. In the absence of camptothecin, 5-aza alone causes a statistically significant decrease in survival only after 2 weeks of continuous treatment (#). Data are from a representative experiment that was repeated on 3 independent occasions. Absorbance is proportional to cell survival. Bars indicate mean +/- SEM of quadruplicate wells.

Task 3 The effect of sub-toxic concentrations of 5-azacytidine (5-aza) in conjunction with camptothecin was tested as a possible strategy to reduce the required dosage or duration of treatment with TOP1 inhibitors.

In order to test the interaction of camptothecin with 5-aza, cytotoxicity assays were performed with MPC 4/30PRR using 0, 0.5 or 1.0 uM camptothecin and a single low dose of 5-aza (1 uM) present during the first week and/or second week of a 2-week experiment. XTT, PARP cleavage and DAPI stains were used as read-outs.

Results:

All cultures treated with 5-aza plus camptothecin showed significantly reduced survival compared to those with camptothecin alone, with 5-aza optimally added during the first week. Further, those cultures from which 5-aza was removed after the first week were not significantly different from those with 5-aza continuously (Fig 1). PARP blots and DAPI stains confirmed increased apoptotic death with the 2-drug combination (Figs. 2 and 3).These results suggest novel strategies for enhancing the efficacy and reducing the toxicity of TOP1 inhibitors by optimizing both the combination and timing of their use in conjunction with other drugs.

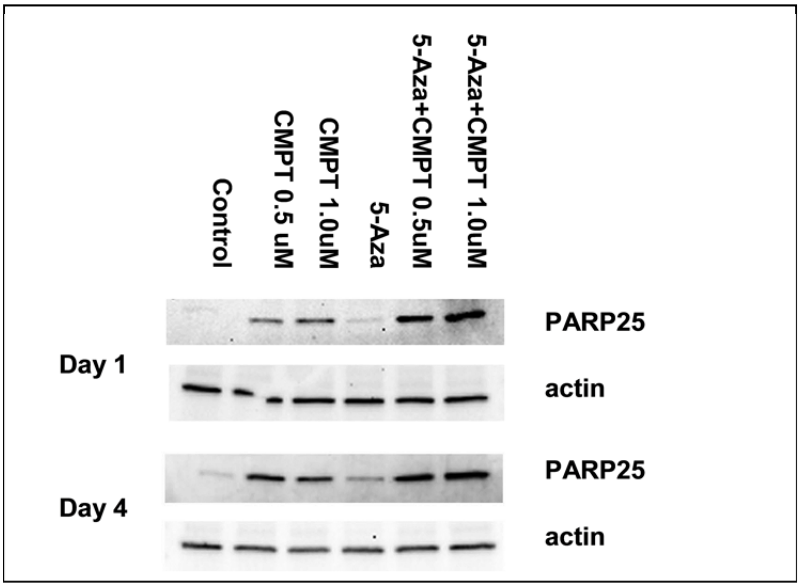


**Fig. 2** Immunoblots showing the effects of camptothecin and 5-azacytidine on MPC cell apoptosis, which is indicated by the presence of a 25 kD fragment of PARP. A marked increase in intensity of the PARP25 band is seen at 24 hrs with the combination of camptothecin and 5-aza, with little effect of 5-aza alone. This pattern is still evident, but diminished, after 4 days.

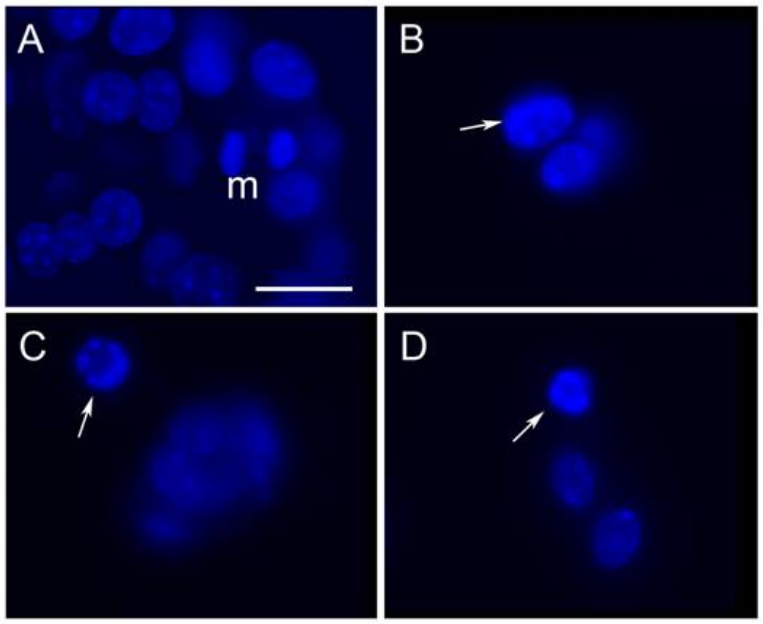


**Fig.3** Representative fluorescence micrographs showing nuclear morphology of DAPI-stained MPC cultures. Panel A shows nuclei of cells maintained in control medium for 7 days. Nuclei are round to oval with finely stippled chromatin. One mitosis is evident (m). Panels B-D show typical apoptotic changes seen at day 7 in cultures with camptothecin or camptothecin + 5-aza. (B, early peripheral margination of chromatin; C, nuclear shrinkage and marked chromatin margination; d, nuclear fragmentation). In addition, B-D contain fewer cells, consistent with ongoing attrition. Bar =20 um. Original magnification 100 X.

Task 4. Because the amount of cell proliferation is an important consideration in the treatment of PCC, we compared the effects of camptothecin against MPC versus MTT, a rapidly growing cell line generated from MPC tumor tissue. MTT serves as a less differentiated counterpart to MPC, and, because of its rapid growth, representing the occasional human PCC that undergoes "explosive" growth after failure of chemotherapy.

Results:

Comparisons of the MPC and MTT cell lines showed that both lines were sensitive to camptothecin, with MTT showing a lower threshold of response than MPC, but comparable cumulative toxicity (Fig. 4).

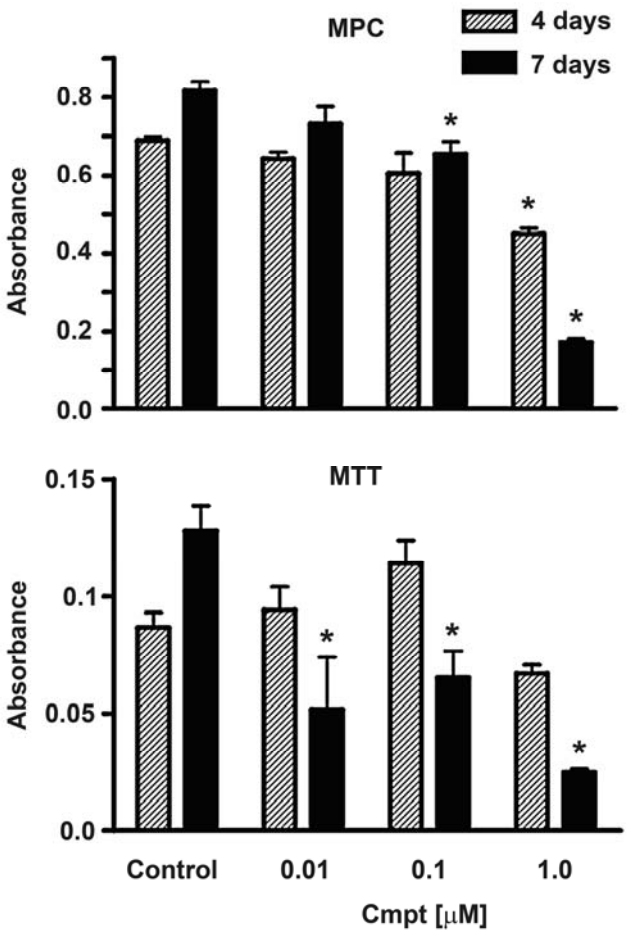


Fig. 4. Parallel tests of camptothecin toxicity on MPC and MTT cell lines at two time points, demonstrating greater sensitivity of MTT to low camptothecin concentrations. Data are from three independent experiments, each with triplicate wells. Bars indicate mean +/- SEM of triplicate wells.

Task 5 Additional TOP1 inhibitors that are currently approved for clinical use were tested for comparison to camptothecin.

- Because native camptothecin is considered too toxic for clinical use, we tested three additional TOP1 inhibitors; topotecan, irinotecan and SN38, the active metabolite of irinotecan, against MPC cells for up to 2 weeks using the same methods as for Task 2. The concentration ranges tested (0.1-10 ng/mL for topotecan, 1-100 ng/mL for SN38) was chosen to match published *in vitro* tests of these drugs against other tumors

Results:
At its highest concentration, SN38 (100ng/mL=0.26 uM) was comparable in cytotoxicity to 1ug/mL camptothecin (=2.7uM), causing ~ 90% cell death, while topotecan at its highest concentration was less effective (<50% cell death). (Fig 5).

This result formed the basis for proceeding with irinotecan as the camptothecin analog to be tested *in vivo* during the second funding period.

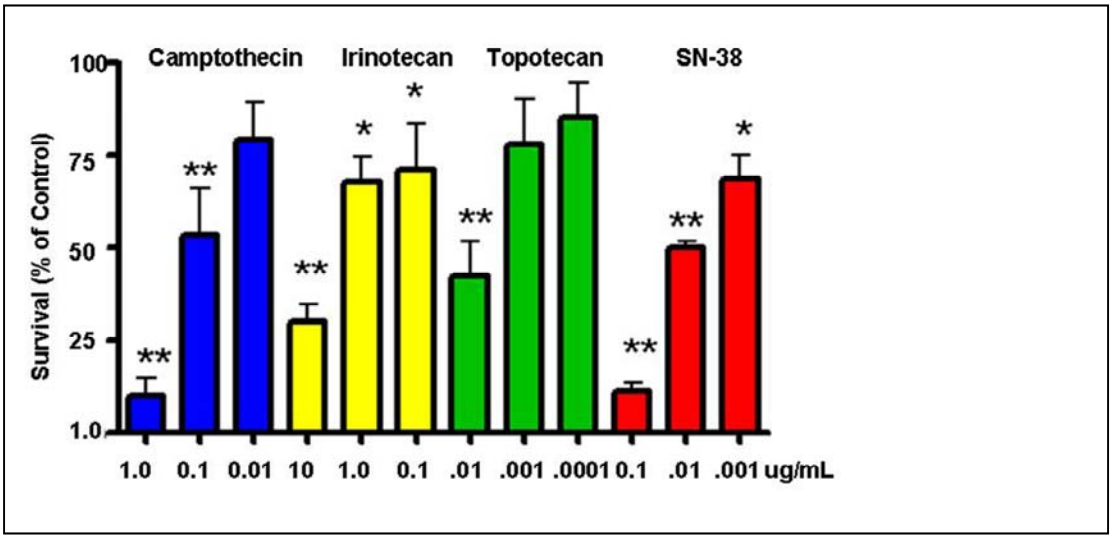


Fig. 5 Concurrent tests of camptothecin versus clinically utilized analogs on MPC cells in monolayer cultures at one week. Comparable sensitivity to camptothecin and SN-38 is seen at the indicated concentrations. Data are from three independent experiments, each with triplicate wells. Bars indicate mean +/- SEM. (**, p<.01; *, p<.05)

Task 6 As a prelude to *in vivo* testing, we tested to determine whether 3-dimensional growth affects drug sensitivity. This was done because tumors *in vivo* grow in 3 dimensions.

Using the same methods as in Task 5, we tested the efficacy of camptothecin and its analogs against MPC cells grown as spherical clusters in suspension.

Results:

Both camptothecin and SN-38 were effective against MPC cells in 3-dimensional as well as monolayer cultures. However, under otherwise identical test conditions, the same drug concentrations of were less effective against 3-dimensional clusters than monolayer cultures (Fig. 6).

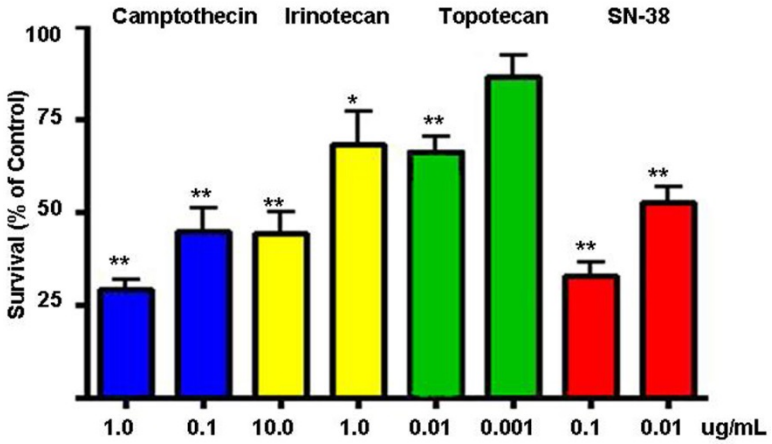


Fig. 6 Concurrent tests of camptothecin versus clinically utilized analogs on MPC cells in 3-dimensional cultures at one week. Comparable sensitivity to camptothecin and SN-38 is seen at the indicated concentrations. However, for both drugs, fewer cells are killed in 3-dimensional cultures than in monolayer cultures during the same time frame (see Fig. 5). Data are from three independent experiments, each with triplicate wells. Bars indicate mean +/- SEM. (**, p<.01; *, p<.05)

Task 7. Two alternative drugs were tested as possible alternatives to TOP1 inhibitors

Using the XTT assay a as screen as in Task 2, we tested a completely new type of drug known as Gamitrinib, developed by our collaborator, Dario Altieri at the Wistar Institute. Gamitrinib accumulates in the mitochondria of tumor cells but not of normal cells, and attacks a mitochondrial chaperone protein called TRAP-1. Cytotoxic effects were measured over a 2 week period.

Results:

At a concentration of 10 uM, Gamitrinib caused 60% MPC cell death at 1 week and > 90% death at 2 weeks, putting it on a par with camptothecin as a potentially useful drug. (Fig. 7)

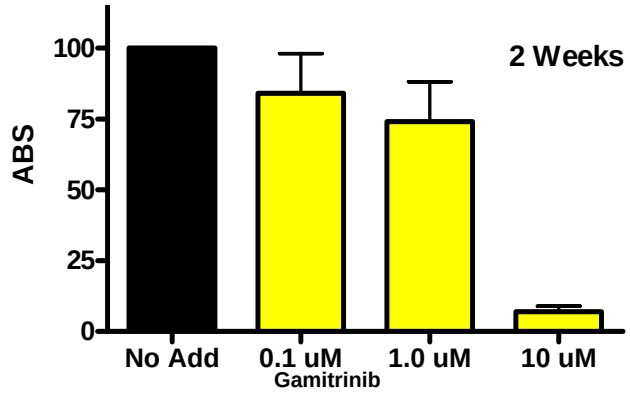


Fig. 7 Toxicity of Gamitrinib to MPC 4/30/PRR, measured by XTT colorimetric assay. Data are from 3 independent experiments with triplicate wells. An unusual aspect of the gamitrinib response is an abrupt dose-response curve with a threshold between 1 and 10 uM

In collaboration with our NIH collaborators, we similarly tested a drug called Torin-1, representing a new class of agents directed against mTOR, the mammalian target of rapamycin, a master regulator of cell proliferation and survival. Subsets of PCC show elevated mTOR signaling. Torin was tested against MTT, an aggressive, rapidly growing derivative of our MPC cells, using the MTT colorimetric assay.

- With this aggressive cell line, Torin-1 was able to significantly inhibit cellular proliferation in a dose-dependent manner over a range of concentrations (1nM to 1 μM) with an $IC_{50}$ of 207 nM and 80% cell death within 48 hours. However, it was much less effective than either camptothecin or Gamitrinib in primary human PCC cultures (see Specific Aim 2 below). and is therefore likely to have limited usefulness

*Specific Aim 2 Validation of drug testing paradigms in primary human cell cultures*

Summary: We tested human tumors in primary cultures with the most promising drugs identified in Specific Aim 1

Task 1. Camptothecin was tested to confirm its cytotoxicity against primary cultures of representative human pheochromocytomas.

Long-term killing of cells from 7 human PCC/PGL with diverse genetic backgrounds was tested in primary cultures. This test series included 3 tumors with SDHB mutations, the genotype most prone to metastasize. The cultures were maintained with 0 (control) (n=7), 1uM (n=7) or 10 uM (n=3) camptothecin for 2 wks, then fixed and stained for

tyrosine hydroxylase to discriminate the tumor cells from other cell types. Counts of surviving cells were derived by counting all stained cells defined by a randomly placed square coverslip in a 35 mm culture dish. (Fig 8, Table 1)

Results:

- Mean tumor cell survival at week 2 was 47 % with 1 uM and 25 % with 10 uM camptothecin (Fig 8, Table 1). All tumors responded, but responses for individual tumors ranged The lower sensitivity of human PCC vs MPC to camptothecin probably reflects the fact that MPC cells proliferate in culture while human PCC do not. It emphasizes the importance of comparing the human and mouse models and the need to develop effective multidrug strategies for the human tumors.

Fig. 8 A. Long-term killing of cells from representative human PCC/PGL s by camptothecin (Cmpt) in primary cultures maintained with 0 (control), 1 or 10 uM Cmpt for 2 wks, then fixed and stained for TH (red cytoplasm) to discriminate the tumor cells from other cell types. At 10 uM, camptothecin eliminated almost all background cells (faintly visible as hematoxylin-counterstained blue nuclei in top row control and 1 uM panels). NOTE: the tumor in the bottom row was identified as *RET*-mutated in an earlier version of this progress report. The genotype data were subsequently corrected.

Table 1. Survival of tumor cells from 7 individual PCCs / PGLs cultured in the presence of 1 uM or 10 uM camptothecin compared to control medium.

| | | **Surviving Cells/Dish (% of Control)*** | |
|---|---|---|---|
| **Tumor** | **Genotype** | **1.0 uM Cmpt** | **10 uM Cmpt** |
| 1 (V49) PCC | VHL | 39.1 | 18.6 |
| 2 (S116) PCC | Sporadic-Neg | 63.3 | 29.1 |
| 3 (M26A) PCC | Sporadic -Neg | 18.6 | 4.7 |
| 4 (TS12-2159) PCC | Unknown NT | 45.7 | |
| 5 (S111B) PGL | SDHB | 33.1 | 2.2 |
| 6 (S189) PGL | SDHB | 71.7 | |
| 7** (S123) PGL | SDHB | 24.0** | 10.1 |

*Counts were derived by counting all stained cells defined by a randomly placed square coverslip in a 35 mm culture dish. All counts were done at 2 weeks except for tumor 7 (**), which was counted at 1 week because of extensive cell death caused by particular sensitivity to camptothecin. Only 5 of the tumors were tested at 10 uM because that concentration eliminated almost all background cells and was therefore considered to exert too much bystander toxicity.

Task 2. Gamitrinib was tested as an alternative drug

We completed testing a series of 21 PCC/PGL representing different genotypes and locations for response to Gamitrinib. This study was begun prior to DoD funding but was continued as the potential usefulness of the drug became clear. Gamitrinib was tested at a concentration of 10 uM based on the results of Specific Aim 1, using the same methods as for Task 1.

Results:

- Individual tumors, shown as symbols in the scatter plot below showing survival at 2-weeks (Fig 9) were variably sensitive.
- Importantly, 3 of 4 tumors caused by mutations of the *SDHB* gene were highly sensitive. PCC/PGL with SDHB mutations are the most likely to be malignant. *SDHB* encodes a subunit of the mitochondrial enzyme succinate dehydrogenase, and therefore show impaired electron transport and pseudo-hypoxic signaling. Because it targets mitochondria in tumors that are driven by abnormal mitochondrial function, Gamitrinib may be both the most effective drug and the one most specifically targeting the majority of malignant PCC. Because Gamitrinib was highly effective against human PCC with relatively little bystander toxicity, we plan to

begin our *in vivo* testing with Gamitrinib rather than a TOP-1 inhibitor in the next funding period.

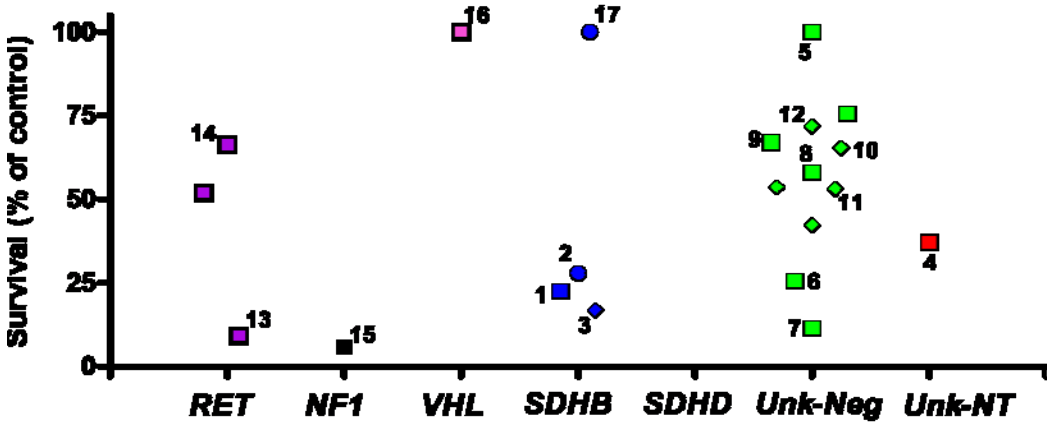


Fig. 9. Scatter plot showing survival at 2-weeks of individual tumors with different causative genetic mutations tested with 10 uM Gamitrinib. (Numbers accompanying the symbols are non-relevant identifiers linking to other characteristics of each tumor).

*Specific Aim 3 In vivo testing of drug-administration paradigms developed in specific aims 1 and 2 using MPC cells as a model*

Summary: We modified the mouse pheochromocytoma cell line used in specific aim 1 to create a novel bioluminescence model for in *vivo* testing .

Task 1 As our principal model for in vivo testing, we generated a cell line designated MPC 4/30/PRR GL-9 (abbreviated to MPC GL-9) that expresses green fluorescent protein (GFP) and firefly luciferase. The luciferase emits light in mice injected with the substrate luciferin, permitting quantitation of tumor growth or regression at repeated intervals using a luminometer designed for small animal imaging, while the GFP permits the cells to be sorted in a cell sorter in order to maintain a stable phenotype or recover pure tumor cells from *in vivo* deposits

- MPC GL-9 was derived from MPC 4/30PRR by transducing the cells with a pre-packaged lentiviral construct (GreenFire1, SBI Systems) containing both the GFP and luciferase genes under control of the CMV promoter. Infection was performed according to the manufacturer's protocol. MPC GL-9, which stably expresses high levels of luciferase, was cloned from a single transduced cell identified by its GFP fluorescence. Clones were initially isolated with glass cloning cylinders and then with a fluorescence activated cell sorter (Fig. 10) Aside from expression of its two marker proteins, MPC G-L9 is similar to its parent tumor.

t

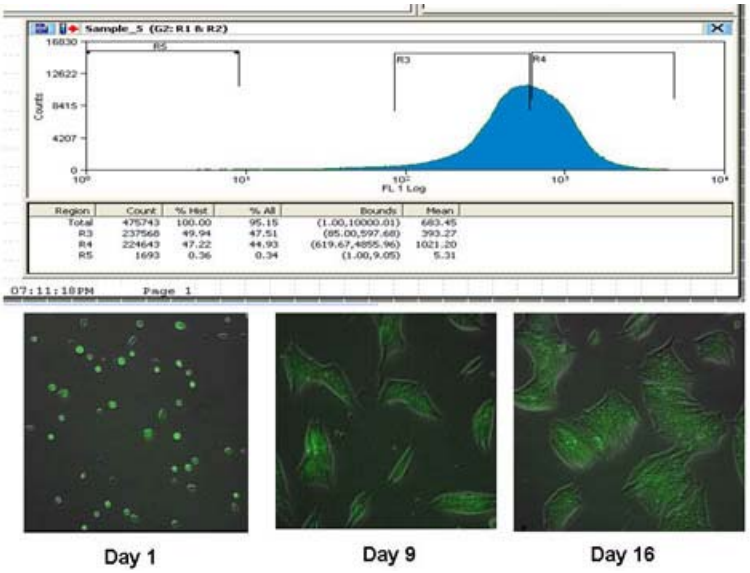


Fig. 10. MPC-GL9 cells sorted by GFP fluorescence. The figure shows sort profile (top), freshly sorted dissociated fluorescent cells at day 1 and fluorescent colonies at days 9 and 16 post-sort.

Task 2 The ability of MPC GL-9 cells to emit detectable light was tested *in vivo* in order to develop protocols *for in vivo* drug testing.

500,000 MPC-GL9 cells (equivalent to a moderately dense small culture dish) were injected into immunodeficient mice by tail vein or subcutaneous injection. The mice were anesthetized and given an intraperitoneal injection of luciferin. After 5 min the mice were imaged in a Xenogen IVIS 200 biophotonic imager at the Tufts Small Animal Imaging Facility.

Results:

Luminescent cells were immediately detectable, distributed between both lungs after tail vein injection (Fig. 11) or in subcutaneous sites. This established the potential utility of the MPC-GL9 model for *in vivo* imaging studies.

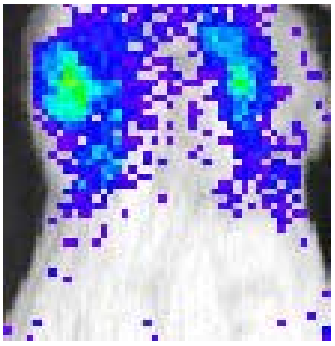

Fig. 11 *In vivo* luminescence of a NOD-SCID mouse imaged immediately after tail vein injection of 500,000 MPC-GL9 cells.

Task 3 We collaborated with colleagues at the NIH on a second luminescent cell line complementary to MPC-GL9

Starting with MPC 4/30PRR cells from our laboratory, our NIH collaborators generated a luminescent cell line known as MTT-Luc. MPC 4/30PRR cells were first injected into tail veins. A rapidly growing cell line designated MTT (for Mouse Tumor Tissue) was cultured from resulting disseminated tumor deposits. Luciferase driven by the CMV promoter was then introduced using a retrovirus vector to create MTT-Luc.

- MTT-Luc and its non-luminescent counterpart MTT serve as a rapidly growing counterpart to the better differentiated MPC GL-9, representing the occasional human PCC that undergoes "explosive" growth after failure of chemotherapy.
- A paper describing MTT-Luc was published (Giubellino A et al, Cancer Lett 2012; **316** 46-52 PMID:22154086) .

*Specific Aim 4 Novel approaches to develop cell lines of human PCC for cell culture and xenografts*

Summary: For this aim we pursued two parallel tracks: Attempts to directly establish cell lines from primary human PCC cell cultures using novel culture conditions, and attempts to establish propagatable xenografts by direct introduction of human PCC cells into favored metastatic sites.

Task 1 Tumor cell proliferation was tested under hypoxic compared to routine normoxic cell culture conditions

We studied 23 PCC/PGL representing different genotypes. Hypoxic culturing was performed in modular incubator chambers (from Billups-Rothenberg Inc) with pre-mixed atmospheres containing 1% -4% $O_2$ Proliferation was assessed by labeling with bromodeoxyuridine (BrdU) as a marker for DNA replication. BrdU was present in the culture medium for 6 days or one week prior to fixation. Double immunohistochemical staining was performed for BrdU and tyrosine hydroxylase to discriminate tumor cells from proliferating fibroblasts and other cell types in primary cultures. Some cultures were studied at two or more time points (Fig. 13). For some tumors, preliminary studies were also performed testing hypoxia/normoxia in several culture media and in media with growth factor or other supplements as shown in Table 2.

Results:

There was no BrdU labeling of tumor cells in either normoxic or hypoxic cultures under any conditions, while labeling of irrelevant cell types was readily detected (Fig 13, Table 2). Because the hypoxic culture approach was unsuccessful, we suspended this work in order to evaluate additonal options (see Areas of Concern section to follow) while focusing on more promising xenograft approaches. Frozen cells from most of the tumors are available for future cell culture experiments.

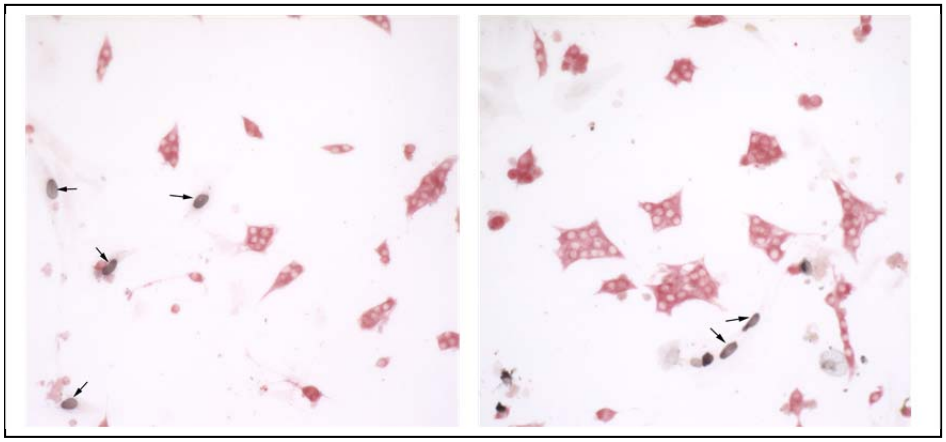

Fig.13. Representative cultures of cells from a human pheochromocytoma in normoxic (left, 20% $O_2$) *versus* hypoxic (right, 4% $O_2$) cultures. BrdU was added to the medium immediately on plating. After 7 days, cultures were fixed and double stained for BrdU (black nuclei) and tyrosine hydroxylase (red cytoplasm). BrdU labeling of fibroblasts is seen under both conditions (arrows), while pheochromocytoma cells show no BrdU incorporation. Numerous pheochromocytoma cells, which are smaller than fibroblasts, are seen in clusters. Clear circles within the red clusters are unlabeled nuclei.

Table 2. Summary of Human Tumors Tested for BrdU Incorporation in Hypoxic *vs*. Normoxic Conditions*

| | **Sex** | **Age** | **Geno-type** | **Site** | **%$O_2$ RPMI** | **%$O_2$ RPMI-HG** | **%$O_2$ RPMI-CS** | **%$O_2$ NSC** | **Hypoxia +adds** |
|---|---|---|---|---|---|---|---|---|---|
| | | | | | | | | | |
| 1 | F | 23 | sporadic-Neg | R adrenal | 2%-6 d | | | | |
| 2 | F | 26 | sporadic-Neg | L adrenal | 3%-18 d | | | 3%-18 d | |
| 3 | F | | sporadic-Neg | | 3%-18 d | | | 3%-18 d | |
| 4 | M | 18 | sporadic-Neg | R adrenal | 3%-18 d | | | 3%-18 d | |
| 5 | M | 31 | VHL | R adrenal | 3%-18 d | | | 3%-18 d | |
| 6 | M | 41 | sporadic-Neg | R adrenal | 3%-18 d | | | 3%-18 d | |
| 7 | M | 16.4 | SDHB | Bladder | 3%-1, 4 wk | | | | |
| 8 | M | 39 | SDHB | Met lung | 4%-1,3 wk | | 4%-1wk | 4%-1 wk | EGF, FGF 1 wk, FA1, FA2, VPA 1,3 wk |
| 9 | M | 54 | ?SDHB | Met | 4%-1 wk | | | 4%-1 wk | EGF, FGF, EGF+FGF, NSC suppl-1wk |

| | | | | | | | | | |
|---|---|---|---|---|---|---|---|---|---|
| 10 | M | 48 | SDHB | met-liver | 4%-<br>1 wk, | | | | |
| 11 | M | 45 | SDHB | Retroperi<br>toneal | 4%-<br>1,8 wk | | | | |
| 12 | M | ? | sporadic-<br>Neg | R<br>adrenal | 4%-<br>1wk | | | | |
| 13 | F | 29 | sporadic-<br>Neg | Infra<br>aortic | 4%-<br>1 wk | | | | IGF II- 7 d |
| 14 | F | | | R<br>perirenal | 4%-<br>1 wk | | | | IGF II- 7 d |
| 15 | M | 44 | sporadic-<br>Neg | R<br>adrenal | 4%-<br>1 wk | | | | IGF II- 7 d |
| 16 | M | 33 | SDHD | L<br>carotid | 4%-<br>1,2,10 wk | | | | |
| 17 | F | 66 | Sporadic<br>? Not<br>tested | R<br>adrenal | 1% -<br>1,3, 8 wk | 1% -<br>1,3, 8 wk | | | |
| 18 | M | 33 | sporadic-<br>neg | Heart | 1% -1,3, 8<br>wk | 1% -<br>1,3, 8 wk | | | |
| 19 | M | 27 | SDHB | Para-<br>spinal | 1%-<br>1 wk | 1%-<br>1,3 wk | | | |
| 20 | F | 50 | sporadic-<br>neg | R thorax | 1%-<br>1, 2, 8 wk | 1%-<br>1, 2, 8 wk | | | |
| 21 | F | ? | RET/<br>MEN2A | | | 4% and<br>1%-<br>1, 2, 6 wk | | | |
| 22 | M | 34 | SDHC | Heart | 4%-<br>1 wk, 60 d | | | | 50% FBS-<br>14, 60 d |
| 23 | M | 74 | Unk | | 4%-<br>1 wk | | | | |
| | M | 58 | Normal<br>Adrenal<br>medulla | | 3%-1 wk | | | Float<br>vs. Att-<br>1 wk | EGF, FGF,<br>NSC suppl |

SUMMARY

| | |
|---|---|
| Total # of Tumors | 23 |
| male | 15 |
| female | 8 |
| | |
| Sporadic (Neg genetic tests) | 10 |
| Indefinite | 5 |
| Definite SDHB | 4 |
| Definite SDHC | 1 |
| Definite SDHD | 1 |
| Definite VHL | 1 |
| Definite RET MEN2A | 1 |

*TABLE LEGEND. All tumors were tested for BrdU incorporation in normoxic (20% $O_2$) *vs* hypoxic cultures at the indicated $O_2$ concentrations and time points. The routine medium for testing all tumors was RPMI 1640 with 15% fetal bovine serum ("RPMI"). For some tumors, additional parallel testing was performed in High Glucose RPMI 1640 with 15% FBS ("RPMI-HG"), RPMI with 15% calf serum ("RPMI-CS"), or synthetic neural stem cell medium ("NSC"). Some tumors were also tested in RPMI 1640 with 15% FBS plus the indicated supplements (EGF, epidermal growth factor; FGF, basic fibroblast growth factor; FA1 & FA2, fatty acid supplements 1 & 2 from Sigma Chemical Co.; IGF II , insulin-like growth factor 2; NSC, neural stem cell supplement, from Neural Stem Cell Technologies Inc.).

Task 2 Approval was obtained from Tufts IACUC for two different methods of xenografting human PCC, i.e. surgical implantation of intact tumor tissue and for intrahepatic injection of dissociated human PCC cells. Pilot studies were performed testing both methods.

Ssurgical implantation of human PCC into the liver:

A small abdominal incision was made in anesthetized mice. The right lobe of the liver was protruded through the incision. A small tumor fragment was implanted through an incision in the liver capsule. The liver capsule incision was rapidly sealed with Vetbond adhesive, the liver lobe was returned to its normal location and the abdominal incision was closed with surgical staples.

- This method permitted tumor fragments to be retained in the liver and subsequently studied histologically.

Intrahepatic injection of dissociated human PCC cells into the liver

Injection of dissociated tumor cells into the right lobe of the liver was tested both with the liver *in situ* under visualization by small animal ultrasound and with surgically exposed liver as in Task 3. Cells were injected in 10 uL of tissue culture medium.

- This method was unsuccessful because intrahepatic pressure forced most of the cells out of the liver despite the low injection volume. This method was consequently abandoned.

Task 3 The bioluminescence methodology from specific aim 3 was adapted to develop a method for tracking the survival of human tumor xenografts

- Transduction of dissociated human PCC cells was first attempted with a lentivirus–luciferase construct using the same method that was successful for MPC cells in specific aim 3. Viral multiplicity of infection (MOI) of 5-50 was tested in medium containing 0-8ug polybreen/mL.
  - Under all conditions infectivity was extremely low (<<1/1000 cells).

- Because of the unsatisfactory infectivity with lentivirus, we next tested an adenoviral luciferase vector (AD-CMV-luciferase, Vector Biolabs).
  - At MOI 10, AD-CMV-luciferase was found to infect 100% of PCC cells.

- To obtain proof of principle, AD-CMV-luciferase was used to test survival of representative intrahepatic xenografts. Small tissue fragments were incubated overnight with AD-CMV-luciferase in complete culture medium. The virus was then washed out and cultures maintained for 1 week with 2 intervening medium changes. Tissue fragments were then implanted into the liver as in Task 2. At intervals the mice were anesthetized and given an intraperitoneal injection of luciferin. After 5 min they were imaged in a Xenogen IVIS 200 biophotonic imager at the Tufts Small Animal Imaging Facility
  - Successfully grafted tissue shows a single brightly luminescent signal (Fig 14).

- This result established a novel model for monitoring graft survival in a series of tumors in the next funding period.

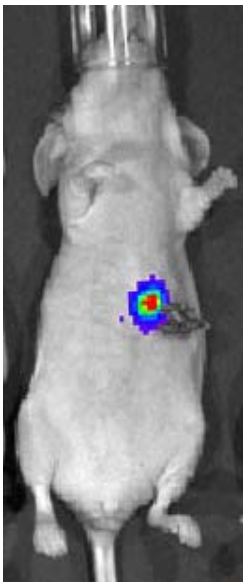

Fig.14. Bioluminescence image of an anesthetized mouse with an intrahepatic graft of a human PCC tissue fragment expressing adenovirus-luciferase, 4 days post–grafting. The graft was implanted in the right lobe of the liver, which is shifted somewhat to the left in the photograph This graft failed to vascularize and did not survive an additional week.

**Year 2 (15 August 2012- 14 September 2013).**

*Specific Aim 1 Development of drug testing paradigms using MPC cell cultures*

Task 1. The HDAC inhibitor, SAHA (vorinostat, Zolinza) was tested against MPC cells in monolayer culture (specific aim 1).

Results:

SAHA is highly effective against MPC cells as a single agent (Figure 1). This finding suggests a potential role for HDAC inhibitors in treating pheochromocytoma. However, these drugs have serious limitations for treating other types of solid tumors, including cardiac toxicity. This provided a rationale for subsequent testing to minimize cardiac and other systemic toxicity by using lower concentrations of the drugs in combination with low concentrations of TOP1 inhibitors (see Task 4).

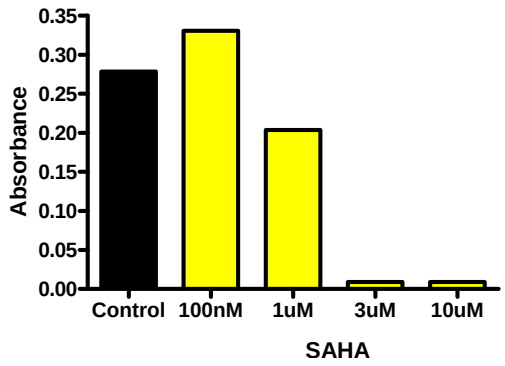


Figure 1. XTT assays showing cytotoxicity of SAHA toward MPC cells in monolayer cultures at one week. Cell survival is proportional to absorbance. Values represent mean ±SEM for quadruplicate wells. (Error bars were extremely small and are not visible on the graph)

Task 2. The HDAC inhibitor, trichostatin was tested against MPC cells in monolayer culture (specific aim 1). (A third HDAC inhibitor mentioned in our original grant proposal, valproic acid, was not further tested because preliminary studies shortly after approval of the grant showed a paradoxical protective effect most likely unrelated to HDAC inhibiton. We therefore tested trichostatin in addition to SAHA as a further confirmation of specificity).

Result:

Like SAHA, trichostatin was highly effective against MPC cells as a single agent (Figure 2).

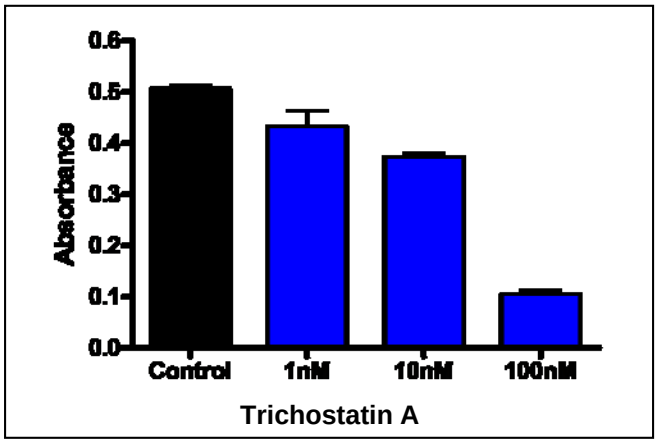


Figure 2. XTT assays showing cytotoxicity of trichostatin A toward MPC cells in monolayer cultures at one week. Cell survival is proportional to absorbance. Values represent mean ±SEM for quadruplicate wells.

Task 3. SAHA was tested in conjunction with two TOP1 inhibitors, camptothecin and SN38, for cytotoxicity against MPC cells. These experiments were performed to determine whether cooperative interactions between the two classes of drugs (HDAC inhibitors and TOP1 inhibitors) would lower the effective concentrations and thereby potentially reduce systemic toxicity.

Results:

- Both TOP1 inhibitors decreased cell survival alone, as shown in the first funding period. There was no apparent cooperativity between these agents and SAHA. However, SAHA alone was effective as a single agent at high concentrations (Figure 3)

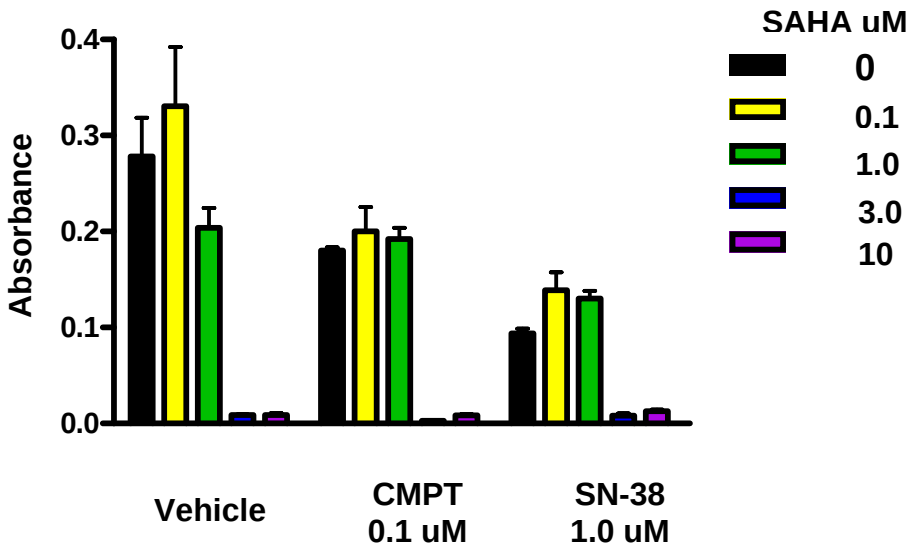


Figure 3. Cytotoxic effects of SAHA and TOP1 inhibitors are not cooperative. MPC cells were maintained in monolayer cultures for one week in control medium or with the indicated concentrations of camptothecin (CMPT), SAHA and SN-38. Cell survival was then measured by XTT assay. Values represent mean ±SEM of quadruplicate cultures. (Note: For increased clarity, the data for SAHA alone versus control from this same experiment are shown as a separate figure in Fig 1.)

Task 4 We tested cytotoxicity toward cultured MPC cells using TOP1 inhibitors in conjunction with lithium, one of the alternate drugs to 5-azacytidine described in the original project narrative and approved SOW. Lithium was tested for this purpose because it can dramatically increase gene transcription in the rat pheochromocytoma cell line PC12 (Dobner PRet al, J Biol Chem. 1988;263:13983-6).
. This concentration is somewhat above the toxic threshold for serum concentration in patients treated with Li for bipolar disorders but is not toxic to PC12 cells.

Results:

At the concentration previously tested with PC12 cells, lithium alone markedly decreased MPC cell number measurable by XTT assay after 1 week. There was also a trend toward cooperativity between Li and 0.5 uM camptothecin or SN-38 during the same time period (Fig 5).

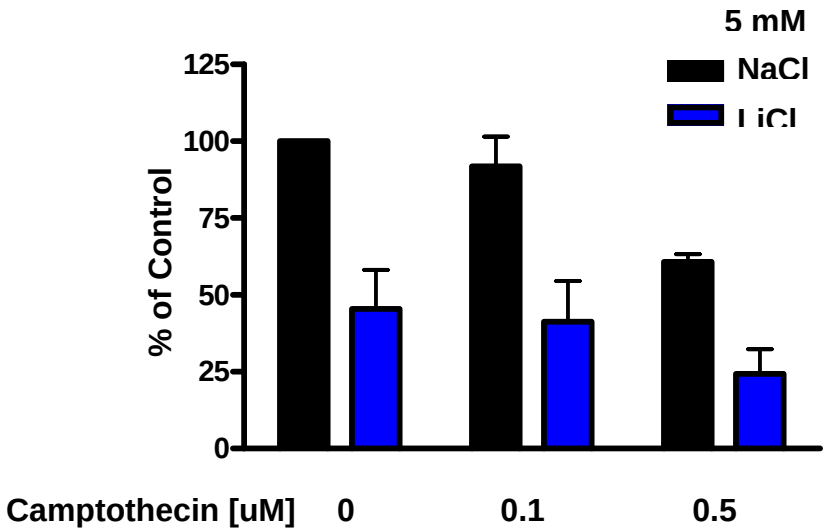


Figure. 5 . MPC cells were maintained in monolayer cultures for one week in control medium or with the indicated drug concentrations. Cell survival was measured by XTT assay. Values represent mean ±SEM of 3independent experiments, each with quadruplicate cultures. Similar results were obtained with SN-38 as the TOP1 inhibitor in place of camptothecin (not shown)

Task 5 To determine whether the dramatically reduced cell number seen with lithium in task 6 was caused by cell death or cytostasis, MPC cultures were cultured with 5mM LiCl or equimolar NaCl as a control for 3 days in the presence of bromodeoxyuridine (BrdU) to label replicating cells. The cultures were then fixed and stained immunocytochemically for BrdU. Cells were counted and labeled cells were expressed as percentage of total.

Results:

- BrdU labeling was present in 47% of MPC cells after 3 days, versus 8.9% with LiCl. This indicates that the short term effect on cell number is caused by cytostasis rather than increased cell death as seen with TOP1 inhibitors. This effect could itself be useful in treatment of metastatic pheochromocytoma and was further studied in the next funding period.

Task 6 We tested cytotoxicity toward cultured MPC cells using TOP1 inhibitors in conjunction with caffeine, another alternate drug to 5-azacytidine described in the original project narrative and approved SOW. Caffeine was tested for this purpose

because it can dramatically increase gene transcription by releasing $Ca^{++}$ from intracellular stores (Zacchetti D et al, J Biol Chem. 1991;266:20152). We performed a two-week experiment with caffeine added during the first and/or second week in the presence or absence of camptothecin.

Results:

- Caffeine did not detectably increase cytotoxicity when added to camptothecin (Fig. 6). However, an interesting observation was that caffeine alone decreased cell survival campared to control medium. This finding is consistent with preliminary data in our original grant proposal showing that caffeine causes a burst of apoptosis in MPC cultures. The effect is variable and small compared to that of the TOP1 inhibitors. However the concentration of caffeine is these experiments was very low (equivalent to the serum caffeine concentration after consuming two cups of instant coffee (Routh JI et al, Clin Chem. 1969;15:661-8)). Further studies of caffeine were performed in the next funding period.

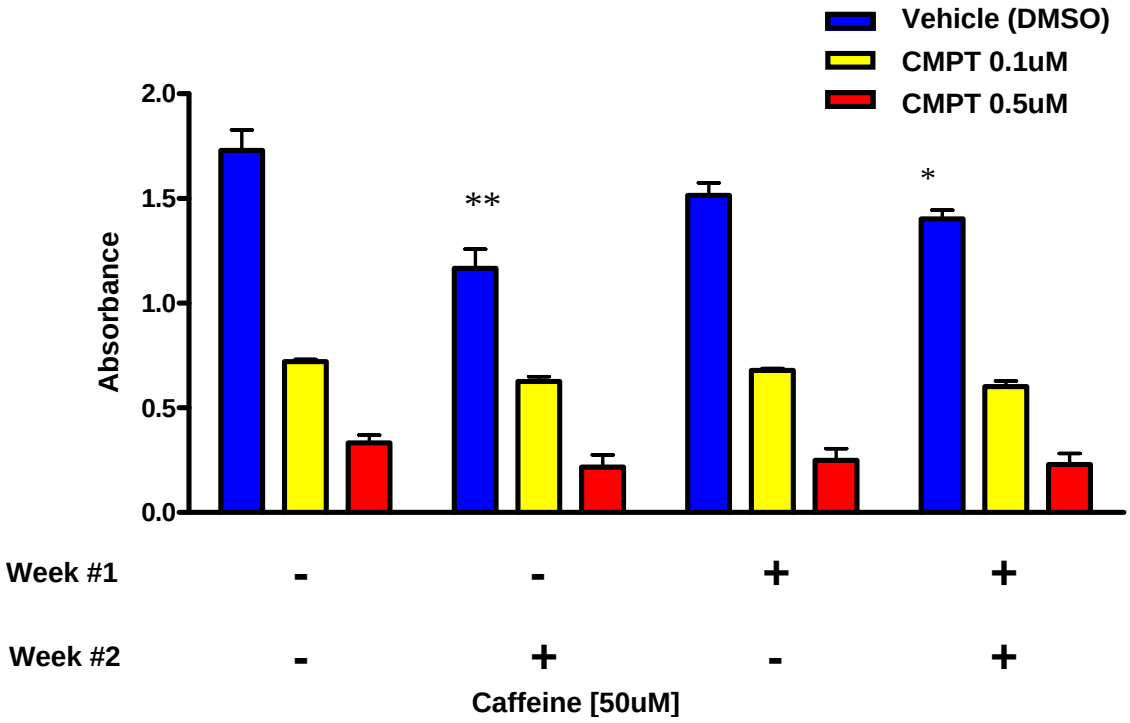


Figure. 6. Caffeine does not enhance toxicity of camptothecin but exerts a small apoptotic effect alone. The effect is most apparent when caffeine is added during week 2, probably indicating that the effect is transient and becomes masked by continued cell replication when caffeine is present continuously from week 1. MPC cells were maintained in monolayer cultures for 2 weeks in control medium or with the indicated drug combinations. Cell survival was measured by XTT assay. Values represent mean ±SEM of quadruplicate cultures. ** $p<.01$; * $p<.05$

***<u>Specific Aim 2</u> validation of drug testing paradigms in primary human cell cultures***

Task 1. SAHA was tested for cytotoxicity against two primary human tumors in primary cultures (specific aim 2). We focused on SAHA for this purpose because SAHA is one of only two HDAC inhibitors currently approved for clinical use (Gryder BE et al, Future medicinal chemistry. 2012;4:505-24).

Results

Both pheochromocytoma (tumor 1) and extra-adrenal paraganglioma (tumor 2) were susceptible to SAHA as a single agent within the concentration range effective against MPC cells. Variation between tumors was evident, as for drugs tested during the first funding period (Table 1).

Table 1. Cytotoxicity of SAHA Against Primary Human Pheochromocytoma/Paraganglioma

| | | **Surviving Cells/Dish (% of Control)*** | |
|---|---|---|---|
| **Tumor** | **Genotype** | **1.0 uM SAHA** | **10 uM SAHA** |
| 1 | *SDHB* | 67.1 | 60.0 |
| 2 | Sporadic- | 122.6 | 22.4 |

*Representative primary human PCC/PGL cells were treated with the indicated concentrations of SAHA or maintained in control medium for one week in monolayer cultures. At the end of the treatment period, cultures were fixed and stained for tyrosine hydroxylase TH to discriminate the tumor cells from fibroblasts and other cell types.

***Specific Aim 3 In vivo testing of drug administration paradigms using MPC cells as a model***

Task 1. We tested the toxicity of Gamitrinib against disseminated MPC GL-9 cells in nude mice (specific aim 3). In order to validate the bioluminescence methodology, we first tested subcutaneous tumor implants with the intention of then moving to the more technically challenging measurements of disseminated tumor. We propagated sufficient cells to inject 20 mice, 2 x $10^6$ cells/mouse (~3 weeks), then waited for discrete tumor masses to form. (~4 weeks) and performed treatment, with interval luminescence imaging. This study was based on a protocol by our collaborators who developed Gamitrinib. It entailed a cycle of 3 days on followed by 2 days off treatment for 21 days (Kang BH et al, British journal of cancer. 2011;104:629-34).

Results:

There was no detectable effect of Gamitrinib *in vivo* using the protocol tested (Fig 1).

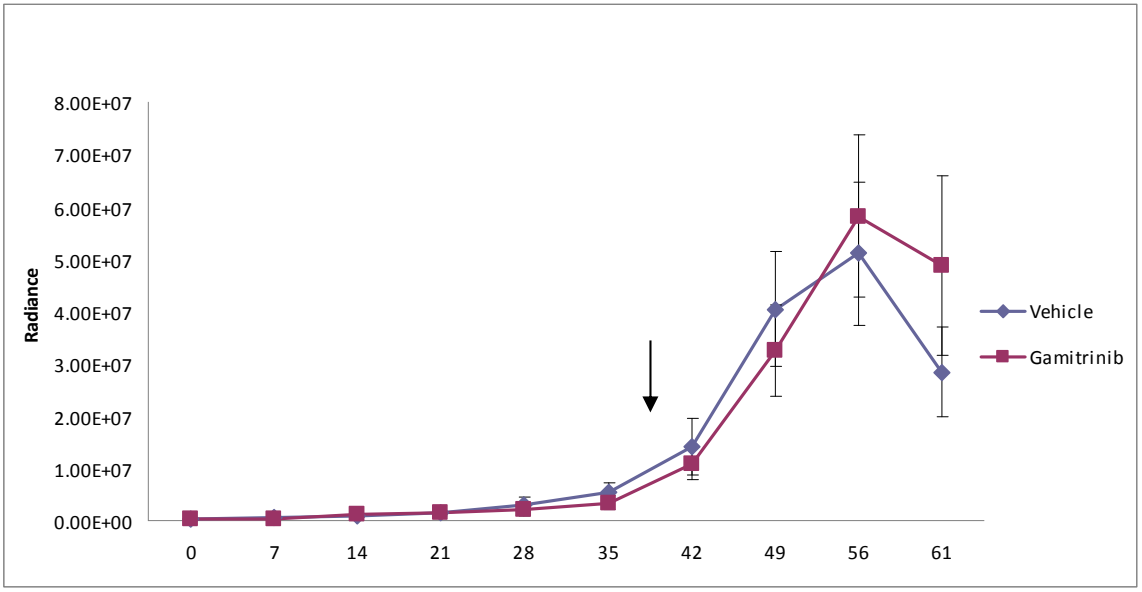


Figure 1. Sequential luminescence imaging of subcutaneously injected MPC GL-9 cells in nude mice before and after start of cyclic Gamitrinib treatment (arrow). There is no detectable effect of the drug using this treatment protocol. The dip in luminescence at day 61 is an artefact resulting from a new lot of luciferin.(Note: In the original Year 2 progress report this figure was erroneously labeled as representing a study of disseminated tumor cells).

***Specific Aim 4 Attempts to develop cell lines of human pheochromocytoma for cell culture and xenografts***

***Task 1***. *Attempt to develop high throughput bioluminescence–based cytotoxicity assay for human PCC/PGL in cell cultures.*

.

We performed a dilution curve with luminescent MPC GL-9 cells to determine the minimal number of luminescent cells detectable in monolayer culture in our luciferin-luciferase bioluminescence assay. These cells, which we generated in the first funding period, stably express the firefly luciferase gene integrated into their genome.

Before progressing to human cells we next used an adenoviral luciferase vector (AD-CMV-luciferase, Vector Biolabs) to transiently introduce firefly luciferase into non-luminescent MPC cells. For this purpose we used AD-CMV –luciferase at a MOI of 10, which we had found to infect 100% of PCC/PGL cells in the previous funding period. The luminescenc of these MPC cells would be commparable to that of primary human PCC/PGL cells, which can be made luminescent only by infection with the adenovirus construct. We then performed a dilution curve and luminescence assay directly comparing the luminescent signal intensity of the AD-CMV-luciferase MPC cells to luminescent MPC GL-9 cells

Results (Fig. 2).

- Although 100% of human PCC/PGL cells are infected with AD-CMV-luciferase, the signal intensity is far lower than with MPC GL-9. Based on Fig. 6, we estimate that a starting number of at least several thousand luminescent human cells per well would be required in order to obtain reliable results from a cytotoxicity assay using this approach. .The combined obstacles of limited tumor cell yield and variable tumor cell enrichment within a dissociated cell population continued to make these attempts unsuccessful. We therefore continued to use our immunohistochemical method for testing primary human cultures.

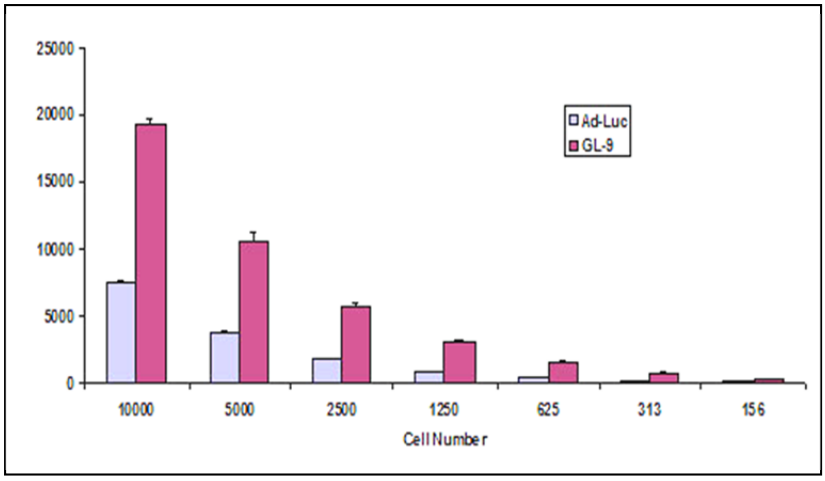


Figure 2. Comparative luminescence intensities of equal numbers of AD-CMV-luciferase MPC cells and luminescent MPC GL-9 cells. Values represent mean ± SEM for quadruplicate wells.

*Task 2. Finalize choice for route of administration of human PCC cells to mice and choice of mouse strain (Specific Aim 4).*

We first generated luminescent human PCC/PGLs using an adenovirus luciferase construct as described in *Goal 3*. Continuing studies begun and preliminarily reported in the first funding period, we compared survival of luminescent human cells introduced by tail vein vs intrahepatic injection and subcutaneous injection in 3 mouse strains (nude, SCID, NOD-SCID). Because the adenovirus construct is not integrated into the genome, we simultaneously maintained cells from representative tumors in cell culture to determine how long luminescence persists before spontaneously being extinguished.

Results

In total, 56 mice were grafted by the end of the second funding period (Table 2). Regardless of the type of graft (dissociated cells or tumor tissue fragments), route of tumor administration, site of grafting or mouse strain, there were no tumor takes from any tumors during periods so far ranging from 21 to 294 days. In the tumors that were tagged

with luciferase, luminescence of cell or tissue grafts invariably extinguished before luminescence of tumor cells in culture (Figure 8). Mice that died or were euthanized for reasons unrelated to tumor were dissected at the end of the observation periods and confirmed that there were no tumor takes *in vivo* that had ceased to be luminescent.

**Table 2. Summary of Mouse Xenografts of Pheochromocytoma (PCC) and Extra-adrenal Paraganglioma (PGL) through August 2013**

| Age | Sex | Tumor Type | Gene | Mouse | # | Route | Result | Tag |
|---|---|---|---|---|---|---|---|---|
| 47 | F | PGL | Sporadic-Neg | Nude | 4 | Liver implant | No Tumor take | Ad-Luc |
| | | | | Nude | 2 | Liver implant | No Tumor take | Ad-Luc |
| 55 | F | PCC | Not Tested | Nude | 4 | Liver implant (coated with matrigel) | No Tumor take | Ad-Luc |
| 54 | M | PGL-CB | SDHB | Nude | 2 | Liver injection | No Tumor take | Ad-Luc |
| 51 | M | PCC | Sporadic-Neg | Nude | 1 | Liver injection | No Tumor take | Ad-Luc |
| 11 | F | PGL | SDHB | Nude | 1 | Liver injection | No Tumor take | Ad-Luc |
| | F | PCC | MEN2A | SCID-Balb | 3 | Liver injection | No Tumor take | Ad-Luc |
| 66 | F | PCC | Not Tested | SCID-Balb | 3 | Liver injection | No Tumor take | Ad-Luc |
| 33 | M | PGL | Sporadic-Neg | SCID-Balb | 2 | Liver injection, SC-neck | No Tumor take | Ad-Luc |
| | | | | NOD-SCID | 2 | Liver injection, SC-neck | No Tumor take | Ad-Luc |
| 27 | M | PGL | SDHB+ | NOD-SCID | 3 | Liver injection | No Tumor take | Ad-Luc |
| 50 | F | PGL | Sporadic-Neg | NOD-SCID | 3 | Liver injection | No Tumor take | Ad-Luc |
| | | | | | | | | |

| | | | | | | | | |
|---|---|---|---|---|---|---|---|---|
| 39 | F | PGL | SDHB+ | NOD-SCID | 1 | IV-Tail vein | No Tumor take | Ad-Luc |
| 61 | M | PCC | Not Tested | Nude | 2 | SC-flank, SC-tail | Pending | Ad-Luc |
| 25 | F | PCC | Pending | Nude | 2 | SC-flank | Pending | Ad-Luc vs. GreenFire |
| 30 | M | PGL | SDHB | Nude | 1 | SC-flank | Pending | Ad-Luc |
| 9 | F | PGL | SDHB | Nude | 2 | SC-flank | Pending | Ad-Luc |
| 48 | M | PGL | SDHB | Nude | 1 | SC-flank | Pending | Ad-Luc |
| 45 | M | PGL | SDHB | Nude | 1 | SC-flank | No Tumor take | Ad-Luc |
| 27 | M | PGL | SDHB+ | Nude | 1 | SC-flank | Pending | Ad-Luc |
| 46 | F | PCC | SDHB | Nude | 1 | SC-flank | Pending | Ad-Luc |
| 39 | M | PGL | SDHB | Nude | 1 | SC-flank | Pending | Ad-Luc |
| 54 | M | PGL | SDHB | Nude | 1 | SC-flank | Pending | Ad-Luc |
| 28 | F | PCC | SDHB | Nude | 1 | SC-flank | Pending | Ad-Luc |
| 55* | M | PGL-skull metastasis | SDHB | Nude | 2 | SC-flank (tissue chunks) | 1-negative 1-pending | |
| | | PGL-liver metastasis | SDHB | Nude | 2 | Liver injection through skin | No Tumor Take | |
| | | | | Nude | 3 | Abdomen through incision (tissue chunks) | 1-negative 2-pending | |
| | | | | Nude | 4 | Liver injection through skin | Pending | Ad-Luc vs. GreenFire |

* Highlighted case is discussed in Task 2

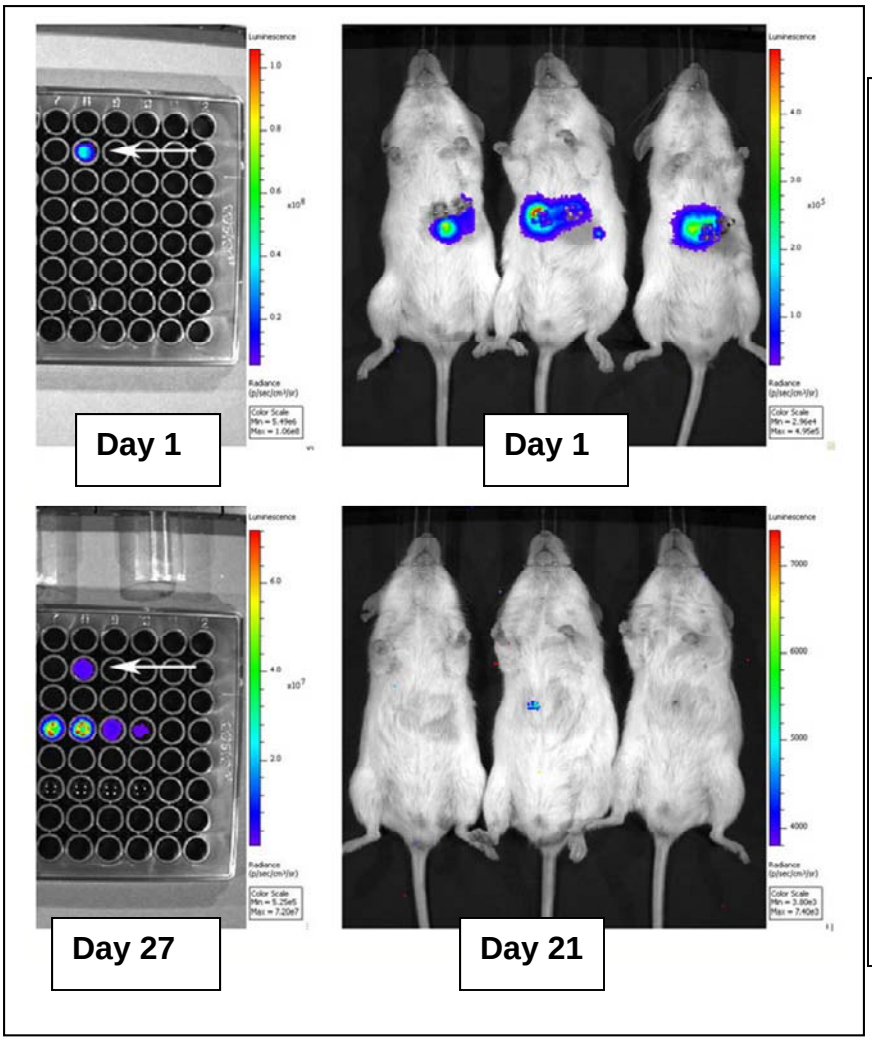


Figure 8. Right: Bioluminescence imaging of SCID mice with intrahepatic grafted human PGL cells tagged with adenovirus-luciferase. Left, arrows: Concurrent cell cultures of the tagged cells. Signal is essentially gone in the mice by day 21 while still persistent, though diminished, in the cultures at day 27. Luminescent wells in the row below the arrow at day 27 contain dilutions of mouse MPC GL-9 cells.

Task 2. To rule out the possibility that the absence of tumor takes *in vivo* might have merely reflected the slow growth typical of most PCC/PGLs, we used rapidly growing metastatic tumor cells from a single tumor derived from a patient with hepatic and peritoneal metastases. This unusual tumor also enabled us to test and compare multiple routes of administration from a single tumor, which was not possible in most other cases because of limited cell yields. We tested subcutaneous and intrahepatic tumor cell injection and intraperitoneal implantation of tumor fragments from this tumor in a total of 11 nude mice (highlighted case in Table 2).

Result:
All but 2 of the mice with cells or tissue from this tumor survived no evidence of tumor after 7 months, despite the fact that these aggressive tumor cells were returned to the same anatomic sites from which they were derived. The two dead mice were euthanized for unrelated lesions and necropsies showed no evidence of tumor. Tumor cells in culture survived for the same period with no cell proliferation.

Task 3 We attempted to develop a protocol to use lentivirus for transduction and stable luciferase expression in human PCC/PGL. Using the Greenfire 2 lentivirus luciferase construct that we previously employed to generate luminescent MPC GL-9 cells, we tested transduction efficiency comparing our previously optimized protocol vs 2 new commercial reagents purported to increase transduction rate (Transdux reagent, from System Biosciences and MACSDuctin, from Miltenyi Biotec). Two tumors were tested using the manufacturers' suggested protocols.

Results:

Regardless of the protocol employed, only extremely rare primary human cells (estimated < 1/1000 cells) express the lentivirus construct. Our existing protocol was subjectively superior to the others tested.

*Task 4* Attempt to address lack of human PCC/PGL cell proliferative response to hypoxic culture

Although we framed this goal in terms of hypoxic cultures, it soon became clear that this was not the appropriate perspective because there is no proliferation under any culture conditions. This is the case even for tumors with *SDHB* or *VHL* mutations, which are characterized by intrinsically activated hypoxic signaling pathways (Dahia PL et al, PLoS Genet. 2005;1:e8). We therefore reframed the goal in order to address the broader problem and reformulated the tasks in order to begin testing new concepts.

We tested all tumors in Table 2 for proliferation under routine culture conditions as described in the first funding period. We focused on tumors with *SDHB* mutations for two reasons. The first is their intrinsic hypoxic signaling profile, which makes a hypoxic culture system redundant. The second is that *SDHB*-mutated tumors are most likely to be malignant and therefore pose the most urgent need for cell lines to be used for pre-clinical drug testing. For each tumor, dissociated cells were plated in RPMI 1640 medium with 15% fetal bovine serum. Proliferation was assessed by labeling with bromodeoxyuridine (BrdU) as a marker for DNA replication as we have previously reported (Tischler AS et al, The journal of histochemistry and cytochemistry : official journal of the Histochemistry Society. 1992;40:1043-5). BrdU was added immediately upon plating and cultures were maintained one week prior to fixation. Double immunohistochemical staining was performed for BrdU and tyrosine hydroxylase to discriminate tumor cells from proliferating fibroblasts and other cell types in primary cultures. Some cultures were studied at two or more time points.

Results:

There was no BrdU labeling of tumor cells under any conditions, while labeling of fibroblasts and other irrelevant cell types was readily detected. It was especially informative that the tumor highlighted in the Table, which grew rapidly *in vivo*, was the same as all of the other tumors in showing absolutely no labeled tumor cells, even though

unlabeled cells have survived for > 7 months. This suggests that culture conditions either lack a required mitogenic signal (a missing "on" switch) or provide signals that suppress mitogenesis (an "off" switch).

Task 5 We reviewed > 20 years of our laboratory notes describing testing of human PCC/PGL for responses to a variety of small molecules that we had previously found to be mitogenic for rodent chromaffin cells, including several activators of adenylate cyclase/protein kinase A (principally cholera toxin and forskolin), and phorbol esters that activate protein kinase C (Tischler AS et al, Neurosci Lett. 1994;168:181-4).

Results

- We confirmed that we have already tested tumors representing a variety of genotypes including *SDH*x and *VHL* mutations and found no response to activators of PKA or PKC. We concluded that these agents are therefore unlikely to be effective as single agents under either normoxic or hypoxic conditions and would be more appropriately incorporated into combinatorial protocols to provide the missing "on" switch (Task 3).

Task 6 It is now apparent that expression of markers associated with embryonic stem cells often drives neoplastic progression, and that these markers can in some tumors be acquired in response to external signals (Martinez-Outschoorn UE et al, Cell Cycle. 2011;10:1271-86). We therefore began to systematically test protocols that reprogram "stemness". To begin this new approach we tested a protocol based on the use of a Rho kinase (ROCK) inhibitor, Y-27632, that increases proliferation of keratinocytes and a variety of normal stem cells (Chapman S et al, The American journal of pathology. 2012;180:443-5). This method employs the ROCK inhibitor, a feeder cell layer of irradiated mouse fibroblasts, and a medium containing several small molecule growth factors and a low concentration of serum (Chapman S et al, The Journal of clinical investigation. 2010;120:2619-26). We extensively tested the separate and combined components of this protocol using cells from 2 human tumors as diagrammed in Tables 3A-C. Both tumors were also routinely cultured in RPMI 1640 medium with 15% fetal bovine serum and tested according to our standard protocol described in Task 1, where they showed no tumor cell proliferation.

Results

- There was no significant proliferation using this protocol as reported or with any modifications tested

Table 3A

Human PGL Cells seeded on $2.5x10^4$ J2 3T3 feeder cells in 2 different media

* indicates complete protocol as reported (Chapman S et al, The Journal of clinical investigation. 2010;120:2619-26) except for cholera toxin, which was toxic to this tumor under these conditions

| Medium | Y27632 (uM) | Hydrocortisone (ug/mL) | Insulin (ug/mL) | rhEGF (ng/mL) | Adenine (ug/mL) | Result (BrdU+) |
|---|---|---|---|---|---|---|
| F3(F12:DMEM 3:1, FBS 5%) | 10 | 0.4 | 5 | 10 | 24 | |
| + | | + | + | + | + | 0 |
| + * | + | + | + | + | + | 0 |
| + | + | + | + | + | | 0 |
| + | + | + | + | | | 0 |
| + | + | + | | | | 0 |
| + | + | | | | | 0 |
| + | | + | | | | 0 |
| + | | | | | | 0 |
| Medium | Y27632 (uM) | Hydrocortisone (ug/mL) | Insulin (ug/mL) | rhEGF (ng/mL) | Adenine (ug/mL) | Result (BrdU+) |
| McCoy's FBS (15%) | 10 | 0.4 | 5 | 10 | 24 | |
| + | | + | + | + | + | 0 |
| + | + | + | + | + | + | 0 |
| + | + | + | + | + | | 0 |
| + | + | + | + | | | 0 |
| + | + | + | | | | 0 |
| + | + | | | | | 0 |
| + | | + | | | | 0 |
| + | | | | | | 0 |

Table 3B: Human PGL Cells plated immediately in 2 different media, no feeder cells

| Medium | Y27632 (uM) | Hydrocortisone (ug/mL) | Insulin (ug/mL) | rhEGF (ng/mL) | Adenine (ug/mL) | Cholera Toxin (ng/mL) | Result (BrdU+) |
|---|---|---|---|---|---|---|---|
| F3(F12:DMEM 3:1, FBS 5%) | 10 | 0.4 | 5 | 10 | 24 | 8.4 | |
| + | + | + | + | + | + | + | 0 |
| + | + | + | + | + | + | | 0 |
| + | + | + | + | + | | | 0 |
| + | + | + | + | | | | 1 cell |
| + | + | + | | | | | 1 cell |
| + | + | | | | | | 0 |
| Medium | Y27632 (uM) | Hydrocortisone (ug/mL) | Insulin (ug/mL) | rhEGF (ng/mL) | Adenine (ug/mL) | Cholera Toxin (ng/mL) | Result (BrdU+) |
| McCoy's FBS (15%) | 10 | 0.4 | 5 | 10 | 24 | 8.4 | |
| + | + | + | + | + | + | + | 0 |
| + | + | + | + | + | + | | 0 |
| + | + | + | + | + | | | 0 |
| + | + | + | + | | | | 0 |
| + | + | + | | | | | 0 |
| + | + | | | | | | 0 |

Table 3C Cultures started in high serum medium (Mc Coy's 15%FBS) then switched to indicated conditions at 48 hours, no feeder layers

| Medium | Y27632 (uM) | Hydrocortisone (ug/mL) | rhEGF (ng/mL) | Insulin (ug/mL) | Adenine (ug/mL) | PMA (nM) | Cholera Toxin (ng/mL) | Result (BrdU +) |
|---|---|---|---|---|---|---|---|---|
| F3(F12:DMEM 3:1, FBS 5%) | 10 | 0.4 | 10 | 5 | 24 | 50 | 20 | |
| + | + | + | + | + | + | | | 0 |
| + | + | + | + | + | + | + (48 hrs) | | 0 |

**Year 3. (15 August 2013- 14 September 2014).**

*Specific Aim 1 Development of drug testing paradigms using MPC cell cultures*

By year 3 the proposed testing of drugs on MPC cell cultures was largely complete and a paper was published reporting the results (Powers JF, et al. PloS one. 2014;9(2):e87807. PMID: 24516563).
(see attached References).

Key findings in the published paper are:

- Enhanced cytotoxic efficacy is achieved by combining 5-azacytidine with TOP1 inhibitors in dividing cell populations. For optimal timing, the two drugs are initially administered together and 5-azacytidine is then removed.

- 5-azacytidine is not effective against non-dividing cells

An additional finding in the course of these studies was the discovery that 5-azacytidine demethylates the cytomegalovirus promoter and causes increased luminescence of cells transduced with reporter constructs expressing luciferase driven by the cytomegalovirus promoter. This was an important unexpected finding that dictates caution in the interpretation of bioluminescence imaging studies. However, it precluded further use of our CMV-driven bioluminescent MPC cells for in vivo imaging studies proposed in Specific Aim 3.

Specific aim 2. Validation of drug testing paradigms in primary human cell cultures

Using human cells in primary cultures, we followed up and continued cell culture testing of promising non-toxic or minimally toxic drugs identified in Year 2 as single agents or adjuncts to conventional chemotherapy drugs including TOP1 inhibitors. These included lithium and caffeine, which had been particularly promising in studies using MPC cells. Three agents were tested- lithium, caffeine and dichloroacetic acid (Lin G et al, British journal of cancer. 2014;111(2):375-85 PMID: 24892448, Xuan Y et al, Experimental cell research. 2014;321(2):219-30 PMID: 24342832.), singly and in combination with SN-38, the active metabolite of the TOP1 inhibitor irinotecan, in cell cultures of human pheochromocytomas.

Results (Figures 1-3)

Lithium, caffeine or dichloroacetic acid individually showed no toxicity against human pheochromocytoma cells and did not enhance the cytotoxic effect of SN38.

Figure 1
Cytotoxicity of 0.1ug/mL SN-38 against disassociated human pheochromocytoma cells was tested in combination with [5mM] lithium chloride (LiCl) by XTT assay. Cells were cultured in 96 well plate in complete medium and either left untreated (NA) or treated for 1 week with a feeding with additions on day 4. Absorbance is proportional to cell survival. Bars indicate

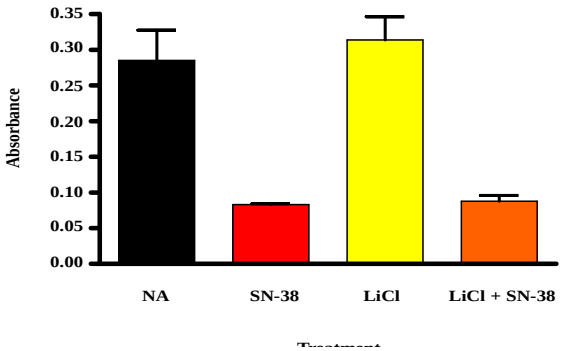


Figure 2
Cytotoxicity of 0.1ug/mL SN-38 against disassociated human pheochromocytoma cells was tested in combination with either [50 uM] or [100 uM] caffeine (Caf) by XTT assay. Cells were cultured in 96 well plate in complete medium and either left untreated (NA) or treated for 1 week with a feeding with additions on day 4. Absorbance is proportional to cell survival. Bars indicate mean +/- SEM of quadruplicate wells.

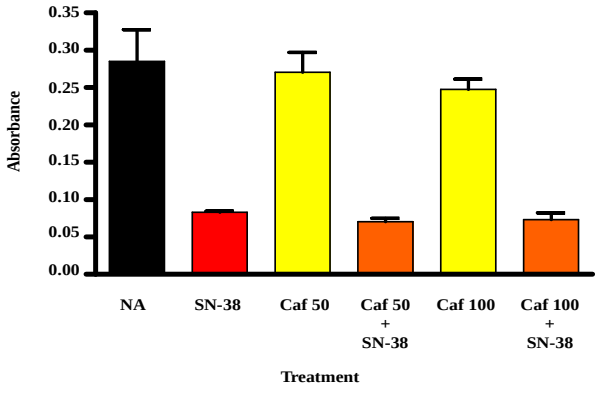

Figure 3
Dose response curve testing the cytotoxicity of dichloroacetic acid against disassociated human pheochromocytoma cells in XTT assay. Cells were cultured in 96 well plate in complete medium and either left untreated (NA), treated with vehicle (Cntrl) or treated with indicated doses of dichloroactic acid for 1 week with a feeding with additions on day 4. Absorbance is proportional to cell survival. Bars indicate mean +/- SEM of quadruplicate wells.

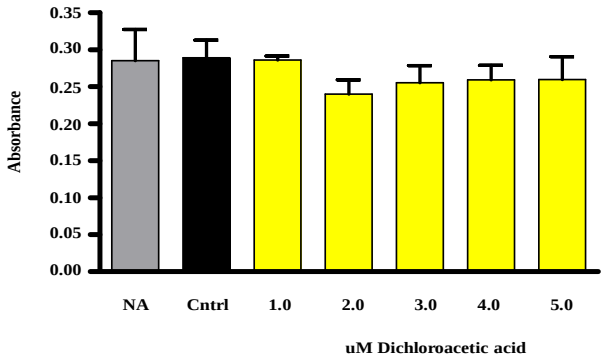


Specific Aim 3 In Vivo testing of drug administration paradigms using MPC cells as a model

In year 2 we had tested Gamitrinib in vivo against cultured mouse pheochromocytoma MPC cells in nude mice using one of two protocols published by our collaborators who developed the drug. That protocol, which entailed a cycle of 3 days on followed by 2 days off treatment for 21 days (Kang BH, et al, J Clin Invest 2009;119(3):454-64. PMID: 19229106;) was ineffective. This time we tested a regimen of continuous administration described in the second protocol, which was found with other tumors to be more effective while still causing minimal toxicity (Kang BH, et al British Journal of Cancer. 2011;104(4):629-34. PMID: 21285984)

Task 1. Repeat testing toxicity of Gamitrinib against MPC GL-9 cells in nude mice.

We first propagated sufficient cells to inject 20 mice, 2 x $10^6$ cells/mouse (~3 weeks), then waited for discrete tumor masses to form (~4 weeks). Gamitrinib was then administered daily (10mg/kg i.p. dissolved in 20% cremophor/80% saline) and interval caliper measurements of the tumors were performed. 1c.Tumor tissue was harvested for histologic sections from control and treated animals at termination of the experiment.

Results (Figure 4)

Gamitrinib suppressed tumor growth for 7 days but then ceased to be effective. Tumor growth in treated animals accelerated and caught up with growth in untreated controls. There were no histological differences between treated and control groups.

Figure 4. Sequential caliper measurements of subcutaneous MPC GL-9 cells in nude mice before and after start of Gamitrinib treatment (on day 0). The initial anti-tumor effect of the drug disappears by day 14, when tumor size is the same in treated and control animals that received the cremophor/saline vehicle only. n=10 mice per group.

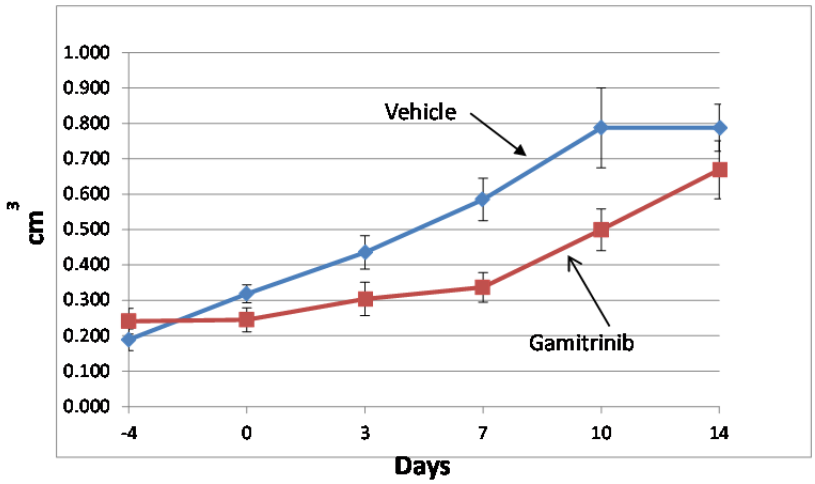


Specific Aim 4 Novel attempts to develop cell lines of human pheochromocytoma for cell culture and xenografts

At the end of the 2012-2013 funding period a number of nude mice that had received xenografts of human PCC or PGL were still alive with no evidence of tumor takes. These mice died or were euthanized by the end of the 2013-2014 period, still with no takes. Early during 2013-2014 funding period a new strain of immunodeficient mice known as Nod SCID Gamma (NSG) became available at our institution. These mice lack B-cells, T-cells and NK-cells, and are generally considered to be superior to nude mice for xenografting. Further, they accept subcutaneous grafts, which are easily observed and measured, as readily as grafts to other locations. We therefore switched to this new strain for our experiments.

Task 1. Necropsies were performed on thirteen mice of several strains (nude, SCID or NOD-SCID) that had been grafted with human PCC/PGL and were alive at the end of the 2012-2013 funding period and either died or were euthanized during the 2013-2014 period.

Results
No tumor takes, regardless of mouse strain or tumor genotype

Task 2. In order to compare NSG mice to the strains previously tested, we thawed stored aliquots of viable frozen primary human pheochromocytoma/paragangliomas that had previously been tested and injected them subcutaneously into NSG mice. Three newly acquistioned tumors were similarly injected into NSG mice, as summarized in Table 1. Mice were monitored for development of masses at the injection site.

Results (Table 1)

No gross tumor takes. However, histologic sections of the implantation sites showed vascularization of the Matrigel matrix in which the cells were injected and long-tern survival of dormant tumor cells. (Figure 1). This was an important finding because it is the only successful demonstration of human PCC/PGL xenografting and it establishes the NSG mouse as a model for future studies.

**Table 1**

| Age | Sex | Tumor Type | Gene | Mouse | # | Route | Result |
|---|---|---|---|---|---|---|---|
| 37 | F | PGL | Not Tested | NSG | 1 | SC-flank (coated with matrigel) | No gross tumor take |
| 50 | F | PCC | Not Tested | NSG | 2 | SC-flank (coated with matrigel) | No gross tumor take |
| 13 | F | PGL | SDHB | NSG | 1 | SC-flank (coated with matrigel) | No gross tumor take |
| 54 | M | PGL | SDHB+ | NSG | 1 | SC-flank (coated with matrigel) | No gross tumor take |
| 41 | M | PGL | Not Tested | NSG | 1 | SC-flank (coated with matrigel) | No gross tumor take |
| 52 | M | PGL | SDHB | NSG | 1 | SC-flank (coated with matrigel) | No gross tumor take |
| 45 | M | PGL | SDHB | NSG | 1 | SC-flank (coated with matrigel) | No gross tumor take |
| 61 | F | PGL | Not Tested | NSG | 1 | SC-flank (coated with matrigel) | No gross tumor take |
| 29 | F | PCC | SDHB | NSG | 1 | SC-flank (coated with matrigel) | No gross tumor take |
| 9 | F | PGL | SDHB | NSG | 1 | SC-flank (coated with matrigel) | No gross tumor take |
| 46 | F | PCC | SDHB | NSG | 1 | SC-flank (coated with matrigel) | No gross tumor take |
| 53 | M | PGL | SDHB | NSG | 1 | SC-flank (coated with matrigel) | No gross tumor take |
| 27 | M | PGL | SDHB+ | NSG | 1 | SC-flank (coated with matrigel) | No gross tumor take |
| 55 | M | PGL-liver met | SDHB | NSG | 1 | SC-flank (coated with matrigel) | No gross tumor take |

Figure 1. Histologic section of the subcutaneous implantation site of *SDHB*-mutated PGL cells in a NSG mouse 10 months after implantation. The image on left shows extensive vascularization of the Matrigel matrix in which the cells were injected, with only sparse scattered aggregates of tumor cells (arrows), highlighted by immunohistochemical stain for tyrosine hydroxylase on right.

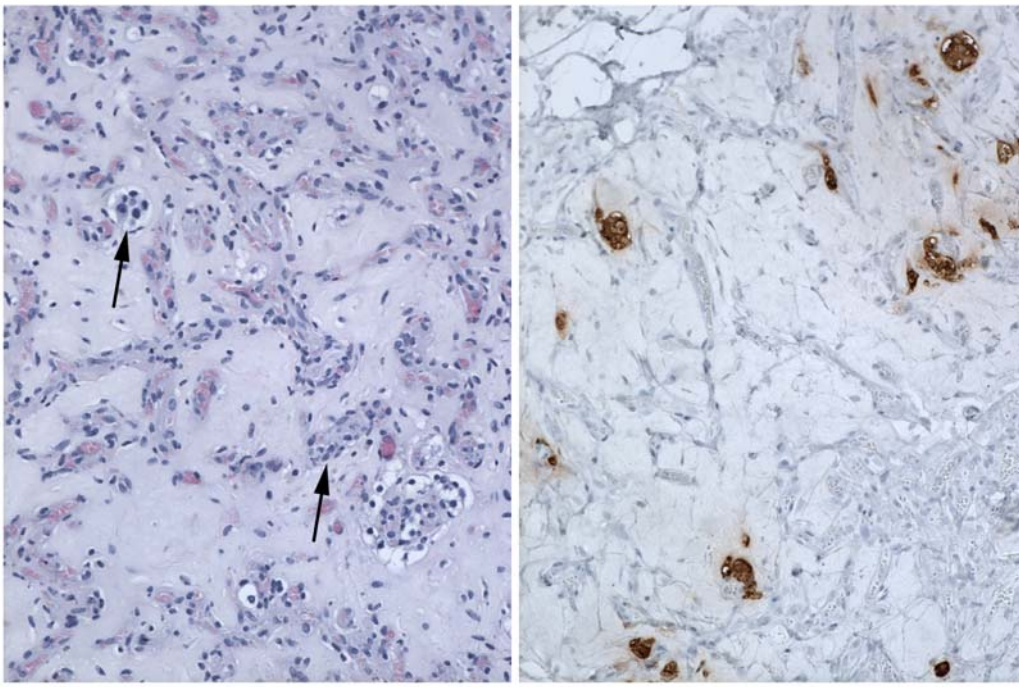

*Task 3.* We continued and expanded attempts to establish human PCC/PGL cell lines from primary cultures.

1. Cell cultures were plated from each thawed tumor and each newly acquired tumor that was grafted into mice as listed in Table 1. Dissociated cells were plated routinely in RPMI 1640 medium with 15% fetal bovine serum, which we have previously found optimal for survival of almost all human PCC/PGL. Cultures were kept for up to 1 year or until there were no surviving tumor cells. Cultures were tested for tumor cell proliferation at week 1 or 2 and one year by double immunocytochemical staining for BrdU incorporation and tyrosine hydroxylase (TH) expression as we previously described (Tischler AS et al, J Histochem Cytochem. 1992;40(7):1043-5).Staining TH discriminates tumor cells from fibroblasts and other cell types.

Results (Figure 1)

No BrdU incorporation into tumor cells at one week or one year. Proliferation of tumor cells ceases immediately on plating, despite long term cell survival. (Fig 1)

Figure 1

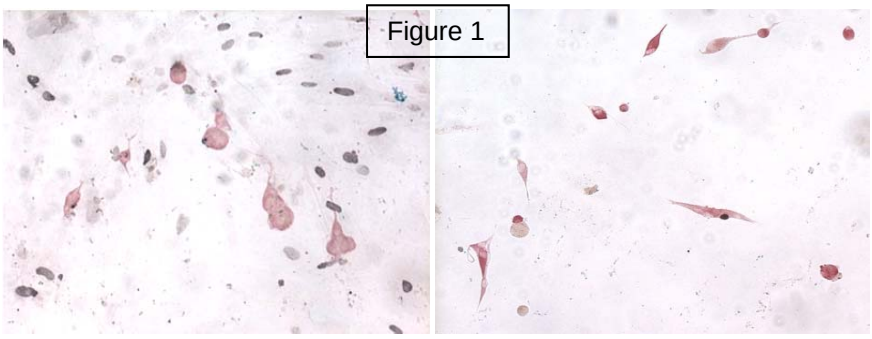

Human PCC culture, 14 days. BrdU-labling is present in TH-negative fibroblasts but not in TH-positive tumor cells (pink cytoplasm)

Human PCC culture, 1 year, trypsinized and replated. Fibroblasts, have become senescent. Still no labeling in tumor cells.

2. Cultures of representative tumors were tested with BrdU labeling and TH staining as above for proliferative responses to peptide growth factors and small molecules that we previously showed to be mitogenic for normal rat adrenal medullary cells, which are the normal counterpart of pheochromocytoma (Tischler AS et al, Neurosci Lett. 1994;168(1-2):181-4). Agents tested and results with four tumors representing different locations and genotypes are shown in Table 2.

Results (Table 2)

No proliferation of tumor cells in response to any mitogen tested

Table 2. BrdU-labeled TH positive cells at 1 week in cultures with the indicated putative mitogens

| Tumor type& mutated gene | No Add | NGF 50 ng/mL | bFGF 20 ng/mL | Forskolin 5 μM | PMA 50 nM |
|---|---|---|---|---|---|
| PGL-*SDHC* | 0 | 0 | 0 | 0 | 0 |
| PCC-*NF1* | 0 | 0 | 0 | 0 | 0 |
| PCC-*RET* (MEN2A) | 0 | 0 | 0 | 0 | 0 |
| PGL-CB-Not tested | 0 | 0 | 0 | 0 | 0 |

CB= carotid body

*Task 4*

We tested novel approaches to maintaining proliferation of PCC/PGL cells using protocols that were developed for maintaining stemness of normal neural stem cells, based the presence of recombinant leukemia inhibitory (hrLIF) plus several other growth factors. We tested 2 protocols (Zhang Het al, Neuroscience research. 2005;51(2):157-65. PMID: 15681033, Walasek MA et al, Blood. 2012; 119(13):3050-9. PMID: 22327222). The studies were performed using frozen freshly dissociated viable cells from three tumors including the last metastatic tumor in Table 2 because that tumor contained an unusually high proportion of proliferating cells *in vivo*, was particularly likely to respond to this approach. Proliferation was assessed as in Tasks 1 and 2.
Results Tables (3 and 4):

No proliferation of tumor cells under any condition tested

Table 3. BrdU-labelled TH positive cells at 1 week in cultures with the indicated putative mitogens +/- the histone deacetylase inhibitor valproic acid (VPA) or leukemia inhibiting factor (LIF), which are reported to maintain "stemness". The combination of VPA and Li prevents terminal stem cell differentiation

| | No Add | Forskolin 5μM | PMA 50nM | bFGF 20ng/mL | rhNGF 50ng/mL | rhLIF 10ng/mL |
|---|---|---|---|---|---|---|
| No Add | 0 | 0 | 0 | 0 | 0 | 0 |
| VPA 1mM | 0 | 0 | 0 | 0 | 0 | 0 |
| VPA 1mM + LiCl 5mM | 0 | 0 | 0 | 0 | 0 | 0 |

Table 4. BrdU-labelled TH positive cells at 1 week in representative cultures under conditions used to culture neural stem cells.

| Additions to Basic medium * | 10% FBS + 1mM Hydrocortisone | 1% BSA + 1mM Hydrocortisone |
|---|---|---|
| None | 0 | 0 |
| BME | 0 | 0 |
| LIF 1000 IU/mL | 0 | 0 |
| BMP4 10 ng/mL | 0 | 0 |
| LIF + BMP4 | 0 | 0 |
| N2 supplement | 0 | 0 |
| N2 + LIF | 0 | 0 |
| N2 + BMP4 | 0 | 0 |
| N2 + LIF +BMP4 | 0 | 0 |
| N2 + LIF + Insulin +bFGF +EGF | 0 | 0 |

* Basic Medium= DMEM:F12 (1:1), 0.3g/100 mL D-glucose, 2 mM glutamine, 3 mM sodium bicarbonate, 5ug/mL heparin; BME =beta mercaptoethanol; BMP = bone morphogenetic protein; N2 is a commercial medium supplement for culturing neural cells. FBS= fetal bovine serum; BSA = bovine serum albumen

*Task 5*

In order to confirm that human pheochromocytoma cells are actually able to respond to LIF, we extracted and electrophoretically resolved proteins from cultures stimulated with LIF and probed immunoblots for phosphorylation of STAT-3, a downstream readout for activated LIF signaling (Dowell KG, et al. Stem Cells. 2014;32(5):1161-72. PMID: 24307629).

Results (Figure 2).

LIF activates STAT-3 signaling in human pheochromocytoma cells, despite the absence of a proliferative response.

Fig.2. Representative assay showing LIF causes phosphorylation of STAT3 in human PCC cells without altering total STAT3 levels

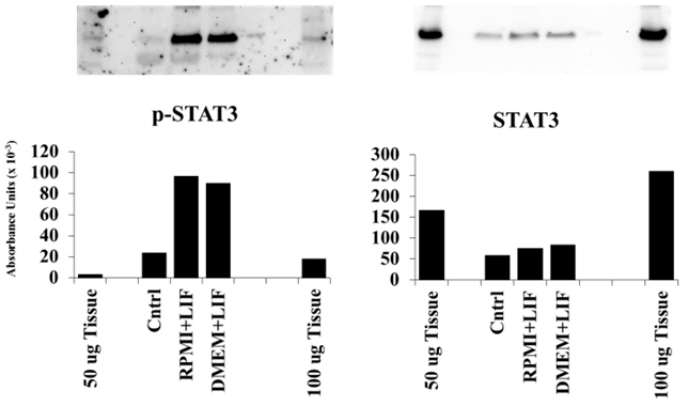


Task 6

We tested a novel approach to maintaining proliferation of PCC/PGL cells using protocols developed for maintaining stemness of normal neural stem cells based on the use of a low concentration of the HDAC inhibitor trichostatin A (Lee JH et al, Genesis. 2004;38(1):32-8 PMID: 14755802, Milhem M et al, Blood. 2004;103(11):4102-10 PMID: 14976039), LIF or small molecule mitogens. The experiments were performed as for Task 3.

Results (Tables 5 and 6)

No proliferation of tumor cells under any condition tested

Table 5. BrdU-labelled TH positive cells at 1 week in representative human PCC cultures with the indicated putative mitogens +/- the histone deacetylase inhibitor trichostatin A or leukemia inhibiting factor (LIF), which are reported to maintain "stemness". Hydrocortisone is a survival factor,

| Trichostatin A | LIF 1000 IU/mL | Hydrocortisone 1 μM | LIF 1000 IU/mL + Hydrocortisone 1 μM |
|---|---|---|---|
| 0 | 0 | 0 | 0 |
| 1 nM | 0 | 0 | 0 |
| 10 nM | 0 | 0 | 0 |
| 100 nM | 0 | 0 | 0 |

Table 6. BrdU-labelled TH positive cells at 1 week in representative human PCC cultures with the indicated putative mitogens +/- the histone deacetylase inhibitor trichostatin A (TSA), which are reported to maintain "stemness"

| | No Add | Forskolin 5μM | PMA 50nM | bFGF 20ng/mL | rhNGF 50ng/mL | rhLIF 10ng/mL |
|---|---|---|---|---|---|---|
| No Add | 0 | 0 | 0 | 0 | 0 | 0 |
| TSA 1nM | 0 | 0 | 0 | 0 | 0 | 0 |

*Task 7* We tested a novel approach to forcing growth-arrested PCC/PGL cells to resume proliferation by introducing cyclinD1 + constitutively active CDK4 as described by Kendall et al (12). This approach has been successful with normal somatic human cells but had never been attempted with growth-arrested tumor cells.

Results (Fig 3)
We initially attempted to transduce cultured tumor cells with a cyclinD1 + CDK4R24C construct cloned into a lentivirus vector by our collaborator at Tufts University School of Medicine, Prof. Brent Cochran. However, the construct did not successfully introduce both inserts. We therefore attempted to achieve the same objective using two separate lentivirus constructs. This was not successful because low infectivity of non-dividing PCC/PGL cells prevented us from obtaining double infections. Fibroblasts in the same cultures apparently were doubly infected and showed increased proliferation compared to fibroblasts in control cultures.

Fig.3. Human pheochromocytoma cells transduced with cdk4 and green fluorescent protein tag. The GFP shows that only occasional cells have been successfully transduced

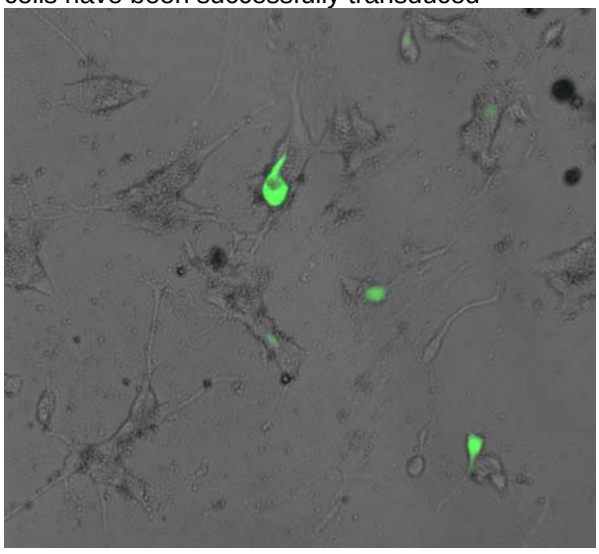

**2. Key Research Accomplishments During the Third Year (15 August 2013-14 September 2014).**

- Completed the major experiments proposed in our original SOW showing cooperative interactions between topoisomerase 1 inhibitors and 5-azacytidine and published the results in a significant journal.

- Completed testing of Gamitrinib, a new type of drug that we previously found to be highly effective in cultures of both human and mouse PCC/PGL cells, against mouse pheochromocytoma xenografts in nude mice. The results were an initial suppression of tumor growth followed by loss of anti-tumor effect

- Showed that several drugs (5-azacytidine, lithium and caffeine) that supplement topoisomerase-1inhibitors in targeting mouse pheochromocytoma cells are ineffective against non-dividing human PCC/PGL cells .

- Tested a new strain of immunodeficient mice called NSG for grafting human PCC/PGL cells and concluded that these mice, as with previously tested strains, are unlikely to be effective in establishing human PCC/PGL xenografts or cell lines.

- Tested novel approaches for directly deriving human PCC/PGL cell lines from primary cultures using protocols designed to maintain or induce stem cell properties in the cultured tumor cells and concluded that these are also unlikely to be effective in establishing cell lines

**Year 4 (15 August 2014- 14 September 2015)**

Overview

The final period was a no-cost one year extension for which we had very limited residual funds. We focused exclusively on testing novel approaches to establish human PCC/PGL cell lines because all previous attempts in Years 1-3 had failed. These studies were performed in collaboration with Prof. Brent Cochran at Tufts University School of Medicine.

*Task1*. Continue attempts begun in Project Year 3 to test transduction with cyclinD1 + CDK4R24C as a means of driving tumor cell proliferation

Cultures were plated as previously. We tested one additional tumor with a higher multiplicity of infection (m.o.i.) than previously employed (m.o.i. 10 vs 3) and with a double cycle of infection with existing separate cyclinD1 and CDK4R24C lentivirus

constructs as a way to increase infection rate. Cultures were maintained for up to 3 months.

Results

No proliferation was detected, and cell survival was decreased.

*Task2*. We conducted preliminary tests for possible metabolomic differences between human PCC/PGL tumor tissue and primary cultures from the same tumors that could account for proliferation arrest in the cultures. Soluble metabolites were extracted from representative tumor tissue and corresponding cell cultures and metabolite profiles were analyzed as described by Dettmer et al. (Analytical and Bioanalytical Chemistry. 2011;399(3):1127-39. PMID: 21125262) These studies were performed on three tumors, two with SDH mutations and one sporadic (Figure 1).

Results

As anticipated, succinate content was high in SDH-mutated tumor tissue and almost undetectable in the sporadic tumor. Interestingly, succinate levels declined markedly in cultured cells (Figure 1)..

Because succinate is believed to be a driver of tumorigenesis (Baysal & Maher. *Endocr Relat Cancer* 2015; **22** T71-82, PMID: 26113606), we followed up with two independent experiments testing for proliferation in freshly plated cultures of the same tumors supplemented with 1-20 mM sodium succinate or 1-10 mM diethyl succinate. Proliferation was assessed by BrdU labeling and double immunocytochemical staining for BrdU and tyrosine hydroxylase.

No proliferation was detected.

Figure 1. Altered concentrations of succinate in cultured cells versus tumor tissue. (Tumor 1, *SDHC* mutation; Tumor 2, sporadic; Tumor 3, *SDHB* mutation)

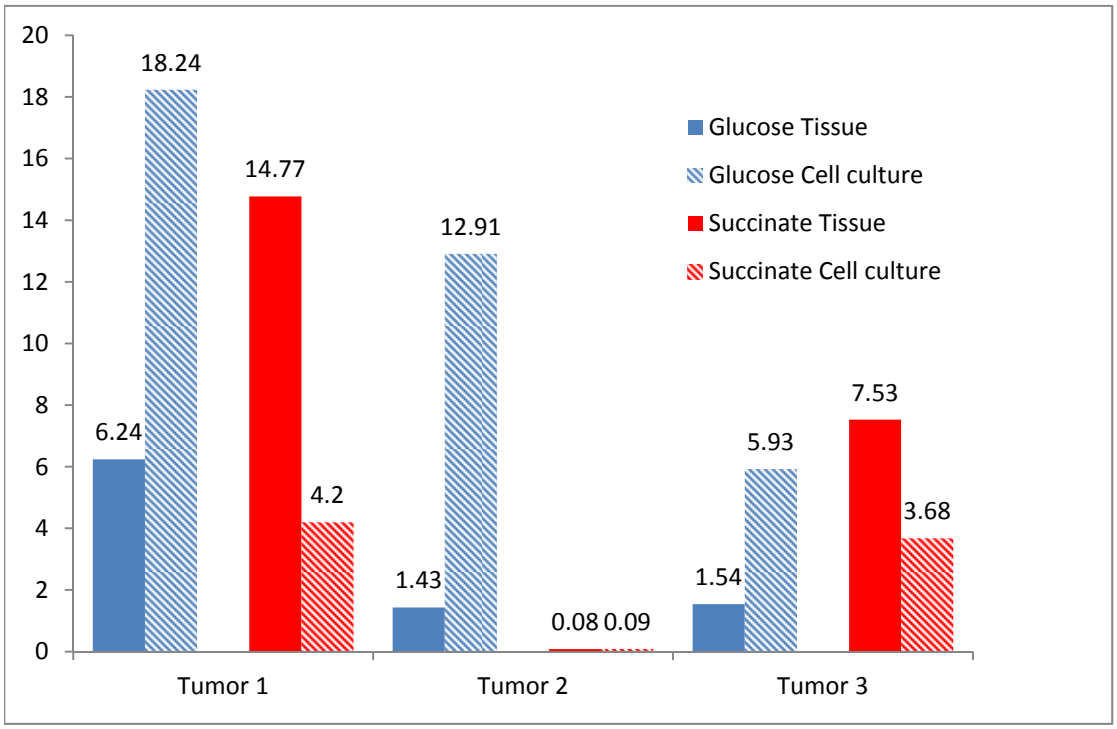


*Task 3* We conducted a preliminary test of a novel high-throughput method attempting to establish tumor stem cell lines by selective gene knockdown

Primary cultures of representative human PCC/PGL were transduced at low multiplicity of infection (m.o.i.) with commercially available modular libraries delivering sh-RNA to knock down expression of > 10,000 individual genes that could affect proliferation, followed by positive selection of proliferating clones (RNAi Screening with Pooled Lentiviral shRNA Libraries, A. Chenchik, Cellecta, Inc, www.cellecta.com). These studies were performed with cultured cells from 13 tumors. Each experiment used two separate library modules (Modules 2 and 3) targeting different signaling pathways. Cultures were maintained for 28 days after transduction. To test for tumor cell proliferation cultures were pulsed with BrdU for the final week to test for proliferation, followed by double immunocytochemical staining for BrdU and tyrosine hydroxylase.

Results
No proliferation of tumor cells was detected.

*Task 4.* Conduct preliminary test of transduction with a pathway-activating library as a means of driving tumor cell proliferation (Martz et al, Sci Signal. 2014;7(357): PMID 25538079).

Primary cultures of representative human PCC/PGL were transduced at low multiplicity of infection (m.o.i.) with a Lentivirus library containing activating components of 17 signaling pathways (Martz et al, Sci Signal. 2014;7(357): PMID 25538079). Proliferation was assessed by BrdU labeling and double immunocytochemical staining for BrdU and tyrosine hydroxylase. The library was provided to Dr Cochran by Dr Kris C. Wood.

Results

Studies were performed with cells from two tumors. In one of these, small numbers of BrdU-labeled cell doublets that we had never previously observed appeared and peaked during week 3-4 post-transduction (Figure 3). However, labeling for longer periods than one week did not demonstrate further doubling. We hypothesize that tumor stem cells underwent a final division and terminal differentiation

Figure 3. Primary human pheochromocytoma cell culture showing one week of cumulative BrdU labeling between weeks 3-4 post-transduction. Arrows indicate clusters of tumor cells stained for tyrosine hydroxylase (red cytoplasm) containing one to three BrdU-labeled cells (black nuclei) amidst much more numerous unlabeled cells. E indicates two endothelial cells.

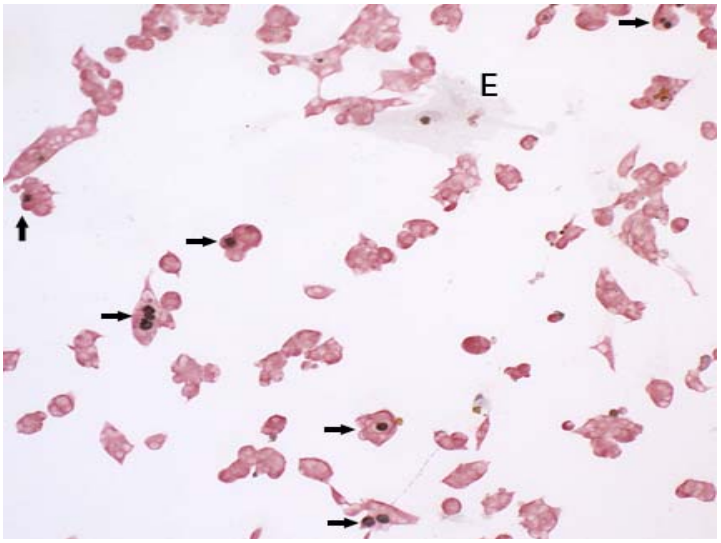


*Task 5*. We conducted a preliminary test of co-culture with glioblastoma cells, which can produce "oncometabolites" potentially mitogenic for some human PCC/PGL genotypes.

Representative PCC/PGL and glioblastoma were co-cultured in separate compartments of membrane-divided wells. Test for PCC/PGL cell replication by BrdU labeling and double immunocytochemical staining for BrdU and tyrosine hydroxylase. Studies were performed with cells from two tumors. Cells were co-cultured with U251 glioblastoma

cells in wells separated by a permeable membrane or were maintained in filtered conditioned medium from ~ 80% confluent U251 cells.

Results
No tumor cell proliferation was detected in cells maintained for up to 4 months

**Key Research Accomplishments During the Entire Funding Period (15 August 2011-14 September 2015).**

- We developed mouse pheochromocytoma cell lines that are now widely utilized in other laboratories for pre-clinical studies of pheochromocytoma paraganglioma (PCC/PGL).

- By testing chemotherapeutic agents on primary tumor cell cultures in parallel with mouse cell lines we demonstrated that chemotherapy regimens for treating metastatic pheochromocytomas and paragangliomas face a distinct obstacle in that most of the tumor cells are non-dividing at any given time, reducing their sensitivity to many types of drugs. Testing of conventional drugs with existing cell lines is likely to overestimate efficacy in many cases.

- We demonstrated that topoisomerase 1 (TOP1) inhibitors, a class of conventional drug not currently used to treat pheochromocytoma/paraganglioma, are effective against both dividing and non-dividing cells and are a potential addition to the therapeutic armamentarium. However, higher concentrations are required for the non-dividing cells, potentially entailing unacceptable systemic toxicity.

- We demonstrated cooperative interactions between TOP1 inhibitors and 5-azacytidine suggesting possible treatment strategies employing both agents in dividing cell populations that could reduce individual drug concentrations.

- We demonstrated the efficacy of a new type of drug called gamitrinib that targets mitochondrial integrity. Gamitrinib might provide an important new key to specific targeted treatment of malignant PCC/PGL because many of these tumors are caused by hereditary inactivating mutations of genes encoding subunits of the mitochondrial enzyme succinate dehydrogenase (SDH). Inactivation of SDH causes interruption of mitochondrial electron transport and accumulation of reactive oxygen species, which leads to apoptotic cell death in many cell types but not in SDH-deficient tumors. We hypothesize that the protective effect is mediated at least in part by proteins that are potential targets for gamitrinib or other mitochondriotoxic agents and we hope to pursue this line of investigation.

- We developed a protocol for implanting human PCC/PGL cells in a new strain of immunodeficient mice called NSG. Although there were no overt tumor takes, histologic sections of the implantation site show long-term cell survival consistent with clinical observations that PCC/PGL metastases often remain stable for years or decades

and then appear to undergo explosive growth. Our findings with NSG mice are important in that no previous investigation has ever demonstrated survival of human PCC or PGL in xenografts. We now have an optimized model that can be used for future studies of tumor growth, survival and drug responses by means of micro-imaging.

- We discovered that both TOP1 inhibitors and 5-azacytidine paradoxically increase luciferase expression in bioluminescence imaging, thereby masking cytotoxic drug effects. We investigated and reported the mechanism, which involves effects on the cytomegalovirus (CMV) promoter driving expression of the luciferase gene. The results are important in dictating a need for caution in the use of CMV promoter- regulated constructs for cancer-related imaging studies.

**Remaining Problem Areas**

1. Although our mouse pheochromocytoma cell lines are a valuable model for some types of pre-clinical drug testing, we have shown that this is not true in every case. This is in part attributable to the relatively rapid proliferation of the mouse cells compared to little or no proliferation of human PCC/PGL cells. Tumor genotype and still unidentified species differences probably also play a role. This problem emphasizes a continued need to develop human PCC/PGL cell lines. However, a paradox is that human lines that grow rapidly enough to provide a practical model would likely also overestimate the efficacy of most types of chemotherapy.

2. We have not been able to devise any means to make human PCC/PGL cells proliferate in culture. Even tumor cells that proliferated rapidly in patients *in vivo* immediately ceased proliferating in culture.

3. Because human PCC/PGL cells do not replicate in culture, the only way to permanently introduce genes that cause proliferatiion is by transduction using Lentivirus vectors. Although Lentivirus is known to be able to transduce non-prolifereating cells, in our experience and that of other investigators Lentivirus infection is very inefficient with PCC/PGL cells. We have so far been unable to achieve sufficient amounts of infection.

## 5. Conclusion

This project utilized cultures of mouse pheochromocytoma cell lines developed in our laboratory as the principal model for pre-clinical testing of strategies to improve the efficacy of existing chemotherapeutic drugs and for testing potential new drugs that might be used to treat patients with malignant pheochromocytoma. Findings made with the mouse model were then tested against primary cultures of human tumors and then tested *in vivo* with grafts to mice of the mouse cell lines. This approach was necessary because there are no human pheochromocytoma cell lines. However, there are important differences between the mouse pheochromocytoma cells and their human counterparts, caused in part by the fact that the human cells proliferate very slowly in vivo and

completely cease proliferating when placed into cell cultures. We identified two classes of drugs potentially effective against non-dividing human pheochromocytoma cells, i.e. topoisomerase 1 inhibitors and the mitochondriotoxic agent gamitrinib. However, there remains a pressing need for human cell lines for more extensive study. We exhaustively tested ways to propagate human pheochromocytoma cells from primary tumors in cell cultures under conventional and hypoxic conditions and using protocols directed at maintaining or inducing stem cell characteristics of tumor cells, but were unsuccessful. We also tested xenografts of human tumor cells to all currently available strains of immunosuppressed mice and developed a protocol for implanting human pheochromocytoma cells in a new strain of immunodeficient mice called NSG. Although there were no overt tumor takes in mice, histologic sections of the implantation sites show long-term cell survival consistent with clinical observations that PCC/PGL metastases often remain stable for years or decades and then appear to undergo explosive growth. Our findings with NSG mice are important in that no previous investigation has ever demonstrated survival of human PCC or PGL in xenografts. This provides a new model that can be used for future studies of tumor growth, drug responses and micro-imaging *in vivo*.

## 6. Publications, Abstracts and Presentations

Papers Supported By This Grant

Powers JF, Korgaonkar PG, Fliedner S, Giubellino A, Pacak K, Sahagian GG, **Tischler** AS. Cytocidal activities of topoisomerase 1 inhibitors and 5-azacytidine against pheochromocytoma/paraganglioma cells in primary human tumor cultures and mouse cell lines. PloS one. 2014;9(2):e87807. doi: 10.1371/journal.pone.0087807. PubMed PMID: 24516563; PMCID: 3917832.

Chae YC, Angelin A, Lisanti S, Kossenkov AV, Speicher KD, Wang H, Powers JF, **Tischler** AS, Pacak K, Fliedner S, Michalek RD, Karoly ED, Wallace DC, Languino LR, Speicher DW, Altieri DC. Landscape of the mitochondrial Hsp90 metabolome in tumours. Nature communications. 2013;4:2139. Epub 2013/07/12. doi: 10.1038/ncomms3139. PubMed PMID: 23842546; PMCID: 3732457.

Giubellino A, Woldemichael GM, Sourbier C, Lizak MJ, Powers JF, **Tischler** AS, Pacak K. Characterization of two mouse models of metastatic pheochromocytoma using bioluminescence imaging. Cancer letters. 2012;316(1):46-52. Epub 2011/12/14. doi: 10.1016/j.canlet.2011.10.019. PubMed PMID: 22154086; PMCID: 3253957.

Giubellino A, Bullova P, Nolting S, Turkova H, Powers JF, Liu Q, Guichard S, Tischler AS, Grossman AB, Pacak K. Combined inhibition of mTORC1 and mTORC2 signaling pathways is a promising therapeutic option in inhibiting pheochromocytoma tumor growth: in vitro and in vivo studies in female athymic nude mice. Endocrinology. 2013;154(2):646-55. Epub 2013/01/12. doi: 10.1210/en.2012-1854. PubMed PMID: 23307788; PMCID: 3548182.

Other Related Papers

Oudijk L, van Nederveen F, Badoual C, Tissier F, **Tischler** AS, Smid M, Gaal J, Lepoutre-Lussey C, Gimenez-Roqueplo AP, Dinjens WN, Korpershoek E, de Krijger R, Favier J. Vascular pattern analysis for the prediction of clinical behaviour in pheochromocytomas and paragangliomas. PloS one. 2015;10(3):e0121361. doi: 10.1371/journal.pone.0121361. PubMed PMID: 25794004; PMCID: PMC4368716.

Papathomas TG, Oudijk L, Persu A, Gill AJ, van Nederveen F, **Tischler** AS, Tissier F, Volante M, Matias-Guiu X, Smid M, Favier J, Rapizzi E, Libe R, Curras-Freixes M, Aydin S, Huynh T, Lichtenauer U, van Berkel A, Canu L, Domingues R, Clifton-Bligh RJ, Bialas M, Vikkula M, Baretton G, Papotti M, Nesi G, Badoual C, Pacak K, Eisenhofer G, Timmers HJ, Beuschlein F, Bertherat J, Mannelli M, Robledo M, Gimenez-Roqueplo AP, Dinjens WN, Korpershoek E, de Krijger RR. SDHB/SDHA immunohistochemistry in pheochromocytomas and paragangliomas: a multicenter interobserver variation analysis using virtual microscopy: a Multinational Study of the European Network for the Study of Adrenal Tumors (ENS@T). Modern Pathology 2015;28(6):807-21. doi: 10.1038/modpathol.2015.41. PubMed PMID: 25720320.

**Tischler** AS, deKrijger RR. 15 YEARS OF PARAGANGLIOMA: Pathology of pheochromocytoma and paraganglioma. Endocr Relat Cancer. 2015;22(4):T123-33. doi: 10.1530/ERC-15-0261. PubMed PMID: 26136457.

Yang SE, Kim C, Wang H, Tatishchev S, Wray C, Nourmand H, Zarrinpar A, **Tischler** AS. RE: Anesthetic Management for Resection of Hepatic Paraganglioma Metastatic From the Donor Organ in an Orthotopic Liver Transplant Recipient: A Case Report. Transplant Proc. 2015;47(6):2072-3. doi: 10.1016/j.transproceed.2015.07.012. PubMed PMID: 26293099.

Mete O, **Tischler** AS, de Krijger R, McNicol AM, Eisenhofer G, Pacak K, Ezzat S, Asa SL. Protocol for the examination of specimens from patients with pheochromocytomas and extra-adrenal paragangliomas. Arch Pathol Lab Med. 2014;138(2):182-8. Epub 2014/01/31. doi: 10.5858/arpa.2012-0551-OA. PubMed PMID: 24476517; PMCID: 3909881.

**Tischler** AS, Pacak K, Eisenhofer G. The adrenal medulla and extra-adrenal paraganglia: then and now. Endocr Pathol. 2014;25(1):49-58. Epub 2013/12/24. doi: 10.1007/s12022-013-9286-3. PubMed PMID: 24362581.

Pacak K, Jochmanova I, Prodanov T, Yang C, Merino MJ, Fojo T, Prchal JT, **Tischler** AS, Lechan RM, Zhuang Z. New Syndrome of Paraganglioma and Somatostatinoma Associated With Polycythemia. Journal of clinical oncology : official journal of the American Society of Clinical Oncology. 2013;31(13):1690-8. Epub 2013/03/20. doi: 10.1200/JCO.2012.47.1912. PubMed PMID: 23509317.

Papathomas TG, de Krijger RR, **Tischler** AS. Paragangliomas: Update on differential diagnostic considerations, composite tumors, and recent genetic developments. Semin Diagn Pathol. 2013;30(3):207-23. Epub 2013/10/23. doi: 10.1053/j.semdp.2013.06.006. PubMed PMID: 24144290.

Shankavaram U, Fliedner SM, Elkahloun AG, Barb JJ, Munson PJ, Huynh TT, Matro JC, Turkova H, Linehan WM, Timmers HJ, **Tischler** AS, Powers JF, de Krijger R, Baysal BE, Takacova M, Pastorekova S, Gius D, Lehnert H, Camphausen K, Pacak K. Genotype and tumor locus determine expression profile of pseudohypoxic pheochromocytomas and paragangliomas. Neoplasia. 2013;15(4):435-47. Epub 2013/04/05. PubMed PMID: 23555188; PMCID: 3612915.

**Tischler** AS, Pacak K, Eisenhofer G. The Adrenal Medulla and Extra-adrenal Paraganglia: Then and Now. Endocr Pathol. 2013. Epub 2013/12/24. doi: 10.1007/s12022-013-9286-3. PubMed PMID: 24362581.

Eisenhofer G, **Tischler** AS, de Krijger RR. Diagnostic tests and biomarkers for pheochromocytoma and extra-adrenal paraganglioma: from routine laboratory methods to disease stratification. Endocr Pathol. 2012;23(1):4-14. Epub 2011/12/20. doi: 10.1007/s12022-011-9188-1. PubMed PMID: 22180288.

Fliedner SM, Kaludercic N, Jiang XS, Hansikova H, Hajkova Z, Sladkova J, Limpuangthip A, Backlund PS, Wesley R, Martiniova L, Jochmanova I, Lendvai NK, Breza J, Yergey AL, Paolocci N, **Tischler** AS, Zeman J, Porter FD, Lehnert H, Pacak K. Warburg Effect's Manifestation in Aggressive Pheochromocytomas and Paragangliomas: Insights from a Mouse Cell Model Applied to Human Tumor Tissue. PloS one. 2012;7(7):e40949. Epub 2012/08/04. doi: 10.1371/journal.pone.0040949. PubMed PMID: 22859959; PMCID: 3409208.

Invited Presentations

**Tischler AS** Thirty-five years of pheochromocytoma models: where do we stand today? 4th International Symposium on Pheochromocytoma, Symposium on Pheochromocytoma, Kyoto, Japan September 17th - 20th, 2014

Commentary

**Tischler** AS, Favier J. Models of pheochromocytoma: what's on the horizon? Int J Endo Oncol. 2015;2(3):171–4.

Eisenhofer G, **Tischler AS**. Closing the GAPP on predicting metastases. Nat Rev Endocrinol. 2014;10:315-6. Epub 1 April. doi: 10.1038/nrendo.2014.41.

**Tischler** AS. What happens in "chromospheres"? Stem cells translational medicine. 2013;2(12):1020. Epub 2013/11/28. doi: 10.5966/sctm.2013-0009. PubMed PMID: 24282324; PMCID: 3841082.

Gimenez-Roqueplo AP, **Tischler** AS. Pheochromocytoma and Paraganglioma: progress on all fronts. Endocr Pathol. 2012;23(1):1-3. Epub 2012/01/17. doi: 10.1007/s12022-011-9190-7. PubMed PMID: 22246920.

Chapters

**Tischler AS,** Nyska A, Elmore SA. Toxic Responses of the Adrenal Medulla. In: Caplan M, Reference Module in Biomedical Sciences, Elsevier, available in late 2014.

Nosé V**, Tischler AS**. Adrenal Medullary Hyperplasia. In: Nosé V et al. Diagnostic Pathology: Familial Cancer Syndromes. Salt Lake City, UT: Amirsys Publishing, Inc.; 2014: ll-5-28.

Nosé V**, Tischler AS**. Pheochromocytoma/Paraganglioma. In: Nosé V et al. Diagnostic Pathology: Familial Cancer Syndromes. Salt Lake City, UT: Amirsys Publishing, Inc.; 2014: ll-5-40.

**7. Inventions, Patents and Licenses** None

**8. Reportable Outcomes** None

**9. Other Achievements** Not applicable

**10. References**

References are included in the text.

**11. Appendices**

Powers JF, Korgaonkar PG, Fliedner S, Giubellino A, Pacak K, Sahagian GG, **Tischler** AS. Cytocidal activities of topoisomerase 1 inhibitors and 5-azacytidine against pheochromocytoma/paraganglioma cells in primary human tumor cultures and mouse cell lines. PloS one. 2014;9(2):e87807. doi: 10.1371/journal.pone.0087807. PubMed PMID: 24516563; PMCID: 3917832.

Chae YC, Angelin A, Lisanti S, Kossenkov AV, Speicher KD, Wang H, Powers JF, **Tischler** AS, Pacak K, Fliedner S, Michalek RD, Karoly ED, Wallace DC, Languino LR, Speicher DW, Altieri DC. Landscape of the mitochondrial Hsp90 metabolome in tumours. Nature communications. 2013;4:2139. Epub 2013/07/12. doi: 10.1038/ncomms3139. PubMed PMID: 23842546; PMCID: 3732457.

Giubellino A, Woldemichael GM, Sourbier C, Lizak MJ, Powers JF, **Tischler** AS, Pacak K. Characterization of two mouse models of metastatic pheochromocytoma using

bioluminescence imaging. Cancer letters. 2012;316(1):46-52. Epub 2011/12/14. doi: 10.1016/j.canlet.2011.10.019. PubMed PMID: 22154086; PMCID: 3253957.

Giubellino A, Bullova P, Nolting S, Turkova H, Powers JF, Liu Q, Guichard S, Tischler AS, Grossman AB, Pacak K. Combined inhibition of mTORC1 and mTORC2 signaling pathways is a promising therapeutic option in inhibiting pheochromocytoma tumor growth: in vitro and in vivo studies in female athymic nude mice. Endocrinology. 2013;154(2):646-55. Epub 2013/01/12. doi: 10.1210/en.2012-1854. PubMed PMID: 23307788; PMCID: 3548182.

OPEN ACCESS Freely available online

PLOS ONE

# Cytocidal Activities of Topoisomerase 1 Inhibitors and 5-Azacytidine against Pheochromocytoma/Paraganglioma Cells in Primary Human Tumor Cultures and Mouse Cell Lines

**James F. Powers[1]*, Parimal G. Korgaonkar[2], Stephanie Fliedner[3,4], Alessio Giubellino[3], Karel Pacak, G. Gary Sahagian, Arthur S. Tischler[1]**

**1** Department of Pathology, Tufts Medical Center, Boston, Massachusetts, United States of America, **2** Small Animal Imaging/Preclinical Testing Facility, Tufts University School of Medicine, Boston, Massachusetts, United States of America, **3** Program in Reproductive and Adult Endocrinology, Eunice Kennedy Shriver National Institute of Child Health and Human Development, National Institutes of Health, Bethesda, Maryland, United States of America, **4** 1st Department of Medicine, University Medical Center Schleswig-Holstein Lübeck, Lübeck, Germany

## Abstract

There is currently no effective treatment for metastatic pheochromocytomas and paragangliomas. A deficiency in current chemotherapy regimens is that the metastases usually grow very slowly. Drugs that target dividing tumor cells have therefore had limited success. To improve treatment, new strategies and valid experimental models are required for pre-clinical testing. However, development of models has itself been hampered by the absence of human pheochromocytoma/paraganglioma cell lines for cultures or xenografts. Topoisomerase 1 (TOP1) inhibitors are drugs that interfere with mechanisms that maintain DNA integrity during transcription in both quiescent and dividing cells. We used primary cultures of representative human tumors to establish the cytotoxicity of camptothecin, a prototypical TOP1 inhibitor, against non-dividing pheochromocytoma/paraganglioma cells, and then employed a mouse pheochromocytoma model (MPC) to show that efficacy of low concentrations of camptothecin and other TOP1 inhibitors is increased by intermittent coadministration of sub-toxic concentrations of 5-azacytidine, a DNA methylation inhibitor that modulates transcription. We then tested the same drugs against a clonal MPC derivative that expresses CMV reporter-driven luciferase and GFP, intended for in vivo drug testing. Unexpectedly, luciferase expression, bioluminescence and GFP expression were paradoxically increased by both camptothecin and SN38, the active metabolite of irinotecan, thereby masking cell death. Expression of chromogranin A, a marker for neuroendocrine secretory granules, was not increased, indicating that the drug effects on levels of luciferase and GFP are specific to the GFP-luciferase construct rather than generalized cellular responses. Our findings provide proof of principle for use of TOP1 inhibitors against pheochromocytoma/paraganglioma and suggest novel strategies for enhancing efficacy and reducing toxicity by optimizing the combination and timing of their use in conjunction with other drugs. The paradoxical effects of TOP1 inhibitors on luciferase and GFP dictate a need for caution in the use of CMV promoter-regulated constructs for cancer-related imaging studies.

**Citation:** Powers JF, Korgaonkar PG, Fliedner S, Giubellino A, Pacak K, et al. (2014) Cytocidal Activities of Topoisomerase 1 Inhibitors and 5-Azacytidine against Pheochromocytoma/Paraganglioma Cells in Primary Human Tumor Cultures and Mouse Cell Lines. PLoS ONE 9(1): e87807. doi:10.1371/journal.pone.0087807

**Editor:** Michal Hetman, University of Louisville, United States of America

**Received** August 16, 2013; **Accepted** December 30, 2013; **Published** January 31, 2014



**Funding:** JF Powers and AS Tischler were supported by grant PR100171 from the Department of Defense and by a grant from the Pheo Para Alliance (http://www.pheo-para-alliance.org/). The funders had no role in study design, data collection and analysis, decision to publish, or preparation of the manuscript.

**Competing Interests:** The authors have declared that no competing interests exist.

* E-mail: jpowers1@tuftsmedicalcenter.org

## Introduction

Pheochromocytomas (PCC) are neuroendocrine tumors that arise from chromaffin cells in the adrenal medulla. Closely related extra-adrenal tumors are arbitrarily classified by the World Health Organization as paragangliomas (PGL) [1]. Up to 30% of PCC/PGL give rise to metastases, for which there is currently no effective treatment [2]. An additional subset of these tumors is surgically unresectable. A major deficiency in current treatment strategies that they do not account for the fact that, in contrast to many other types of malignant tumors, PCC/PGL usually grow very slowly and most of the cells are quiescent at any given time. Mitotic counts and expression of cell cycle markers both in primary tumors and in their metastases are usually very low [3]. Treatments that target replicating tumor cells or tumor angiogenesis have therefore met with only limited success. Patients with metastases or inoperable tumors often die from complications of catecholamine hypersecretion, or from invasive and expansile tumor growth that occurs over many years.

The need to improve treatment of metastatic or unresectable PCC/PGL requires new strategies and a valid experimental model for pre-clinical testing of those strategies. However, development of a model has itself been hampered by failure to establish any human PCC cell lines for cell culture or xenograft studies, despite many efforts to establish them over a period of more than 35 years [4] and several initially promising reports. Factors contributing to these failures are that there are very few dividing cells even in vivo,

as shown by staining for Ki-67 or other markers [3]., and that whatever dividing cells are present immediately undergo growth arrest in culture [4]. One recent paper reports the establishment of a putative PCC progenitor line using a TERT construct [5], but the cells appear to bear minimal resemblance to PCC and are also not generally available.

Topoisomerases are enzymes that alleviate topological stresses such as supercoiling that occur when DNA strands are unwound during transcription or replication. The enzymes function by introducing transient single strand (topoisomerase 1, TOP1) or double strand (topoisomerase 2, TOP2) DNA breaks. Inhibition of topoisomerases initiates apoptotic cell death [6,7]. The prototypical TOP1 inhibitor, camptothecin, causes DNA damage both during S-phase and during transcription [8], thereby potentially activating apoptotic pathways in both dividing and non-dividing cells. Further, cytotoxicity of camptothecin on both dividing and non-dividing PCC cells was demonstrated by Greene and colleagues, who first showed in the 1990's that the drug causes apoptotic death of nerve growth factor-treated PC12 cells [9]. We therefore hypothesized that camptothecin and other TOP inhibitors might be effective chemotherapeutic agents for treatment of metastatic PCC/PGL.

Camptothecin is known to be toxic to many kinds of cancer cells, but systemic toxicity and a long time course required for its effect have prevented its general use in chemotherapy. Several camptothecin analogs currently are in use, including topotecan and irinotecan. These have been employed in combination with other agents to treat a variety of aggressive neuroendocrine carcinomas, with mostly modest results in terms of patients' survival [10,11]. However, new TOP1 and TOP2 inhibitors are under development [6,7], as is a particle-bound form of camptothecin that might have reduced toxicity and increased efficacy [12,13], and increasing numbers of publications in recent years attest to growing awareness of the potential value of camptothecin or its analogs as chemotherapeutic agents.

This *in vitro* study was undertaken in preparation for the clinical availability of new camptothecin derivatives, and had two objectives. The first was to test the effectiveness of TOP1 inhibition against pheochromocytoma cells using camptothecin to obtain proof of principle. The second. was to develop strategies for enhancing the efficacy and reducing the toxicity of TOP1 inhibitors by optimizing the combination and timing of their use in conjunction with other drugs. Because there are no human PCC/PGL cell lines, we first used primary cultures of representative human tumors to establish the cytotoxicity of camptothecin against non-replicating human PCC/PGL cells. We then used a mouse pheochromocytoma cell line (MPC) as a model to further test camptothecin and other TOP1 inhibitors in conjunction other drugs. As a prototype for complementary drugs, we used the DNA methyltransferase inhibitor, 5-azacytidine (5-aza), which we hypothesized would potentiate the effect of camptothecin because it is known to increase transcription of multiple genes by causing promoter demethylation. Combinations of existing TOP1 inhibitors with other drugs have previously been tested against other tumors in clinical or experimental settings, with mixed results. These include a strategy for staggered initiation of combined treatment with irinotecan and 5-aza-2′-deoxycytidine reported by Ishiguro et al to be highly effective against a colorectal cancer cell line *in vivo* and in cell culture [14]. Promoter demethylation in response to 5-aza has until recently been considered to be dependent on DNA replication in dividing cell populations. However, increasing evidence indicates that DNA can be demethylated in a process of dynamic remodeling that occurs in both dividing and non-dividing cells [15].

## Materials and Methods

### Ethics Statement

Studies of human tumor samples were approved by the Institutional Review Boards of the National Institutes of Health and Tufts Medical Center. Patients provided written informed consent.

### Human Tumor Cultures

Seven human PCCs/PGLs representing different genotypes and locations were enzymatically dissociated and plated in 35 mm culture dishes at a density of ~5000 cells/dish in RPMI 1640 medium with 15% fetal bovine serum. Cultures were maintained for 1–2 weeks before the start of drug testing to allow for firm attachment. During the pre-testing interval, representative dishes were pulsed for at least 5 days with 10 uM bromodeoxyuridine (BrdU), which is incorporated into the DNA of proliferating cells, then fixed and double stained for BrdU and tyrosine hydroxylase (TH), a marker of catecholamine-synthesizing ability, to discriminate tumor cells from non-neoplastic fibroblasts and other cell types in primary cultures [16]. At the start of drug testing, camptothecin (Sigma Chemical Co, St Louis, MO) and/or additional drugs were added for the time intervals and at the concentrations indicated in the figure legends. At the end of the experiments cultures were fixed and stained for TH in order to identify surviving tumor cells.

To measure drug-induced cytotoxicity, surviving TH-positive cells were counted in an area of the culture dish defined by a randomly placed 22×22 mm square coverslip.

Protocols for dissociation and culture of PCC/PGL cell cultures were as previously described for similar studies by Powers et al [17]. Cytotoxicity assays were performed without knowledge of tumor genotype or location until final tabulation of the data.

### Mouse Pheochromocytoma Cell Lines

The mouse pheochromocytoma cell line MPC 4/30PRR was developed in our laboratory [18] and previously utilized for testing of other potential chemotherapeutic agents [19]. Cells tested were from passages ~20–25 maintained as described by Powers et al [18]. The less differentiated derivative of MPC 4/30PRR designated MTT (for mouse tumor tissue) established from MPC tumor tissue formed after reinjection of the original cell line into nude mice [20], was maintained as described by Martiniova et al [20]. The MPC and MTT lines are complementary for drug testing purposes in that MTT best reflects aggressive metastases, while MPC is better differentiated and more comparable to slowly growing, hormonally active metastases [21] [22].

We derived an additional cell line designated MPC 4/30/PRR GL-9 (abbreviated to MPC GL-9) expressing copepod green fluorescent protein (copGFP) and firefly luciferase from MPC 4/30PRR by transducing the cells with a pre-packaged lentiviral construct (GreenFire1, SBI Systems) containing both genes under control of the CMV promoter. Infection was performed according to the manufacturer's protocol and MPC GL-9, which stably expresses high levels of luciferase, was cloned from a single transduced cell identified by its GFP fluorescence. Aside from expression of its two marker proteins, MPC G-L9 is similar to its parent tumor. It is intended to be used for in vivo bioluminescence imaging of tumor deposits comparably to the recently described MTT derivative known as MTT-luc [23].

### Cytotoxicity Testing and Immunostaining of MPC and MTT Cell Lines

Drug testing regimens were as described in the figure legends. Cytotoxicity against MPC 4/30PRR and MTT cells was tested in parallel using the XTT colorimetric assay to quantitate cell survival (Cell Proliferation Kit II, Roche, Indianapolis IN). Additional XTT assays were performed to compare cytotoxicity against MPC 4/30PRR and MPC GL-9 cells, and a parallel assay using bioluminescence as the reporter was performed on MPC GL-9 cells. The luminescence assay was essentially as described by Giubellino et al [23]. All cytotoxicity experiments with mouse cell lines were performed on 3 occasions unless otherwise specified.

To assess BrdU incorporation into MPC cells, cultures were pulsed with 10 uM BrdU for 24 h, then fixed and stained for BrdU and TH by the same method as the primary human cell cultures.

### Effects of Other TOP1 Inhibitors on MPC and Human Pheochromocytoma Cells

In order to determine the cytotoxicity of camptothecin analogs currently in clinical use, we first used MPC in XTT assays to test four drugs: camptothecin, topotecan, irinotecan and SN38, the active metabolite of irinotecan. The concentrations of these drugs were based on published preclinical studies of other cell types [24].

### Assessment of Apoptosis

To test and compare the effects of different combinations of camptothecin and 5-aza on apoptosis, MPC cells were cultured with the two drugs separately or in combination for up to 2 weeks, with a switch in sequence of addition at one week corresponding to the schedule of cytotoxicity testing by XTT assay. Immunoblots were then probed for a 25 kDa fragment of poly (ADP-ribose) polymerase (PARP), that is cleaved from the 116 kDa nuclear enzyme by activated caspase 3 and serves as an apoptosis marker [25]. To confirm the morphological changes of apoptosis, fixed cultures were stained with 4′-6-diamidino-2-phenylindole (DAPI, 0.5 uM) (Abbot Molecular, Abbott Park IL) and examined by fluorescence microscopy.

### Immunoblots

Protocols for protein extraction and immunoblotting were as previously described [17]. Cleaved PARP was detected with a rabbit monoclonal antibody from Epitomics Inc, (Burlingame, CA, USA). Firefly luciferase protein was detected with mouse monoclonal antibody Luci 1–107 from Abcam (ab7358, 1:000), copepod GFP was detected with TurboGFP polyclonal rabbit antibody PA5-22688 from Thermo Scientific Pierce, and chromogranin A was detected with a polyclonal rabbit antibody provided by Dr. Reiner Fischer-Colbrie, Innsbruk, Austria.

### Statistics

Statistical significance of drug effects on survival of human PCC/PGL cells studied by immunocytochemistry on MPC cells in XTT assays was analyzed by one-way ANOVA. Statistics for luminescence imaging analyses are as described by Tao et al [26].

## Results

### Cell Culture Studies

**Primary human tumor cell cultures.** Progressive, dose-dependent killing of human PCC/PGL cells was observed in cultures maintained for up to 2 weeks in the presence of camptothecin *versus* control medium. At two weeks, mean survival was approximately 13% with 10 uM camptothecin and 38% with 1 uM (Table 1 and Fig. 1). Cytotoxicity was independent of tumor genotype or location in this series. Staining of additional control cultures for BrdU and TH showed no BrdU incorporation into TH-positive cells and robust incorporation into TH-negative cells in the pre-testing period. This finding was consistent with our previous observations that human PCC/PGL do not proliferate in primary cultures [4], and indicated that the effect of camptothecin on human PCC/PGL cells does not require DNA replication.

The proportion of TH-negative contaminating cell types in control cultures was estimated at $<10\%$ to $>80\%$, reflecting the composition and varying ease of dissociation of individual tumors. Cytotoxicity of camptothecin against TH-positive tumor cells was not obviously affected by the relative presence or absence of other cell types. However, bystander toxicity on TH-negative cells was evident, particularly in cultures with 10 uM camptothecin, indicating a need for strategies to reduce the effective camptothecin dose.

### MPC versus MTT Cells

Initial comparisons of the MPC and MTT cell lines showed that both lines were more sensitive to camptothecin than their human counterparts, with MTT showing a lower threshold of response than MPC (Fig. 2). Both cell lines showed approximately 20% survival in the presence of 1 uM camptothecin at 7 days and no survival at 7 days in the presence of 10 uM camptothecin. Because the responsiveness of MPC more closely resembled that of human pheochromocytomas, MPC was used as the focus for subsequent studies.

### Responses to Camptothecin and 5-azacytidine

To test the interaction of camptothecin with 5-aza, cytotoxicity assays with MPC cells were performed over a 2-week period with camptothecin present continuously and 5-aza added during either the first or second week (Fig. 3), Two concentrations of camptothecin (0.5 uM and 1 uM) and a single (1 uM) concentration of 5-aza were tested. Mean survival at two weeks was significantly decreased in cultures treated with 5-aza plus camptothecin compared to either concentration of camptothecin alone, However, cooperativity was optimal during the first week of culture and was reduced when 5-aza was present only for the second week. Further, when 5-aza was removed after one week from cultures initially receiving camptothecin plus 5-aza, survival was equivalent to that in cultures containing both drugs for the entire 2 weeks (Fig. 3). A small decrease in survival seen with 5-aza alone was cumulative over the two week period and significant at 2 weeks (Fig. 3). In contrast to human primary cultures, MPC cells from passage numbers used in this study showed approximately 30% BrdU labeling/24 hrs at the onset of cytotoxicity testing (not shown).

Immunoblots for the cleaved p25 PARP fragment showed a marked increase within 24 hrs in apoptosis caused by the combination of camptothecin and 5-aza, with little or no effect of 5-aza alone (Fig. 4). This pattern of cooperativity was still evident after 4 days (Fig. 4). However, it was no longer detectable at day 7, when the intensity of the PARP band was increased in cultures with 5-aza alone. Consistent with this finding, fluorescence microscopy at day 7 showed many cells with nuclei in final stages of apoptotic death [27] in cultures with camptothecin alone or camptothecin plus 5-aza, and a few similar cells were seen in cultures with 5-aza alone. (Fig. 5).

With MPC GL-9, the results of cytotoxicity testing by XTT assay were comparable to those with the parent tumor. However, in the parallel bioluminescence assays a paradoxical increase in

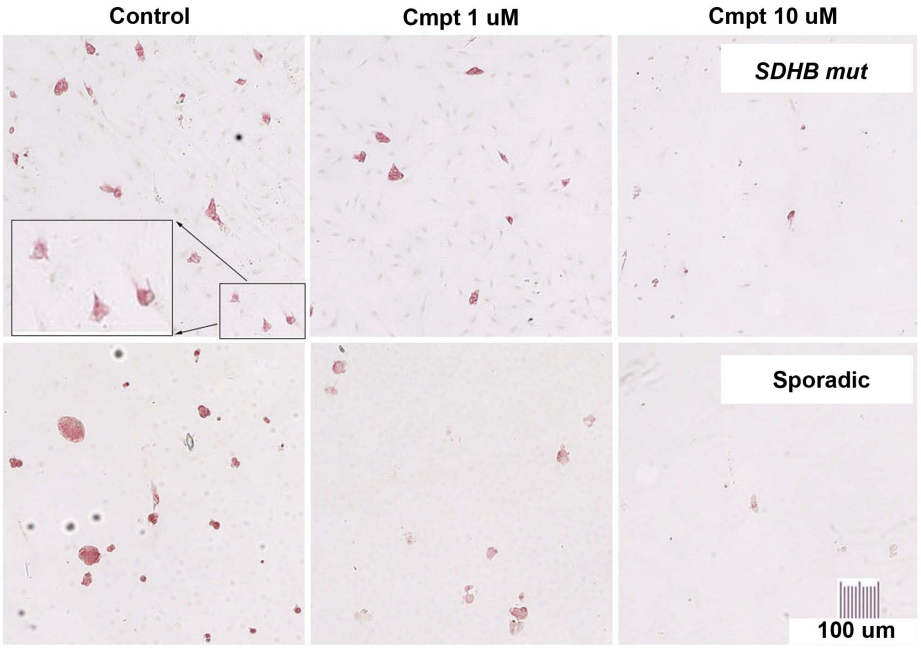


**Figure 1. Killing of cells from *SDHB*-mutated and apparently sporadic human PCC/PGL s by camptothecin.** Dissociated human tumor cells in primary cultures maintained with 0 (control), 1 or 10 uM camptothecin (Cmpt) for 2 wks, then fixed and stained for TH (red cytoplasm) to discriminate the tumor cells from other cell types. At 10 uM, camptothecin eliminated almost all background cells (faintly visible as hematoxylin-counterstained blue nuclei in top row control and 1 uM panels) and was therefore considered too toxic for the purposes of this investigation.
doi:10.1371/journal.pone.0087807.g001

luminescence above control levels was caused by camptothecin despite the presence of drug-induced apoptosis and cell death. A comparably large increase was not detectable in the presence of 5-aza alone (Fig. 6A), However, cultures with 5-aza alone maintained a constant level of luminescence in the presence of decreased cell numbers shown by XTT assay, consistent with a smaller luminescence increase. Immunoblotting for luciferase protein supported this interpretation, showing increased band intensities in camptothecin-treated cells and also a small increase in cells treated with 5-aza (Fig. 6B). Parallel increases were seen in GFP bands, while chromogranin A bands in the same immunoblot decreased in response to camptothecin and showed no effect of 5-aza. Because CgA is a marker for neuroendocrine secretory granules, this finding indicates that the drug effects on levels of luciferase and GFP are specific to the GFP-luciferase construct rather than increased granule content or other generalized cellular responses.

**Table 1.** Cytotoxicity of camptothecin against human PCC/PGL cells in primary cultures.

| | | Surviving Cells/Dish (% of Control) | |
|---|---|---|---|
| | | 1.0 uM Cmpt | 10 uM Cmpt |
| **Tumor** | **Genotype** | | |
| 1 PCC | VHL | 39.1 | 18.6 |
| 2 PCC | Sporadic-Neg | 63.3 | 29.1 |
| 3 PCC | Sporadic -Neg | 18.6 | 4.7 |
| 4 PCC | Unknown NT | 45.7 | |
| 5 PGL | SDHB | 33.1 | 2.2 |
| 6 PGL | SDHB | 71.7 | |
| 7** PGL | SDHB | 24.0** | 10.1 |

Dissociated primary tumor cells from PCCs or PGLs representing different genotypes were cultured in the presence of 1 uM or 10 uM camptothecin compared to control medium. Counts were derived by counting all stained cells defined by a randomly placed square coverslip in a 35 mm culture dish (see Figure 1). All counts were done at 2 weeks except for tumor 7 (**), which was counted at 1 week because of extensive cell death caused by particular sensitivity to camptothecin. The two tumors listed as sporadic negative were tested negative for MEN2 *RET* mutation and for *SDHB*, *SDHC* and *SDHD* mutations and deletions.
doi:10.1371/journal.pone.0087807.t001

## Responses to other TOP1 Inhibitors

Because native camptothecin is considered too toxic for clinical use, we tested three additional TOP1 inhibitors; topotecan, irinotecan and SN38, the active metabolite of irinotecan, against MPC cells for up to 2 weeks using the same methods as for camptothecin. The concentration ranges tested (0.1–10 ng/mL for topotecan, 1–100 ng/mL for SN38, 0.1–10 ug/mL for irinotecan) were chosen to match published *in vitro* tests of these drugs against other tumors [24]. The relatively high concentration of irinotecan required in cell cultures reflects the fact that the enzyme required for *in vivo* metabolic activation is not present. On a molar basis the most potent drug was SN38, which was approximately 10 times as potent as camptothecin, with 100 ng/mL SN38 (0.26 uM) or 1 ug/mL camptothecin (2.7 uM) each causing ~90% cell death (Fig. 7). Irinotecan was less potent as expected but did show some effect, suggesting that some conversion to SN38 might take place in the cultures.

Following the above result, we tested SN38 in a XTT assay against one representative human pheochromocytoma for which a sufficient number of highly purified tumor cells could be obtained by multiple rounds of plating and differential detachment prior to testing. The human cell population tested in the XTT assay was

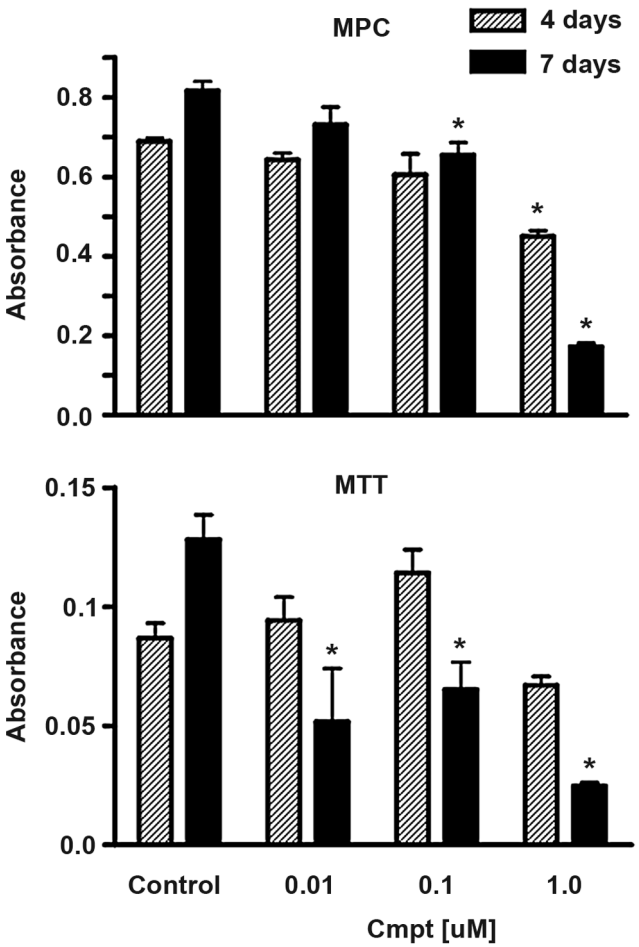


**Figure 2. Comparative cytotoxicity of camptothecin against MPC and MTT cells.** Parallel tests of camptothecin toxicity on MPC and MTT cell lines at two time points, demonstrate greater sensitivity of the more aggressive MTT line to low camptothecin concentrations. Data are from a representative experiment that was repeated on 2 independent occasions. Bars indicate mean +/− SEM of quadruplicate wells.
doi:10.1371/journal.pone.0087807.g002

confirmed to consist of >90% TH-positive cells by immunohistochemical staining of an additional culture. As shown in Fig. 8, SN38 killed human PCC cells similarly to camptothecin, although both drugs were less effective against human PCC than against MPC cells. A set of immunohistochemically stained cultures of the same tumor tested for 2 weeks with SN-38 as described for the camptothecin experiments in Fig. 1 showed 38.6% survival. This experiment also included 5-aza, which showed no enhancement of the SN-38 effect (37.3% survival).

## Discussion

In this study we used primary cultures to show that human PCC/PGL are highly sensitive to camptothecin, a prototypical TOP1 inhibitor. Importantly, the representative tumors tested included three from patients with germline *SDHB* mutations, which are the most likely to metastasize [2]. All *SDHB*-mutated tumors were sensitive to camptothecin, and one such tumor was extremely sensitive, supporting a potential role for TOP1 inhibitors in treating metastases. We then demonstrated that mouse pheochromocytoma cells respond similarly, providing a

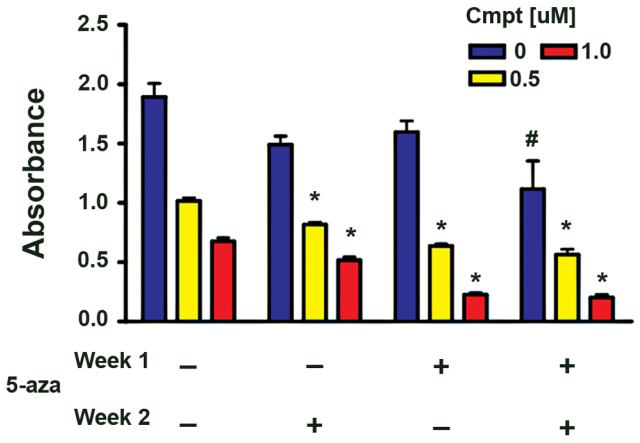


**Figure 3. Cytotoxicity of camptothecin against MPC cells is increased in the presence of 5-azacytidine.** Cytotoxicity of camptothecin against MPC 4/30/PRR cells was tested in the presence or absence of 5-azacytidine (1 uM) by XTT assay. Absorbance is proportional to cell survival. Captions under each bar indicate whether 5-aza was present during the first week/second week of a 2-week experiment. Data are from a representative experiment that was repeated on 3 independent occasions. Bars indicate mean +/− SEM of quadruplicate wells.
doi:10.1371/journal.pone.0087807.g003

physiologically relevant model for further studies. Other authors have previously advocated the use of primary cultures or primary tumor xenografts for testing chemotherapy regimens in parallel with human tumor cell lines because it is recognized that even human cell lines often do not accurately reflect the properties of their parent tumors [24]. The use of mouse cells was necessary in this study because there are currently no human PCC/PGL cell lines. However, we were unable to fully rely on primary cultures

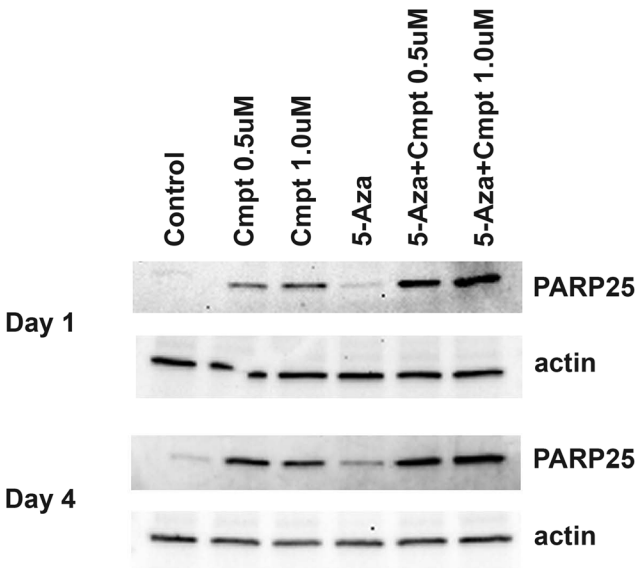


**Figure 4. Camptothecin and 5-azacytidine cooperatively increase MPC cell apoptosis.** Immunoblots show the cooperative effects of camptothecin and 5-azacytidine on MPC cell apoptosis, which is indicated by the presence of a 25 kDa fragment of PARP. A marked increase in intensity of the PARP25 band is seen at 24 hrs with the combination of camptothecin and 5-aza, with little effect of 5-aza alone. This pattern is still evident, but diminished, after 4 days.
doi:10.1371/journal.pone.0087807.g004

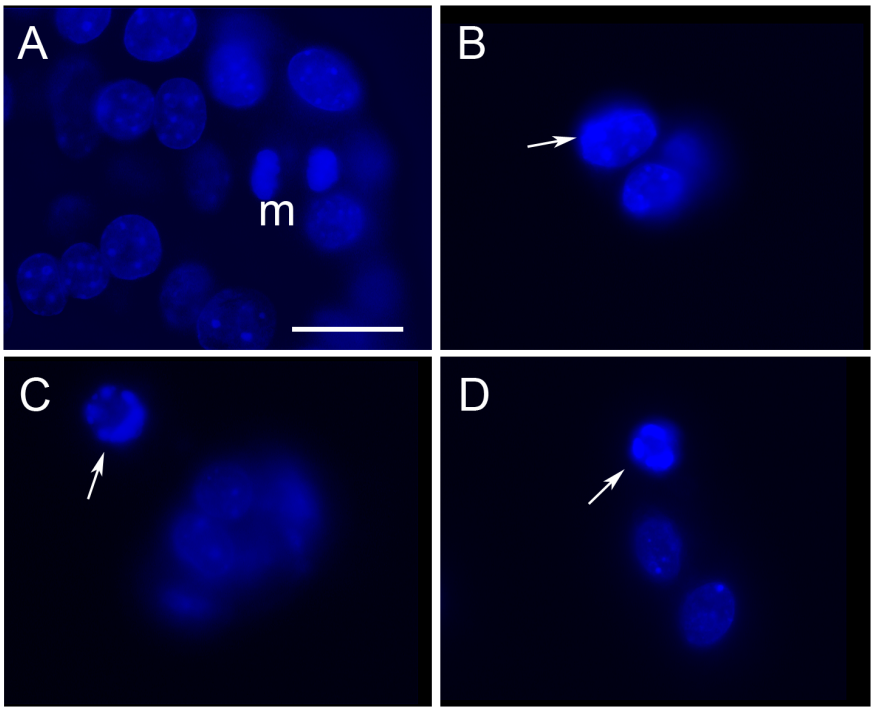


**Figure 5. MPC cells treated with camptothecin show morphological changes of apoptosis.** Representative fluorescence micrographs showing nuclear morphology of DAPI-stained MPC cultures. Panel A shows nuclei of cells maintained in control medium for 7 days. Nuclei are round to oval with finely stippled chromatin. One mitosis is evident (m). Panels B–D show typical apoptotic changes seen at day 7 in cultures with camptothecin or camptothecin +5-aza. (B, early peripheral margination of chromatin; C, nuclear shrinkage and marked chromatin margination; d, nuclear fragmentation). In addition, B–D contain fewer cells, consistent with ongoing attrition. Bar = 20 um. Original magnification 100 x.
doi:10.1371/journal.pone.0087807.g005

because of the rarity of PCC/PGL and the considerable difficulty of obtaining cells in sufficient number and purity from any individual tumor. It was therefore important to document that mouse pheochromocytoma cells represent in fact a valid model.

A major consideration for testing any drug on human PCC/PGL is the fact that most human PCC/PGL *in vivo* grow very slowly even when metastatic, and the vast majority of cells are non-replicating *in vivo* as well as in cell culture [3]. In this study we therefore first used human primary cultures to provide the foundation for further testing by establishing the fact that camptothecin is cytotoxic to non-replicating PCC/PGL cells. We then employed the mouse model to show that efficacy of a low concentration of camptothecin is increased by intermittent coadministration of a minimally toxic concentration of 5-aza, and that efficacy of the drugs in combination can be optimized by timing the sequence and duration of 5-aza administration. In the MPC model, the optimal effectiveness of the latter strategy was seen in a period of less than one week.

The rationale for use of 5-aza was our hypothesis that it would sensitize cells to camptothecin by its reported ability to alter transcription in both replicating and non-replicating cells [28], facilitated by dynamic DNA remodeling. [15]. However, we were unable to detect an effect of 5-aza in studies of representative non-replicating human PCC cells tested similarly to MPC. It remains possible that other relatively non-toxic drugs known to evoke large transcriptional changes in pheochromocytoma cells and in non-dividing neurons might be similarly tested. These include caffeine [29] and lithium [30]. In addition, methylation inhibitors might still play a role in the treatment of metastatic PCC/PGL because the growth of metastases is dependent on the small numbers of dividing cells that these deposits do contain. Those dividing cells are likely to be particularly susceptible to methylation inhibitors because the tumors are often characterized by a "methylator phenotype" [31,32].

Modes of action of 5-aza in addition to effects on DNA methylation have not been ruled out in MPC cells, and methylation-independent effects of 5-aza or (DAC) on transcription have been reported in other cell types [33]. However, at the concentration tested, the relatively potent effect of 5-aza in conjunction with TOP1 inhibition versus the small effect alone at least suggest that the proapoptotic effect of the drug is strongly, if not completely, transcription dependent.

Although generally concordant effects of camptothecin in the primary human and MPC models validates the use of MPC cells to study the cytotoxicity of TOP1 inhibitors, a caveat is that the effects of low camptothecin concentrations were greater on MPC cells than on their human counterparts. This is very likely attributable to the fact that MPC cells do proliferate, increasing their sensitivity to some chemotherapy drugs. In contrast to human PCC/PGL, which showed no BrdU incorporation at the onset of cytotoxicity testing, 30% of MPC cells in this study showed BrdU labeling in 24 hours. Further, in preliminary studies we found that exposure to 5 aza at a relatively high concentration (50 uM) for 72 hours can completely and reversibly inhibit BrdU incorporation (JF Powers and AS Tischler, unpublished data). In the present studies, inhibition of proliferation could have contributed only minimally to the cooperativity between camptothecin and the low concentration of 5-aza that we employed because a robust increase in apoptosis assayed by PARP cleavage was observed in response to the two agents within 24 hours, and markedly decreased cell numbers were detected by the XTT colorimetric assay within one week. In contrast, significantly

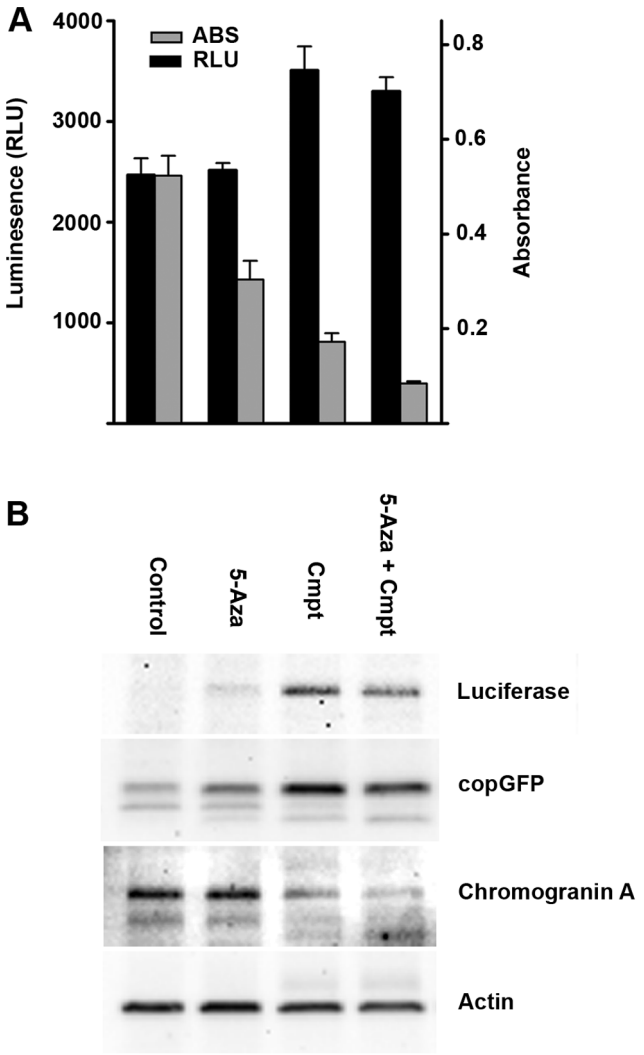


**Figure 6. Camptothecin paradoxically increases bioluminescence and luciferase expression.** (A) Effects of camptothecin and 5-azacytidine on bioluminescence of MPC GL-9 cells compared to survival measured by Absorbance in XTT assay at 1 week. (B) corresponding immunoblot from the same experiment showing increased levels of firefly luciferase protein and copepod GFP (copGFP) in camptothecin-treated cultures. Expression of CgA is not increased, indicating that the effect is specific for the luciferase construct. The paradoxically increased bioluminescence of cells treated with camptothecin obscured obvious actual toxicity that was quantifiable by XTT assay.
doi:10.1371/journal.pone.0087807.g006

decreased cell number in cultures with 5-aza alone were detectable by XTT assay only after 1–2 weeks. Nonetheless, the inhibitory effect of a high concentration of 5-aza on MPC cell proliferation suggests a further novel strategy that could be developed in future studies. Specifically, the effect could be exploited by cyclic timing and staggering of drug administration, so that TOP inhibitors first target cells in which genes are activated during 5-aza -induced cytostasis, and additional cells are then targeted when 5-aza is removed to permit reactivation of genes controlling cell cycle progression. That approach might be applicable to treatment of metastatic PCC/PGL that show accelerated growth after failure of current chemotherapies, and would be particularly interesting to test with MTT cells. In addition, cytostasis induced by pre-treatment with high concentrations of 5-aza might cause MPC and

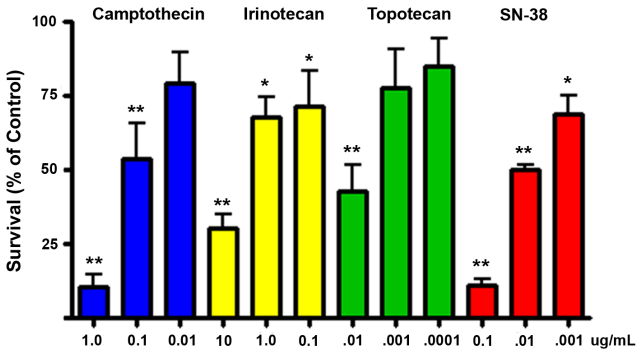


**Figure 7. Clinically utilized TOP1 inhibitors show variable toxicities to MPC cells.** Concurrent tests of camptothecin versus clinically utilized TOP1 inhibitors on MPC cells in monolayer cultures at one week. Equivalency of camptothecin and SN-38 is seen at 10-fold lower concentrations of SN38. Data are from three independent experiments, each with triplicate wells. Bars indicate mean +/− SEM. (**, p<.01; *, p<.05).
doi:10.1371/journal.pone.0087807.g007

MTT cells to more closely resemble primary human PCC/PGL cultures, in which no tumor cells proliferate, thereby possibly increasing the relevance of both models.

Although our cytotoxicity results with human PCC/PGL cells provided proof of principle to justify further testing, cytotoxicity assays of these cells in primary cultures are challenging because the neoplastic cells can be rapidly overgrown by inevitably present fibroblasts and other cell types. The percentage of contaminating cell types varies greatly from tumor to tumor, probably reflecting variable histological characteristics of the tumor tissue [34]. The present study employed staining for a tumor cell specific marker, TH, to establish that tumor cells were being targeted. This methodology is well established but tedious, and future studies will require higher throughput methods.

Human PCC/PGL can be divided into clusters according to their gene expression profiles [35] that might in turn influence

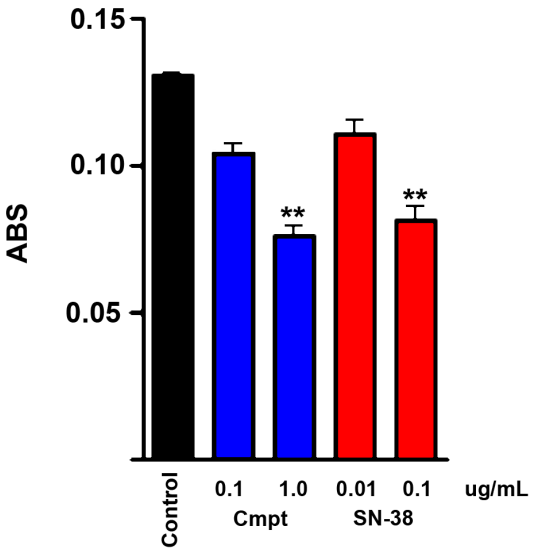


**Figure 8. The active metabolite of irinotecan is toxic to primary human pheochromocytoma cells.** XTT assay results showing killing of human PCC cells by camptothecin and SN-38. Cultures were treated with the indicated drug concentrations for one week. Data represent mean +/− SEM of triplicate wells. (**, p<.01).
doi:10.1371/journal.pone.0087807.g008

drug sensitivity. Tumors with *SDHB* mutations have a distinct pseudo-hypoxic signature. Because we were able to test only a small number of human tumors, we can not draw conclusions as to whether responsiveness to TOP inhibitors correlates with tumor genotype. However, a wide range of responsiveness among the three tested tumors from patients with *SDHB* mutations suggests that characteristics of individual tumors will be more important than genetic background.

A surprising finding in this study was increased expression of both luciferase and GFP in MPC GL-9 cells treated with camptothecin. This effect serves as an important reminder that chemotherapeutic agents can have unanticipated effects on gene expression. Interestingly, camptothecin has been reported to increase the expression of endogenous differentiation-related genes in cell lines derived from human hematopoietic tumors [36]. We therefore probed immunoblots for both luciferase and chromogranin A, a marker of neuroendocrine differentiation, but found that only luciferase and GFP were affected. Our experiments used a construct containing both luciferase and GFP driven by the CMV promoter. Since expression of both proteins is increased in parallel by camptothecin, the drug effect is most likely mediated by the CMV promoter.

Previous publications have called attention to increased CMV promoter-driven GFP expression in response to several drugs and other agents. Examples include 5-azacytidine [37], for which we also observed that effect, as well as histone deacetylase inhibitors, cisplatin and radiation [37,38]. These agents act with different kinetics [38], suggesting a number of possible mechanisms. However, a likely explanation for our observations is drug-mediated demethylation of CpG motifs in the CMV promoter [39]. This can occur either in response to a methylation inhibitor such as 5-azacytidine [37] or to a histone deacetylase inhibitor, which would facilitate chromatin remodeling and removal of methylated DNA [40]. Topoisomerase inhibitors might produce a similar effect as DNA is unwound during transcription and, inversely, methylation can alter the number of cleavage sites produced in chromatin by topoisomerase inhibitors [41]. Transcriptional silencing of transgene expression by methylation has been demonstrated with a number of experimental models, and CpG-depleted DNA vectors have been tested as a tool to improve gene delivery systems [42]. Studies using luciferase constructs for that purpose have shown that CpG-containing reporter vectors are silenced by DNA methylation and that luminescence is increased by use of CpG-depleted vectors [43]. Because the CMV promoter, is widely utilized, it is important for investigators who use CMV-driven reporters for bioluminescence or fluorescence imaging studies to be aware of potential anomalous responses to TOP1 inhibitors or other drugs. In a preliminary in vivo experiment with subcutaneous MPC GL-9 cells we have found this to be a significant concern (JF Powers, unpublished data). A number of alternative approaches might be considered for optimal in vivo imaging and pre-clinical drug testing [44].

In summary, these results provide proof of principle for use of camptothecin or newer generation TOP1 inhibitors against PCC/PGL cells and suggest novel strategies for enhancing their efficacy and reducing their toxicity by optimizing both the combination and timing of their use in conjunction with other drugs. It should be borne in mind that TOP1 inhibitors and other drugs can cause anomalous increases in CMV reporter-controlled expression of luciferase and GFP, potentially confounding the interpretation of tumor imaging studies and pre-clinical drug testing.

## Author Contributions

Conceived and designed the experiments: JFP AST GGS. Performed the experiments: JFP PGK SF AG. Analyzed the data: JFP PGK GGS AST. Contributed reagents/materials/analysis tools: SF AG KP GGS. Wrote the paper: JFP AST KP GGS.

## References


1. DeLellis RA, Lloyd RV, Heitz PU, Eng C, editors (2004) Tumours of Endocrine Organs. Lyon: IARC Press.
2. Pacak K, Eisenhofer G, Ahlman H, Bornstein SR, Gimenez-Roqueplo AP, et al. (2007) Pheochromocytoma: recommendations for clinical practice from the First International Symposium. October 2005. Nat Clin Pract Endocrinol Metab 3: 92–102.
3. Strong VE, Kennedy T, Al-Ahmadie H, Tang L, Coleman J, et al. (2008) Prognostic indicators of malignancy in adrenal pheochromocytomas: clinical, histopathologic, and cell cycle/apoptosis gene expression analysis. Surgery 143: 759–768.
4. Tischler AS, Powers JF, Alroy J (2004) Animal models of pheochromocytoma. Histol Histopathol 19: 883–895.
5. Ghayee HK, Bhagwandin VJ, Stastny V, Click A, Ding LH, et al. (2013) Progenitor cell line (hPheo1) derived from a human pheochromocytoma tumor. PLoS One 8: e65624.
6. Basili S, Moro S (2009) Novel camptothecin derivatives as topoisomerase I inhibitors. Expert Opin Ther Pat 19: 555–574.
7. Nitiss JL (2009) DNA topoisomerase II and its growing repertoire of biological functions. Nat Rev Cancer 9: 327–337.
8. Liu LF, Desai SD, Li TK, Mao Y, Sun M, et al. (2000) Mechanism of action of camptothecin. Ann N Y Acad Sci 922: 1–10.
9. Park DS, Morris EJ, Greene LA, Geller HM (1997) G1/S cell cycle blockers and inhibitors of cyclin-dependent kinases suppress camptothecin-induced neuronal apoptosis. J Neurosci 17: 1256–1270.
10. Kenmotsu Y, Oshita F, Sugiura M, Murakami S, Kondo T, et al. (2012) Nedaplatin and irinotecan in patients with large-cell neuroendocrine carcinoma of the lung. Anticancer Res 32: 1453–1456.
11. Mairs RJ, Boyd M (2008) Optimizing MIBG therapy of neuroendocrine tumors: preclinical evidence of dose maximization and synergy. Nucl Med Biol 35 Suppl 1: S9–20.
12. Gary-Bobo M, Hocine O, Brevet D, Maynadier M, Raehm L, et al. (2012) Cancer therapy improvement with mesoporous silica nanoparticles combining targeting, drug delivery and PDT. Int J Pharm 423: 509–515.
13. Chen KJ, Tang L, Garcia MA, Wang H, Lu H, et al. (2012) The therapeutic efficacy of camptothecin-encapsulated supramolecular nanoparticles. Biomaterials 33: 1162–1169.
14. Ishiguro M, Iida S, Uetake H, Morita S, Makino H, et al. (2007) Effect of combined therapy with low-dose 5-aza-2′-deoxycytidine and irinotecan on colon cancer cell line HCT-15. Ann Surg Oncol 14: 1752–1762.
15. Yamagata Y, Szabo P, Szuts D, Bacquet C, Aranyi T, et al. (2012) Rapid turnover of DNA methylation in human cells. Epigenetics 7: 141–145.
16. Tischler AS, Ruzicka LA, Riseberg JC (1992) Immunocytochemical analysis of chromaffin cell proliferation in vitro. J Histochem Cytochem 40: 1043–1045.
17. Powers JF, Picard KL, Tischler AS (2009) RET expression and neuron-like differentiation of pheochromocytoma and normal chromaffin cells. Horm Metab Res 41: 710–714.
18. Powers JF, Evinger MJ, Tsokas P, Bedri S, Alroy J, et al. (2000) Pheochromocytoma cell lines from heterozygous neurofibromatosis knockout mice. Cell Tissue Res 302: 309–320.
19. Martiniova L, Perera SM, Brouwers FM, Alesci S, Abu-Asab M, et al. (2011) Increased uptake of [(1)(2)(3)I]meta-iodobenzylguanidine, [(1)F]fluorodopamine, and [(3)H]norepinephrine in mouse pheochromocytoma cells and tumors after treatment with the histone deacetylase inhibitors. Endocr Relat Cancer 18: 143–157.
20. Martiniova L, Lai EW, Elkahloun AG, Abu-Asab M, Wickremasinghe A, et al. (2009) Characterization of an animal model of aggressive metastatic pheochromocytoma linked to a specific gene signature. Clin Exp Metastasis 26: 239–250.
21. Korpershoek E, Pacak K, Martiniova L (2012) Murine models and cell lines for the investigation of pheochromocytoma: applications for future therapies? Endocr Pathol 23: 43–54.
22. Nolting S, Grossman AB (2012) Signaling pathways in pheochromocytomas and paragangliomas: prospects for future therapies. Endocr Pathol 23: 21–33.
23. Giubellino A, Woldemichael GM, Sourbier C, Lizak MJ, Powers JF, et al. (2012) Characterization of two mouse models of metastatic pheochromocytoma using bioluminescence imaging. Cancer Lett 316: 46–52.
24. Jonsson E, Fridborg H, Csoka K, Dhar S, Sundstrom C, et al. (1997) Cytotoxic activity of topotecan in human tumour cell lines and primary cultures of human tumour cells from patients. Br J Cancer 76: 211–219.
25. Kaufmann SH, Desnoyers S, Ottaviano Y, Davidson NE, Poirier GG (1993) Specific proteolytic cleavage of poly(ADP-ribose) polymerase: an early marker of chemotherapy-induced apoptosis. Cancer Res 53: 3976–3985.

26. Tao K, Fang M, Alroy J, Sahagian GG (2008) Imagable 4T1 model for the study of late stage breast cancer. BMC Cancer 8: 228.
27. Tone S, Sugimoto K, Tanda K, Suda T, Uehira K, et al. (2007) Three distinct stages of apoptotic nuclear condensation revealed by time-lapse imaging, biochemical and electron microscopy analysis of cell-free apoptosis. Exp Cell Res 313: 3635–3644.
28. Zhuang J, Ye Y, Liu X, Li F, Pan X, et al. (2010) DNA demethylation in retinal neurocytes contributes to the upregulation of DNA repair protein, Ku80. Neuroreport 21: 282–286.
29. Zacchetti D, Clementi E, Fasolato C, Lorenzon P, Zottini M, et al. (1991) Intracellular Ca2+ pools in PC12 cells. A unique, rapidly exchanging pool is sensitive to both inositol 1,4,5-trisphosphate and caffeine-ryanodine. J Biol Chem 266: 20152–20158.
30. Dobner PR, Tischler AS, Lee YC, Bloom SR, Donahue SR (1988) Lithium dramatically potentiates neurotensin/neuromedin N gene expression. J Biol Chem 263: 13983–13986.
31. Kiss NB, Muth A, Andreasson A, Juhlin CC, Geli J, et al. (2013) Acquired hypermethylation of the P16INK4A promoter in abdominal paraganglioma: relation to adverse tumor phenotype and predisposing mutation. Endocr Relat Cancer 20: 65–78.
32. Killian JK, Kim SY, Miettinen M, Smith C, Merino M, et al. (2013) Succinate dehydrogenase mutation underlies global epigenomic divergence in gastrointestinal stromal tumor. Cancer Discov 3: 648–657.
33. Milagre I, Nunes MJ, Moutinho M, Rivera I, Fuso A, et al. (2010) Chromatin-modifying agents increase transcription of CYP46A1, a key player in brain cholesterol elimination. J Alzheimers Dis 22: 1209–1221.
34. Tischler AS (2008) Pheochromocytoma and extra-adrenal paraganglioma: updates. Arch Pathol Lab Med 132: 1272–1284.
35. Gimenez-Roqueplo AP, Dahia PL, Robledo M (2012) An update on the genetics of paraganglioma, pheochromocytoma, and associated hereditary syndromes. Horm Metab Res 44: 328–333.
36. Aller P, Rius C, Mata F, Zorrilla A, Cabanas C, et al. (1992) Camptothecin induces differentiation and stimulates the expression of differentiation-related genes in U-937 human promonocytic leukemia cells. Cancer Res 52: 1245–1251.
37. Kamensek U, Sersa G, Vidic S, Tevz G, Kranjc S, et al. (2011) Irradiation, cisplatin, and 5-azacytidine upregulate cytomegalovirus promoter in tumors and muscles: implementation of non-invasive fluorescence imaging. Mol Imaging Biol 13: 43–52.
38. Grassi G, Maccaroni P, Meyer R, Kaiser H, D'Ambrosio E, et al. (2003) Inhibitors of DNA methylation and histone deacetylation activate cytomegalovirus promoter-controlled reporter gene expression in human glioblastoma cell line U87. Carcinogenesis 24: 1625–1635.
39. Brooks AR, Harkins RN, Wang P, Qian HS, Liu P, et al. (2004) Transcriptional silencing is associated with extensive methylation of the CMV promoter following adenoviral gene delivery to muscle. J Gene Med 6: 395–404.
40. Jones PL, Veenstra GJ, Wade PA, Vermaak D, Kass SU, et al. (1998) Methylated DNA and MeCP2 recruit histone deacetylase to repress transcription. Nat Genet 19: 187–191.
41. Leteurtre F, Kohlhagen G, Fesen MR, Tanizawa A, Kohn KW, et al. (1994) Effects of DNA methylation on topoisomerase I and II cleavage activities. J Biol Chem 269: 7893–7900.
42. Yew NS, Zhao H, Przybylska M, Wu IH, Tousignant JD, et al. (2002) CpG-depleted plasmid DNA vectors with enhanced safety and long-term gene expression in vivo. Mol Ther 5: 731–738.
43. Klug M, Rehli M (2006) Functional analysis of promoter CpG methylation using a CpG-free luciferase reporter vector. Epigenetics 1: 127–130.
44. Gu L, Hall DJ, Qin Z, Anglin E, Joo J, et al. (2013) In vivo time-gated fluorescence imaging with biodegradable luminescent porous silicon nanoparticles. Nat Commun 4: 2326.

nature COMMUNICATIONS

ARTICLE

Received 5 Apr 2013 | Accepted 13 Jun 2013 | Published 10 Jul 2013

DOI: 10.1038/ncomms3139

# Landscape of the mitochondrial Hsp90 metabolome in tumours

Young Chan Chae[1], Alessia Angelin[2], Sofia Lisanti[1], Andrew V. Kossenkov[3], Kaye D. Speicher[3], Huan Wang[3], James F. Powers[4], Arthur S. Tischler[4], Karel Pacak[5], Stephanie Fliedner[5], Ryan D. Michalek[6], Edward D. Karoly[6], Douglas C. Wallace[2], Lucia R. Languino[1,7], David W. Speicher[3] & Dario C. Altieri[1,3]

Reprogramming of tumour cell metabolism contributes to disease progression and resistance to therapy, but how this process is regulated on the molecular level is unclear. Here we report that heat shock protein 90-directed protein folding in mitochondria controls central metabolic networks in tumour cells, including the electron transport chain, citric acid cycle, fatty acid oxidation, amino acid synthesis and cellular redox status. Specifically, mitochondrial heat shock protein 90, but not cytosolic heat shock protein 90, binds and stabilizes the electron transport chain Complex II subunit succinate dehydrogenase-B, maintaining cellular respiration under low-nutrient conditions, and contributing to hypoxia-inducible factor-1α-mediated tumorigenesis in patients carrying succinate dehydrogenase-B mutations. Thus, heat shock protein 90-directed proteostasis in mitochondria regulates tumour cell metabolism, and may provide a tractable target for cancer therapy.

[1] Prostate Cancer Discovery and Development Program, The Wistar Institute, Philadelphia, Pennsylvania 19104, USA. [2] Center for Mitochondrial and Epigenomic Medicine, Children's Hospital of Philadelphia, Philadelphia, Pennsylvania 19104, USA. [3] Molecular and Cellular Oncogenesis Program and Center for Systems and Computational Biology, The Wistar Institute, Philadelphia, Pennsylvania 19104, USA. [4] Department of Pathology, Tufts Medical Center, Boston, Massachusetts 02111, USA. [5] Program in Reproductive and Adult Endocrinology, Eunice Kennedy Shriver National Institute of Child Health and Human Development, National Institutes of Health, Bethesda, Maryland 20892, USA. [6] Metabolon, Inc, Durham, North Carolina 27713, USA. [7] Department of Cancer Biology, Kimmel Cancer Center, Thomas Jefferson University, Philadelphia, Pennsylvania 19107, USA. Correspondence and requests for materials should be addressed to D.C.A. (email: daltieri@wistar.org).

Reprogramming of tumour cell metabolism[1] is increasingly recognized as a multifaceted disease driver, enhancing biomass expansion[2], and promoting various mechanisms of oncogenic signalling[3]. Although these processes have been mostly studied in the context of aerobic glycolysis, the so-called Warburg effect[3], there is evidence that mitochondria continue to have an important role in tumour metabolism[4,5], and organelle-driven oxidative phosphorylation has been associated with tumorigenic potential[6], drug resistance[7,8] and enhanced tumour cell survival[9]. Harnessing these pathways may open new prospects for cancer therapy[10], but the regulators of mitochondrial homeostasis in tumours have remained largely elusive, and their potential suitability as drug candidates is unknown.

With a complex, multi-compartment topology, dependence on import of nuclear-encoded proteins and production of protein-modifying reactive oxygen species (ROS), mitochondria must tightly control their protein folding environment[11]. This is indispensable to maintain metabolic output[2], ensure organelle integrity[12] and prevent the consequences of an unfolded protein response, which may result in cell death[13]. Buffering mitochondrial proteotoxic stress, especially in the protein-dense and energy-producing organelle matrix[14], relies on adaptive responses mediated by molecular chaperones and AAA proteases[15], and dysregulation of these mechanisms has been linked to human diseases, including neurodegeneration and cancer[14].

In this context, a pool of ATPase-directed molecular chaperones, including heat shock protein 90 (Hsp90)[16] and its related homologue, TNF receptor-associate protein-1 (TRAP-1)[17] localize to the mitochondria, almost exclusively in tumour cells[18]. The molecular requirements for the selective accumulation of these chaperones in tumour mitochondria have not been completely elucidated. However, there is evidence that both Hsp90 and TRAP-1 form overlapping complexes with mitochondrial proteins, including cyclophilin D (CypD), a component of the permeability transition pore and control their folding[19]. Accordingly, inhibition of Hsp90 and TRAP-1 chaperone activity selectively in mitochondria triggered acute organelle dysfunction[20], defective hexokinase II (HK-II)-dependent[2] ATP production[21], and anticancer activity in preclinical tumour models, *in vivo*[19].

In this study, we examined the role of Hsp90-directed mitochondrial protein folding on cellular homeostasis. Using combined proteomics and metabolomics approaches, we found that mitochondrial Hsp90 and TRAP-1 are global regulators of tumour metabolic reprogramming, including oxidative phosphorylation, and are required for disease maintenance.

## Results

**Identification of a mitochondrial Hsp90 proteome**. We began this study by setting up a preliminary proteomics screen to identify regulators of mitochondrial protein homeostasis, or proteostasis, in tumours. For these experiments, we used non-cytotoxic concentrations of Gamitrinib (GA mitochondrial matrix inhibitor), a mitochondrial-targeted, small molecule ATPase antagonist that inhibits the chaperone activity of both Hsp90 and TRAP-1 in tumours[20].

Treatment of glioblastoma LN229 cells with non-cytotoxic concentrations of Gamitrinib[21] caused the accumulation of aggregated and misfolded proteins, characterized by resistance to detergent solubilization (Supplementary Fig. S1). Preliminary mass spectrometry analysis of selected bands showing higher intensities with Gamitrinib treatment identified 96 mitochondrial proteins (Supplementary Data 1). Forty-four of these proteins based on spectral counts were elevated by more than threefold after Gamitrinib treatment, indicating a requirement of Hsp90 for their folding. Although gel-based comparison (Supplementary Fig. S1) provides high detection sensitivity for specific bands, individual bands are not single proteins, and slight differences in band excision between control and Gamitrinib treatment can produce artificial differences. To minimize this concern, this experiment focused primarily on band differences at the 2% CHAPS condition, where protein complexity was the lowest, but not necessarily where the largest fold change occurred. To independently validate these initial results, we next performed unbiased proteomics studies using stable isotope labelling by amino acids in culture (SILAC) of control or Gamitrinib-treated cells. Of the original 44 proteins of the mitochondrial Hsp90 proteome identified by 1D mass spectrometry, 33 were independently confirmed for response to Gamitrinib in SILAC experiments (Fig. 1a). Of the remaining 11 proteins, 7 were below adequate detection levels for SILAC quantification, and 4 did not show significant changes.

These verified mitochondrial Hsp90-regulated proteins (Fig. 1a and Supplementary Table S1) comprised the following: transcription factors *TFB1M* and *TFB2M* involved in organelle gene expression[22] and glucose homeostasis[23]; ribosomal proteins (*MRPLs, MTG1* and *ERAL1*) associated with RNA translation[24–26]; regulators of purine biosynthesis and the methyl cycle (*MTHFD2*)[27]; and effectors of oxidative phosphorylation[2], including *SDHB*, *IDH3G, NDUFS3*, *PDHB* and *MDH2* (ref. 28) (Fig. 1b). Mitochondrial proteins participating in redox status and detoxification pathways (*PRDX6, POLDIP2, CYB5R1* and *ETHE1*)[29–31] were also identified in the mitochondrial Hsp90 proteome (Fig. 1b).

**Mitochondrial Hsp90 regulation of tumour metabolism**. The impact of a mitochondrial Hsp90 proteome (Fig. 1b) on cellular homeostasis was next investigated. For these experiments, we quantified the level of 301 individual metabolites in prostate adenocarcinoma PC3 cells treated with non-cytotoxic concentrations of Gamitrinib[21] or, alternatively, silenced for expression of TRAP-1 by small interfering RNA (siRNA)[21]. Both approaches produced global defects in tumour cell metabolism (Supplementary Data 2). Consistent with a requirement of Hsp90 for oxidative phosphorylation (Fig. 1b), Gamitrinib-treated cells exhibited aberrant accumulation of citric acid cycle metabolites, succinate, fumarate and malate (Fig. 2a). This was associated with altered glutaminolysis (elevation in glutamine and α-ketoglutarate) (Supplementary Fig. S2) and deregulated fatty acid metabolism (Fig. 2b), leading to higher levels of palmitate and linoleate, increased long chain fatty acid transport into mitochondria (elevation of palmitoylcarnitine and stearoylcarnitine), and excess lipid oxidation (accumulation of the ketone body 3-hydroxybutyrate (Supplementary Fig. S3). Mitochondrial Hsp90-targeted cells also showed increased AMP/ATP ratio (Supplementary Fig. S3), indicative of cellular starvation, and consistent with the loss of ATP production, phosphorylation of the energy sensor, AMP-activated kinase (AMPK), and inhibition of mammalian target of Rapamycin complex (mTORC1) observed in response to Gamitrinib[21].

Targeting mitochondrial Hsp90s impaired the catabolism of branched-chain amino acids, with accumulation of valine, isoleucine and leucine (Fig. 2c), and decreased levels of branched-chain amino acid catabolites, isobutyryl-carnitine, succinylcarnitine, 2-methylbutyryl-carnitine and isovaleryl-carnitine (Fig. 2c, Supplementary Fig. S4). This was associated with defects in redox status (Fig. 2d), cholesterol homeostasis (Fig. 2e) and purine nucleotide metabolism (Fig. 2f), resulting in higher levels of cholesterol metabolites associated with lipid

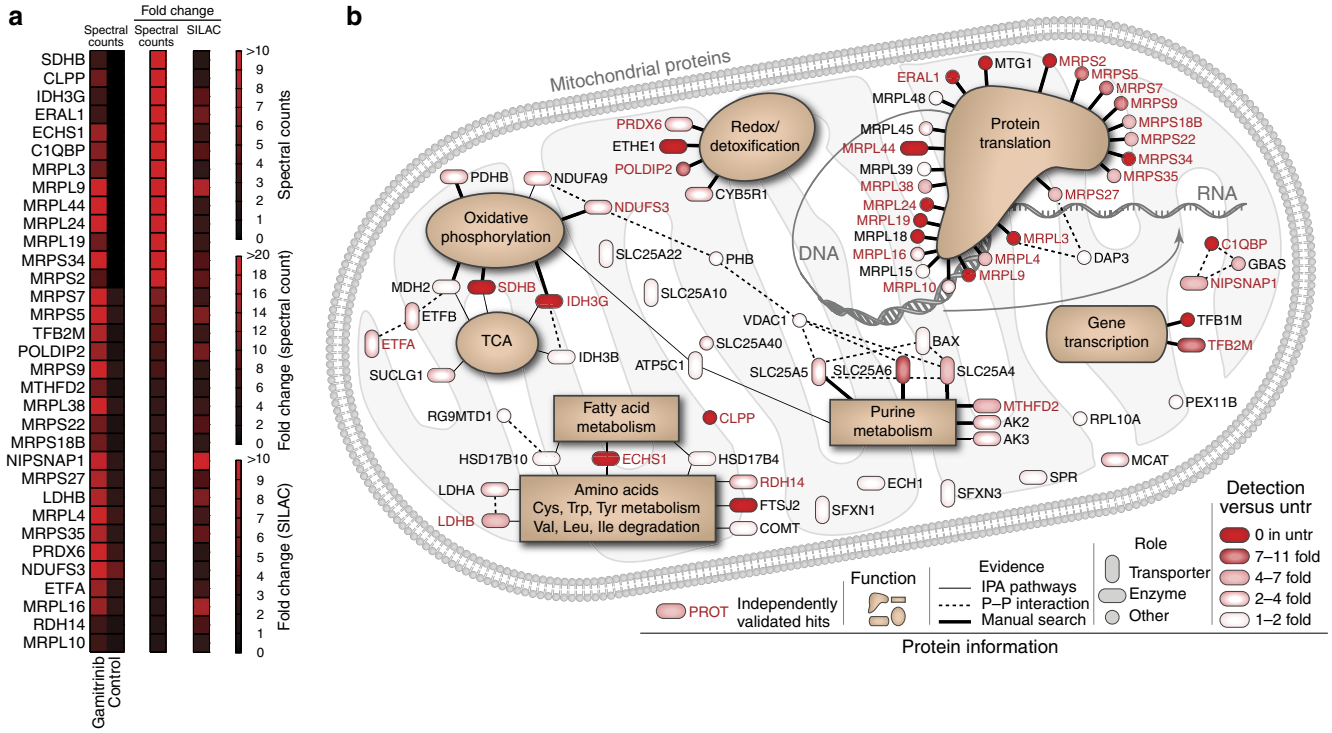


**Figure 1 | Mitochondrial Hsp90 proteome.** (**a**) LN229 cells were treated with vehicle (Control) or non-cytotoxic concentrations of mitochondrial-targeted Hsp90 inhibitor, Gamitrinib, and detergent-insoluble mitochondrial proteins were identified by one dimensional mass spectrometry (spectral counts), or, alternatively, by SILAC technology. The heat map quantifies changes in protein solubility (>3-fold cutoff) between the treatments assessed using the two independent proteomics approaches. (**b**) Schematic representation of the mitochondrial Hsp90 proteome. Proteins are annotated with functions based on literature search and information from Ingenuity software, which was also used to determine known direct protein–protein interactions. All proteins are colour coded to reflect the magnitude of difference in detection between treated and untreated (untr) samples. Proteins marked in 'red' exhibited a >3-fold change difference after Gamitrinib treatment compared with control, and were independently confirmed by both one dimensional mass spectrometry and SILAC technology.

peroxidation, ROS-dependent allantoin generation (Fig. 2f, Supplementary Fig. S5), and increased oxidized glutathione, cysteine-glutathione disulphide and the glutathione catabolic product, 5-oxoproline (Supplementary Fig. S6). Increased ROS production under these conditions may result from dysfunctional mitochondrial metabolism (see above), and/or increased nitric oxide generation from arginine, a possibility suggested by the accumulation of citrulline under these conditions (Fig. 2g, Supplementary Fig. S7).

Overall, Gamitrinib treatment produced more extensive changes in the tumour metabolome, compared with siRNA silencing of TRAP-1 (Fig. 2 and Supplementary Figs S2–S7). This may reflect incomplete TRAP-1 knockdown by siRNA, or, alternatively, compensatory mechanisms provided by mitochondrial Hsp90, which is inhibited by Gamitrinib, but not by TRAP-1 knockdown. As a control, treatment of PC3 cells with 17-allylamino 17-demethoxygeldanamycin (17-AAG), which inhibits Hsp90 in the cytosol, but not mitochondria[20], or transfection of a control, non-targeting siRNA, had minimal effects on metabolic pathways (Supplementary Figs S2–7). In previous experiments, addition of the triphenylphosphonium 'mitochondriotropic' moiety, alone or in the presence of 17-AAG, had no effect on mitochondrial function[20].

**Mechanism of mitochondrial Hsp90 control of tumour metabolism**. To elucidate how mitochondrial Hsp90s regulate tumour bioenergetics, we next focused on SDHB, the iron–sulphur subunit of ETC Complex II[32], which required Hsp90s for proper folding (Fig. 1a,b, Supplementary Table S1, Supplementary Data 1), and functional activity (Supplementary Fig. S2). Treatment of tumour cells with Gamitrinib caused insolubility of Complex II over a range of detergent concentrations (Fig. 3a and Supplementary Fig. S8a). In contrast, mitochondrial proteins comprising other ETC Complexes (I, IV, III and V) were minimally affected (Fig. 3a). Immune complexes precipitated from mitochondrial fractions of tumour cells with two independent antibodies to SDHB, but not control IgG, contained TRAP-1, *in vivo* (Supplementary Fig. S8b). In addition, immunoprecipitated SDHB associated with recombinant TRAP-1, *in vitro* (Supplementary Fig. S8c), demonstrating that these two proteins interact in tumour mitochondria. Suggestive of a chaperone-'client protein' recognition[33], this interaction was required to preserve SDHB stability, as Gamitrinib treatment (Fig. 3b), or siRNA silencing of TRAP-1 (Supplementary Fig. S8d) caused SDHB degradation in tumour cells (Fig. 3c).

We next asked whether a TRAP-1–SDHB complex was important during cellular stress. In control experiments, exposure of tumour cells to concentrations >50 μM of the oxidative agent, hydrogen peroxide ($H_2O_2$), reduced SDHB levels (Fig. 3d). siRNA silencing of TRAP-1 exacerbated this response and induced nearly complete loss of SDHB expression at lower $H_2O_2$ concentrations (Fig. 3d). As a control, the expression of the flavoprotein subunit of Complex II, SDHA[28], was not affected (Fig. 3d). Functionally, treatment of tumour cells with Gamitrinib inhibited Complex II activity in a concentration-dependent manner, whereas 17-AAG had no effect (Fig. 3e). Reciprocally, addition of recombinant TRAP-1

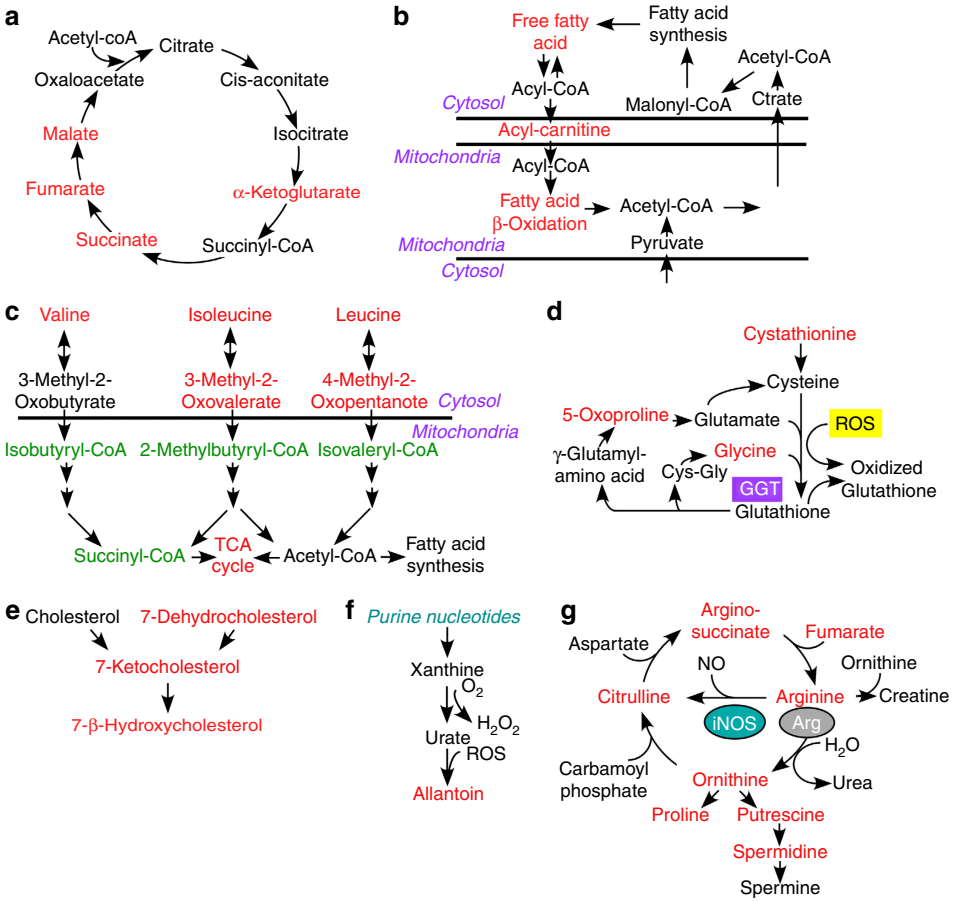


**Figure 2 | Mitochondrial Hsp90 control of tumour cell metabolism.** PC3 cells were transfected with control non-targeting siRNA or TRAP-1-directed siRNA, or, alternatively, treated with non-cytotoxic concentrations of 17-AAG (5 μM) or Gamitrinib (2.5–5 μM), and analysed for changes in expression of 301 individual metabolites by mass spectrometry. The complete summary of metabolic changes induced by targeting mitochondrial Hsp90s is presented in Supplementary Data 2. The experiment was carried out once with five independent replicates per condition tested. The metabolic pathways affected under these conditions are depicted as follows: (**a**) citric acid cycle; (**b**) fatty acid oxidation; (**c**) branched-chain amino acid catabolism; (**d**) redox status; (**e**) cholesterol metabolism; (**f**) purine nucleotide metabolism; and (**g**) arginine metabolism. Significant ($P<0.05$) changes in metabolite levels within each group (Ctrl versus TRAP-1 siRNA or vehicle versus Gamitrinib) are indicated in red (increase) or green (decrease) using Welch's two-sample *t*-test ($n=5$).

to SDHB immuno-affinity isolated from mitochondrial extracts enhanced Complex II activity in a concentration-dependent manner, *in vitro* (Fig. 3f).

**Mitochondrial Hsp90 regulation of bioenergetics stress**. The results above have suggested that Hsp90-directed protein folding preserves the stability and function of SDHB in tumour cells. To determine whether this mechanism regulates oxidative phosphorylation, we next quantified the respiration rates of tumour cells in real time. At the same concentrations that induce SDHB misfolding (Fig. 3a), and impaired mitochondrial metabolism (Figs 1,2), Gamitrinib inhibited the oxygen consumption rate (OCR) in prostate PC3 cancer (Fig. 3g,h, Supplementary Fig. S9a), or glioblastoma LN229 (Supplementary Fig. S9b–d) cells, in a concentration-dependent manner. 17-AAG had no effect on OCR (Fig. 3g,h, Supplementary Fig. 9). siRNA knockdown of TRAP-1 in PC3 (Fig. 3i,j, Supplementary Fig. S10a), or LN229 (Supplementary Fig. S10b–d) cells, partially attenuated the inhibition of OCR mediated by Gamitrinib, compared with control transfectants. In contrast, transfection of tumour cells with non-targeting siRNA had no effect on OCR, with or without Gamitrinib (Fig. 3i,j, Supplementary Fig. S10a–d). The partial reduction in the respiratory capacity and SDHB inhibition produced by Gamitrinib when added after siRNA silencing of TRAP-1, as compared with the near complete inhibition observed when Gamitrinib is added without prior siRNA to TRAP-1, may reflect a compensatory protective response by the mitochondria as a result of the extended partial TRAP-1 inhibition produced by siRNA knockdown of TRAP-1, potentially involving organelle Hsp90.

Most tumours undergo metabolic reprogramming, and utilize aerobic glycolysis as their main energy source[3]. Therefore, we asked whether oxidative phosphorylation enabled by Hsp90-directed protein folding was important for tumour maintenance. Tumour cells transfected with control siRNA and maintained in abundant nutrients (10 mM glucose) exhibited normal cellular respiration (Fig. 4a,b, Supplementary Fig. S10e). This response was increased at lower glucose concentrations (1 mM), suggestive of a compensatory mechanism that elevates ATP output by oxidative phosphorylation during nutrient deprivation (Fig. 4a,b, Supplementary Fig. S10e). Under these experimental conditions, siRNA knockdown of TRAP-1 abolished the compensatory increase in OCR at limiting glucose concentrations (1 mM), whereas cellular respiration in 10 mM glucose was minimally affected (Fig. 4a,b, Supplementary Fig. S10e).

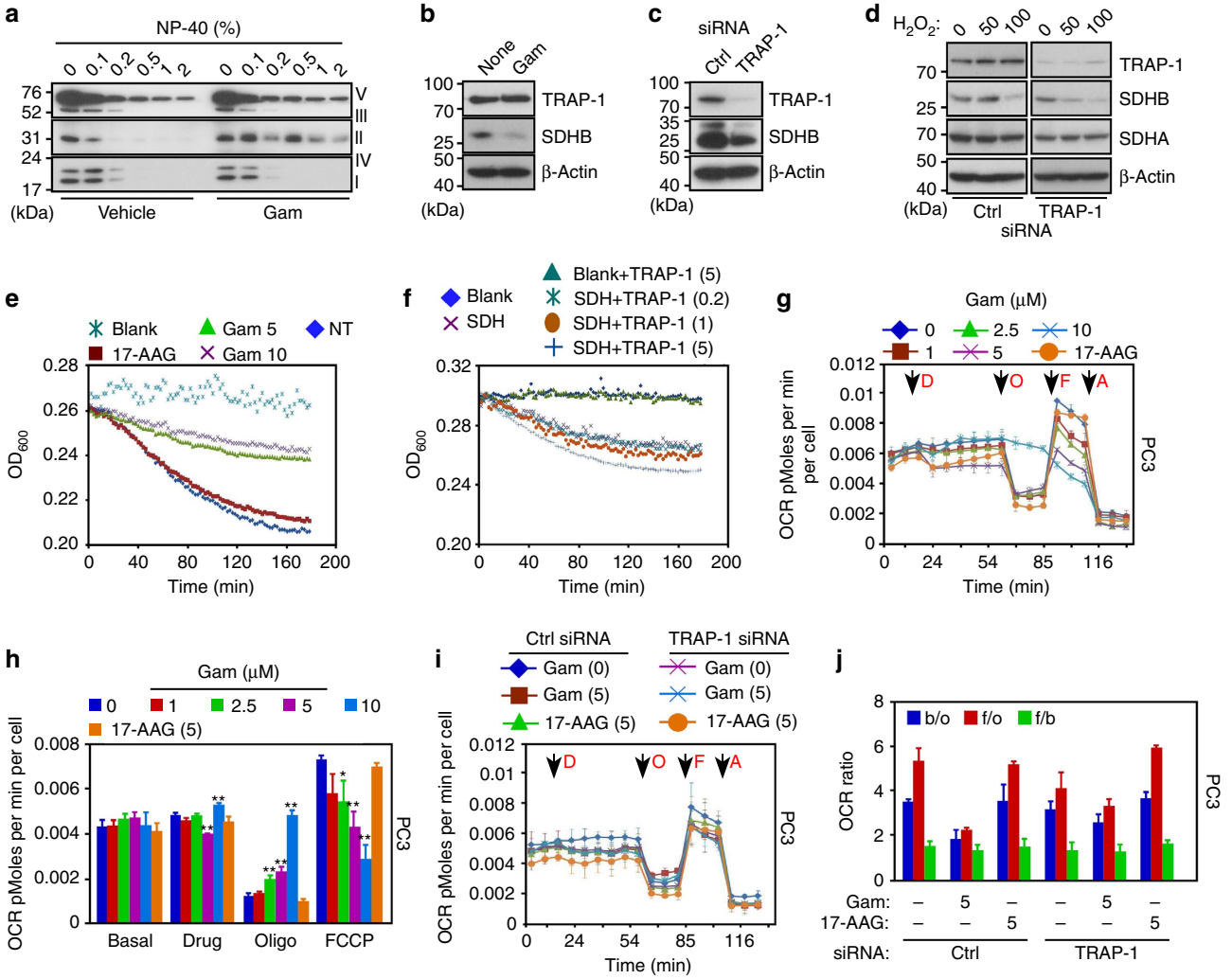


**Figure 3 | Mitochondrial Hsp90 regulation of cellular respiration.** (**a**) PC3 cells were treated with vehicle or Gamitrinib (Gam), solubilized in the indicated increasing concentrations of detergent (NP-40), and insoluble proteins were analysed by western blotting with an antibody cocktail to the OXPHOS complex. (**b**,**c**) PC3 cells were treated with Gamitrinib (**b**) or transfected with control non-targeting siRNA (Ctrl) or TRAP-1-directed siRNA (**c**), and analysed by western blotting. None, untreated. (**d**) PC3 cells were transfected as in (**c**), treated with the indicated increasing concentrations of $H_2O_2$ (μM), and analysed by western blotting. (**e**) PC3 cells were treated with the indicated concentrations of Gamitrinib (Gam, μM) or 17-AAG (10 μM) and analysed for SDHB activity at the indicated time intervals. NT, not treated. (**f**) Endogenous Complex II (SDH) was immunoprecipitated from PC3 cells, and analysed for SDHB activity in the presence of increasing concentrations of recombinant TRAP-1 (μM). Data for panels (**e**,**f**) are from representative experiments out of at least two independent determinations. (**g**) PC3 cells were treated with 17-AAG (5 μM) or the indicated increasing concentrations of Gamitrinib (Gam, μM) and the OCR was measured in real time under basal condition and in response to the indicated inhibitors. Arrows indicate the time of drug addition: D, Gamitrinib (Gam) or 17-AAG; O, oligomicyin (1.25 μM); F, FCCP (0.4 μM); A, antimycin (1.8 μM). (**h**) The OCR was normalized by the number of cells, and the extra-mitochondrial respiration after addition of antimycin was subtracted as background. $^*P<0.05$; $^{**}P<0.01$ versus control sample at each state (two-sided unpaired *t*-test). (**i**) PC3 cells were transfected with control (Ctrl) siRNA or TRAP-1-directed siRNA, treated with Gamitrinib (Gam, μM) or 17-AAG and analysed for OCR as in (**g**). (**j**) Quantification of OCR ratio between: b/o, basal condition (before any addition) and after oligomycin addition; f/o, after FCCP and oligomycin addition; f/b, after FCCP addition and basal condition in PC3 cells transfected with control siRNA (Ctrl) or TRAP-1-directed siRNA. $^*P<0.05$; $^{**}P<0.01$ (two-sided unpaired *t*-test). For all OCR experiments, data are representative of two independent experiments carried out in triplicate, mean ± s.d.

In reciprocal experiments, we transfected a control plasmid or TRAP-1 cDNA in normal NIH3T3 fibroblasts (Fig. 4c), which have low endogenous levels of mitochondrial Hsp90 and TRAP-1 (ref. 18). NIH3T3 fibroblasts transfected with control cDNA exhibited reduced ATP production (Fig. 4c), and phosphorylation of AMPK (Fig. 4d) at limiting glucose concentrations, consistent with cellular starvation. In contrast, transfection of TRAP-1 restored ATP production (Fig. 4c), and reduced AMPK phosphorylation (Fig. 4d) at low glucose concentrations.

**Role of mitochondrial Hsp90s in SDH-mutant tumours.** These experiments suggest that Hsp90 and TRAP-1 control multiple mitochondrial pathways of bioenergetics, and their role in oxidative phosphorylation may support energy production under conditions of nutrient deprivation. To test the implications of this model for tumour cell survival, we next targeted ETC Complex II function using pharmacological inhibitors. Treatment of tumour cells with the Complex II inhibitor, thenoyltrifluoroacetone (TTFA), but not 3-nitropropionic acid, increased the expression

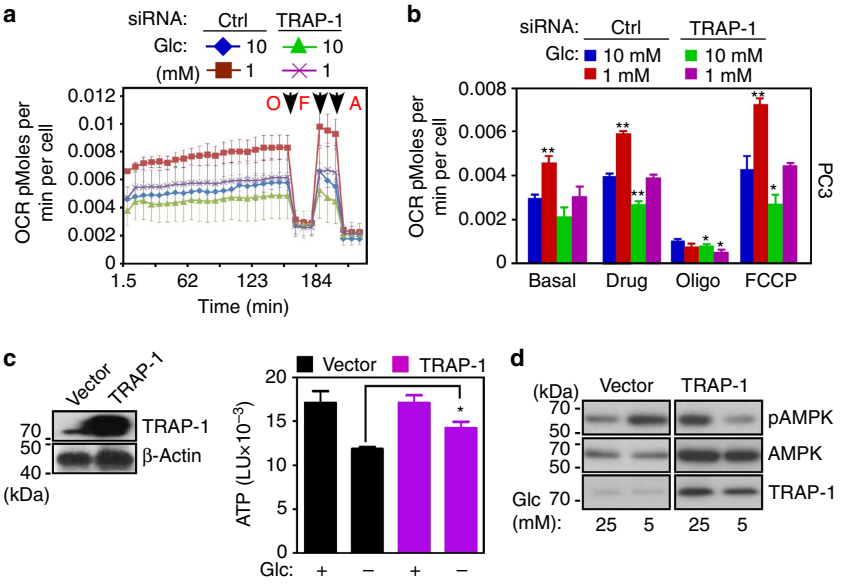


**Figure 4 | Mitochondrial Hsp90 regulation of stress bioenergetics.** (**a**) PC3 cells were transfected with control, non-targeting siRNA (Ctrl) or TRAP-1-directed siRNA and maintained in 1 or 10 mM glucose (Glc) for 3 h before analysis of OCR. Arrows indicate the time of drug addition: O, oligomicyin (1.25 μM); F, FCCP (0.4 μM); A, antimycin (1.8 μM). (**b**) OCR in **a** was quantified in siRNA-transfected cells in different glucose (Glc) concentrations. Data for panels (**a**,**b**) data are representative of two independent experiments carried out in triplicate, mean ± s.d. $^{*}P<0.05$; $^{**}P<0.01$ versus control sample at each state (two-sided unpaired *t*-test). (**c**) Normal NIH3T3 fibroblasts were transfected with control vector or TRAP-1 cDNA and analysed by western blotting (left) or ATP production in the presence (+) or absence (−) of glucose (Glc, 25 mM) (*right*). $^{*}P=0.03$ (two-sided unpaired *t*-test). (**d**) NIH3T3 fibroblasts were transfected as in (**c**), incubated with the indicated concentrations of glucose (Glc, mM), and analysed by western blotting. p, phosphorylated.

of hypoxia-inducible factor-1α (HIF-1α) (Fig. 5a), an oncogenic transcription factor implicated in adaptive responses to cellular stress[34]. Inhibition of mitochondrial Hsp90s with Gamitrinib (Fig. 5b), or siRNA silencing of TRAP-1 (Fig. 5c), was insufficient, alone, to modulate HIF-1α levels, whereas both treatments strongly enhanced TTFA induction of HIF-1α in tumour cells (Fig. 5b,c). In parallel experiments, tumour cells exposed to hypoxia exhibited increased recruitment of Hsp90 to mitochondria, compared with cytosol (Fig. 5d,e), and this response was reversed by HIF-1α silencing by siRNA (Fig. 5f,g). The mitochondrial pool of HK-II was also increased under hypoxic conditions (Fig. 5d,e), and this response was also abolished by siRNA knockdown of HIF-1α (Fig. 5f,g). In contrast, normoxic conditions (Fig. 5d,e), or transfection of tumour cells with non-targeting siRNA (Fig. 5f,g) had no effect.

Mutations in Complex II[35], including SDHB[36], have been linked to hereditary or sporadic pheochromocytoma (PCC)[37], and paraganglioma (PGL)[38], potentially through a mechanism of HIF-1α-dependent tumorigenesis[39]. Consistent with HIF-1α-dependent accumulation of Hsp90 to mitochondria after Complex II inhibition (Fig. 5e,g), TRAP-1 was strongly expressed in PCC/PGL samples carrying *SDHB* and *SDHD* mutations, compared with tumours with mutations in *RET*, *NF1* and *VHL*, or of unknown genotype (Fig. 5h,i). Functionally, PCC/PGL tumours with Complex II mutations and high levels of TRAP-1 (Fig. 5j) were more sensitive to Gamitrinib-mediated killing, *in vitro* (Fig. 5j), suggesting a compensatory pro-survival role of mitochondrial Hsp90s in transformed cells with defective oxidative phosphorylation[39].

## Discussion

In this study, we have identified mitochondrial Hsp90s[18] as global regulators of tumour cell metabolism, including oxidative phosphorylation and redox networks. This pathway hinges on chaperone-directed protein folding in mitochondria[15], and affects a discrete Hsp90/TRAP-1[18] proteome intercalated in multiple, fundamental pathways of cellular homeostasis. This mechanism may be ideally suited to buffer the risk of proteotoxic stress in transformed cells with high biosynthetic needs[19], preserve organelle integrity against CypD-dependent apoptosis[20] and maintain multiple sources of energy production, including HK-II-dependent glycolysis[21], and oxidative phosphorylation (this study), especially under stress conditions of hypoxia and nutrient deprivation.

The considerable interest in aerobic glycolysis[3] as a central feature of tumour metabolic reprogramming[1], together with the signalling role of oncogenes in these responses[40], have brought into question the function of mitochondrial bioenergetics, and in particular oxidative phosphorylation, in tumour maintenance[28]. However, recent studies have suggested that mitochondrial oxidative phosphorylation continues to remain critical for tumour cells[6], favouring resistance to therapy[7,8] and promoting cell survival[9]. The data presented here provide a mechanistic framework in support of these observations, and identify Hsp90/TRAP-1-directed protein folding in mitochondria[18] as a key requirement of oxidative phosphorylation in tumours. This involved the formation of physical complex(es) between Hsp90/TRAP-1 and the iron–sulphur subunit of mitochondrial ETC Complex II, SDHB[32], preserving its folding, stability and enzymatic function under oxidative stress. Functionally, Hsp90/TRAP-1 regulation of SDHB maintained energy production under conditions of low nutrients and hypoxia, which are hallmarks of tumour growth, *in vivo*[41], and dampened biochemical signals of cellular starvation that are typically associated with tumour suppression[42].

SDHB[32] has attracted attention as a gene mutated in certain human neuroendocrine tumours[36]. The molecular requirements

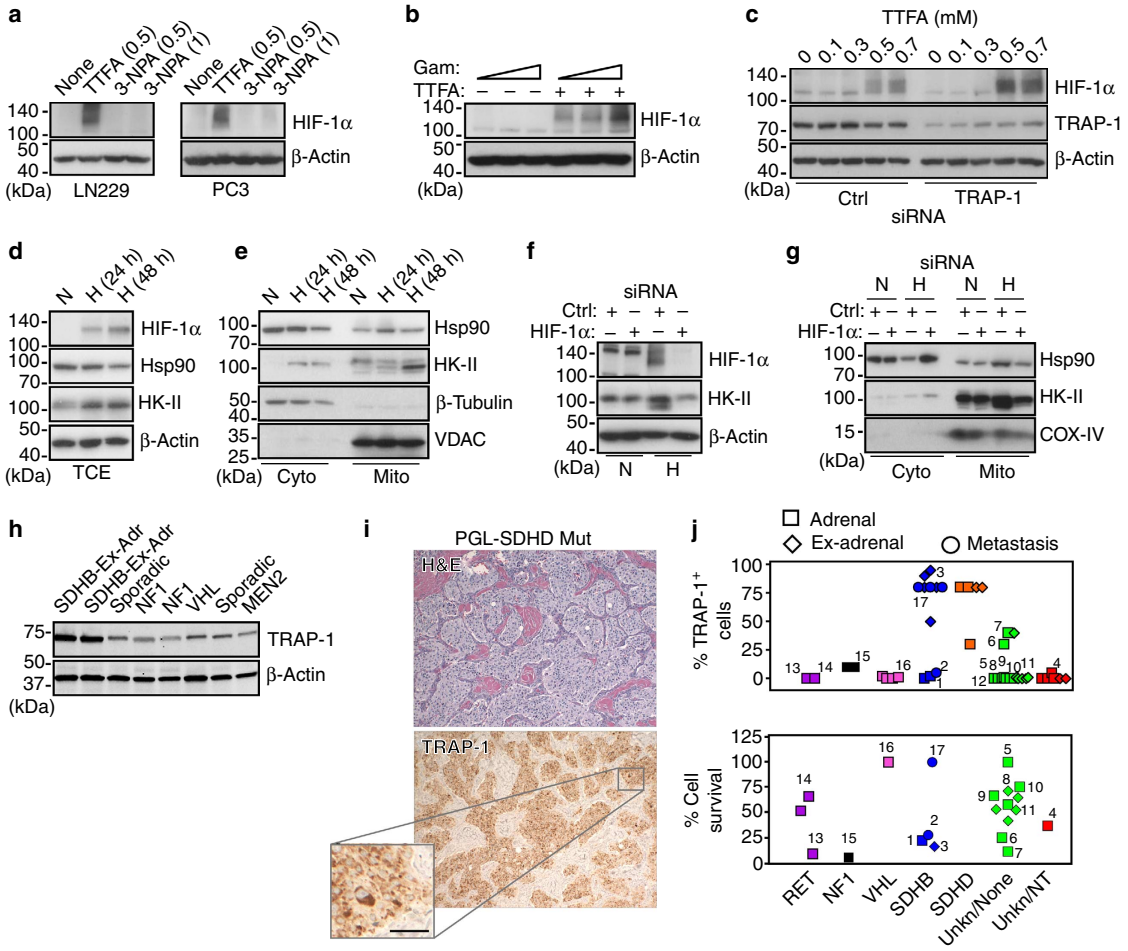


**Figure 5 | TRAP-1–SDHB complex regulates HIF-1α-directed tumorigenesis.** (**a**) The indicated tumour cell types (LN229 or PC3 cells) were treated with the various concentrations (mM) of the SDHB inhibitors, TTFA or 3-nitropropionic acid (3-NPA) and analysed by western blotting. (**b**) PC3 cells were treated with increasing concentrations of Gamitrinib (Gam, 0, 2.5, 5 μM) in the absence ( − ) or presence ( + ) of TTFA (0.3 mM) and analysed by western blotting. (**c**) LN229 cells were transfected with control siRNA (Ctrl) or TRAP-1-directed siRNA and analysed by western blotting in the presence of the indicated increasing concentrations of TTFA. (**d**,**e**) PC3 cells were maintained under conditions of hypoxia (H, 0.5% $O_2$, 5% $CO_2$, and 94% $N_2$ for 24 h) or normoxia (N), and analysed by western blotting in total cell extracts (TCE) (**d**), or fractionated cytosolic (Cyto) or mitochondrial (Mito) extracts (**e**). VDAC or β-tubulin was used as a mitochondrial or cytosolic marker, respectively. (**f**) PC3 cells were transfected with control siRNA (Ctrl) or HIF-1α-directed siRNA, maintained in normoxia (N) or hypoxia (H) conditions, and analysed by western blotting. (**g**) PC3 cells were transfected and treated as in (**f**), and isolated cytosolic (Cyto) or mitochondrial (Mito) fractions were analysed by western blotting. COX-IV was used as a mitochondrial marker. (**h**) Patient-derived tissue samples of PCC/PGL were analysed by western blotting. The mutational status of each tumour is indicated. Ex-Adr, extra-adrenal localization. (**i**) A tissue sample of extra-adrenal PGL with *SDHD* mutation, showing a typical nest-like ('Zellballen') growth pattern was stained with hematoxylin/eosin (H&E, top) or TRAP-1 (bottom), by immunohistochemistry. Scale bar, 50 μm. (**j**) Quantification of immunohistochemical expression of TRAP-1 in PCC/PGL cases with the indicated mutational status (top). Cells from the various tumour samples were maintained in culture and analysed for killing by Gamitrinib (10 μM for 2 weeks) (bottom) measured by counts of tyrosine hydroxylase-positive cells counted in an area defined by a randomly placed 22 × 22 $mm^2$ coverslips in 35 mm round culture dishes. Each point represents a single tumour. Paired samples of the same tumour were available in 12 instances and are indicated by matching numbers. Data are from a representative experiment.

of how these mutations contribute to malignancy are still being worked out[36], but one consequence of pharmacological or genetic inactivation of SDHB observed here was an increased recruitment of Hsp90 to mitochondria[18]. This pathway required HIF-1α, which is deregulated in SDHB-mutant tumours, and may potentially contribute to disease maintenance[39]. The increased accumulation of mitochondrial Hsp90s under these conditions may help compensate for the impaired oxidative phosphorylation resulting from defective SDHB function[36], enhancing organelle integrity against CypD-mediated permeability transition[18] and energy production via HK-II-directed glycolysis[21]. Consistent with this model, SDHB-mutant tumour cells were more sensitive to Gamitrinib-mediated killing than other neuroendocrine malignancies, suggesting that Hsp90-directed protein folding in mitochondria provides an adaptive and potentially 'addictive' survival factor for these cells.

There is now intense interest in pursuing aberrant tumour cell metabolism for cancer therapeutics[10]. However, inhibitors that can safely target these pathways in tumours, as opposed to normal tissues, especially with respect to oxidative phosphorylation[7,8], have not been clearly identified[43]. As a mitochondrial-directed Hsp90 inhibitor[20], Gamitrinib may be ideally suited to function as a general antagonist of tumour cell metabolism. Supported by the differential targeting of

tumour, as opposed to normal mitochondria[18], and a favourable safety profile in preclinical models[20], Gamitrinib inhibition of mitochondrial Hsp90s may simultaneously disable metabolic and survival adaptive networks in genetically heterogeneous tumours.

## Methods

**Antibodies and reagents.** The following antibodies to succinate dehydrogenase complex subunit B (SDHB, 1:500, Abcam), succinate dehydrogenase complex subunit A (SDHA, 1:3000, Abcam), HK-II (1:1000, Cell Signaling), Cox-IV (1:1000, Cell Signaling), hypoxia-inducible factor-1α (HIF-1α, 1:500, Cell Signaling), Hsp90 (1:1000, BD Biosciences), Thr172-phosphorylated AMPKα (1:1000, Cell Signaling), AMPKα (1:1000, Cell Signaling), TRAP-1 (1:1000, BD Biosciences), and β-actin (1:5000, Sigma-Aldrich) were used. A total oxidative phosphorylation antibody cocktail (1:500, Mitoscience) directed against the 20-kDa subunit of Complex I (20 kDa), cytochrome C oxidase subunit II of Complex IV (22 kDa), SDHB subunit of Complex II (30 kDa), core 2 of Complex III ( ~ 50 kDa) and F1α (ATP synthase) of Complex V ( ~ 60 kDa) was used. The complete chemical synthesis, HPLC profile, and mass spectrometry of mitochondrial-targeted small molecule Hsp90 antagonist, Gamitrinib has been reported[20]. The Gamitrinib variant containing triphenylphosphonium as a mitochondrial-targeting moiety[20] was used in this study. Non-mitochondrially directed Hsp90 inhibitor, 17-AAG was obtained from LC-Laboratories. Oligomycin, carbonyl cyanide p-trifluoromethoxyphenylhydrazone (FCCP), antimycin A, 3-nitropropionic acid and (TTFA) were obtained from Sigma-Aldrich.

**Transfections.** For gene knockdown experiments, tumour cells were transfected using control, non-targeting siRNA pool (Dharmacon, cat. no. D-001810) or specific ON-Target SMARTpool siRNAs to TRAP-1 (Dharmacon, cat. no. L-010104) or HIF-1α (Dharmacon, cat. no. L-004018). The various siRNAs were transfected at 10–30 nM using Oligofectamine (Invitrogen). Transfection of plasmid DNA was carried out with Lipofectamine (Invitrogen), as described[20].

**Subcellular fractionation.** Mitochondrial fractions were isolated from Gamitrinib-treated LN229 cells (0–20 μM for 5 h) using an ApoAlert cell fractionation kit (Clontech), as described[20]. Briefly, LN229 cells or PC3 cells were mechanically disrupted by 70 strokes with a Dounce homogenizer in isolation buffer containing 1 mM DTT plus protease inhibitor cocktail. Cell debris was removed by centrifugation at 700 *g* for 10 min. The supernatant was further centrifuged at 10,000 *g* for 25 min, and supernatants or mitochondrial pellets were processed for further analysis.

**Mitochondrial protein folding.** Mitochondrial fractions were isolated from vehicle- or Gamitrinib-treated LN229 cells (5 μM for 12 h), and suspended in equal volume of mitochondrial fractionation buffer containing increasing concentrations of CHAPS (0, 0.05, 0.1, 0.2, 0.5, 1 or 2%). Samples were incubated for 20 min on ice and detergent-insoluble protein aggregates were recovered by centrifugation (20,000 *g*) for 20 min. Pelleted proteins were separated by SDS-gel electrophoresis and visualized by silver staining (Sigma-Aldrich).

**Proteomics studies.** To identify mitochondrial proteins that require organelle Hsp90s for proper folding and/or activity (mitochondrial Hsp90 proteome), individual silver-stained bands isolated from mitochondrial fractions of vehicle or Gamitrinib-treated LN229 cells were analysed by 1D MS (see Supplementary Methods). As an independent experimental approach, global proteomics analysis of vehicle or Gamitrinib-treated LN229 cells was carried out by SILAC technology (see Supplementary Methods). Changes in the expression of 301 metabolites were determined by ultrahigh performance liquid chromatography/mass spectroscopy and gas chromatography/mass spectroscopy in PC3 cells treated with vehicle or Gamitrinib (2.5, 5 μM), non-mitochondrial-targeted 17-AAG (5 μM), or alternatively, transfected with control non-targeting or TRAP-1-directed siRNA (see Supplementary Methods).

**Purification of TRAP-1 proteins.** NIH3T3 cells were transfected with human TRAP-1-Myc plasmid cDNA. After 48 h, cells were washed with PBS and lysed in PBS containing 1% TX-100 plus phosphatase inhibitor cocktail (Roche). Lysates were centrifuged at 14,000 *g* for 10 min at 4 °C, and c-Myc-tagged TRAP-1 proteins were isolated by immunoprecipitation with an antibody to c-Myc coupled to agarose beads (Sigma-Aldrich). Samples were then washed five times with lysis buffer, and TRAP-1-myc was eluted from the immune complex with 100 μg ml$^{-1}$ c-Myc peptide (Sigma-Aldrich) in PBS. To eliminate free c-Myc peptide and further enrich eluted TRAP-1-containing material, samples were purified with centrifugal filter (30 K, Millipore).

**SDH activity assay.** Tumour cells were analysed for SDH complex activity as reduction of the dye 2,6-dichlorophenolindophenol, which recycles the substrate ubiquinone using Complex II enzyme activity. Briefly, mitochondria isolated from PC3 or LN229 cells were lysed in enzyme assay buffer containing 1% *N*-dodecyl-β-D-maltopyranoside plus protease inhibitors (Roche) for 1 h at 4 °C under constant agitation. After centrifugation at 15,000 *g* for 20 min at 4 °C, supernatants were loaded on anti-Complex II antibody-coated 96-well plates, and incubated with increasing concentrations of recombinant TRAP-1 for 2 h. Enzyme activity was determined from SDH-dependent reduction of dye 2,6-dichlorophenolindophenol, and quantified as changes in absorbance at 600 nm for 3 h at 2 min intervals using a plate reader (Beckman Coulter).

**Cellular respiration.** OCRs were assayed using the Extracellular Flux System 24 Instrument (Seahorse Bioscience, Billerica, MD). PC3 or LN229 cells were grown in standard media and after trypsinization and re-suspension in growth media, 25,000 cells were plated in each well of a Seahorse XF24 cell culture plate (100 μl volume). After 4-h incubation to allow the cells to adhere to the plate, an additional 150 μl of media was added to each well, and the cells were grown for 24 h at 37 °C with 5% $CO_2$. The media was then exchanged with unbuffered DMEM XF assay media (Seahorse Bioscience) supplemented with 2 mM glutaMAX, 1 mM sodium pyruvate and 5 mM glucose (pH 7.4 at 37 °C), and equilibrated for 30 min at 37 °C and ~0.04% $CO_2$ before the experiment. Cellular oxygen consumption was monitored in basal condition (before any addition) and after addition of oligomycin (1.25 μM), FCCP (0.4 μM) and antimycin (1.8 μM), all dissolved in DMSO. The three drugs were injected into the XF24 sequentially, and the OCRs measured using the extracellular flux analyser with three cycles of mixing (150 s), waiting (120 s) and measuring (210 s). This cycle was repeated following each injection[44]. To test the effect of mitochondrial Hsp90s on cellular respiration, PC3 or LN229 cells were treated with non-cytotoxic concentrations of Gamitrinib (0–10 μM) or 17-AAG (2.5–5 μM) and continuously analysed for OCR changes. Alternatively, cells were transfected with control or TRAP-1-directed siRNA and analysed after 24–36 h.

**Patient samples.** All experiments involving patient-derived material were approved by the Tufts Medical Center Institutional Review Board following informed consent. A series of genetically characterized PCC/PGL with documented mutations of major susceptibility genes ($n = 10$, *SDHB*; 6 *SDHD*; 4 *VHL;* 3 *RET*; 2 *NF1*), apparently sporadic PCC/PGL ($n = 22$) and normal human adrenal medulla was examined in this study. All of the tumours with *VHL*, *RET* or *NF1* mutations were intra-adrenal, while 10/13 with *SDHB,* 3/6 with *SDHD*, and 10/25 with no known mutations were extra-adrenal. Two of the extra-adrenal tumours with *SDHD* mutations were in the head or neck and the remainder retroperitoneal. For four of the tumours with *SDHB* mutations, tissue was available only from metastatic sites. One *SDHB*-mutated tumour was an adrenal bed recurrence of a primary malignancy that had given rise to metastases. All of the other specimens were primary tumours.

**Statistical analysis.** Data were analysed using the two-sided unpaired *t*-tests using a GraphPad software package (Prism 4.0) for Windows. Data are expressed as mean ± s.d. or mean ± s.e.m. of multiple independent experiments. A *P*-value of $<0.05$ was considered as statistically significant. For pair-wise comparisons in metabolite screening studies, the Welch's t-tests, Wilcoxon's rank sum tests or ANOVA were performed. For classification studies, random forest analyses were performed. Statistical analyses are performed with the program 'R' http://cran.r-project.org/.

## References

1. Kroemer, G. & Pouyssegur, J. Tumor cell metabolism: cancer's Achilles' Heel. *Cancer Cell* **13,** 472–482 (2008).
2. Vander Heiden, M. G., Cantley, L. C. & Thompson, C. B. Understanding the Warburg effect: the metabolic requirements of cell proliferation. *Science* **324,** 1029–1033 (2009).
3. Koppenol, W. H., Bounds, P. L. & Dang, C. V. Otto Warburg's contributions to current concepts of cancer metabolism. *Nat. Rev. Cancer.* **11,** 325–337 (2011).
4. Gao, P. *et al.* c-Myc suppression of miR-23a/b enhances mitochondrial glutaminase expression and glutamine metabolism. *Nature* **458,** 762–765 (2009).
5. Matoba, S. *et al.* p53 regulates mitochondrial respiration. *Science* **312,** 1650–1653 (2006).
6. Weinberg, F. *et al.* Mitochondrial metabolism and ROS generation are essential for Kras-mediated tumorigenicity. *Proc. Natl Acad. Sci. USA* **107,** 8788–8793 (2010).
7. Haq, R. *et al.* Oncogenic BRAF regulates oxidative metabolism via PGC1alpha and MITF. *Cancer Cell* **23,** 302–315 (2013).
8. Caro, P. *et al.* Metabolic signatures uncover distinct targets in molecular subsets of diffuse large B cell lymphoma. *Cancer Cell* **22,** 547–560 (2012).
9. Vazquez, F. *et al.* PGC1alpha expression defines a subset of human melanoma tumors with increased mitochondrial capacity and resistance to oxidative stress. *Cancer Cell* **23,** 287–301 (2013).
10. Wang, J. B. *et al.* Targeting mitochondrial glutaminase activity inhibits oncogenic transformation. *Cancer Cell* **18,** 207–219 (2010).

11. Haynes, C. M. & Ron, D. The mitochondrial UPR—protecting organelle protein homeostasis. *J. Cell. Sci.* **123,** 3849–3855 (2010).
12. Green, D. R. & Kroemer, G. The pathophysiology of mitochondrial cell death. *Science* **305,** 626–629 (2004).
13. Tabas, I. & Ron, D. Integrating the mechanisms of apoptosis induced by endoplasmic reticulum stress. *Nat. Cell. Biol.* **13,** 184–190 (2011).
14. Wallace, D. C. A mitochondrial paradigm of metabolic and degenerative diseases, aging and cancer: A dawn for evolutionary medicine. *Annu. Rev. Genet* **39,** 359–407 (2005).
15. Baker, B. M. & Haynes, C. M. Mitochondrial protein quality control during biogenesis and aging. *Trends Biochem. Sci.* **36,** 254–261 (2011).
16. Taipale, M., Jarosz, D. F. & Lindquist, S. HSP90 at the hub of protein homeostasis: emerging mechanistic insights. *Nat. Rev. Mol. Cell. Biol.* **11,** 515–528 (2010).
17. Leskovar, A., Wegele, H., Werbeck, N. D., Buchner, J. & Reinstein, J. The ATPase cycle of the mitochondrial Hsp90 analog Trap1. *J. Biol. Chem.* **283,** 11677–11688 (2008).
18. Kang, B. H. *et al.* Regulation of tumor cell mitochondrial homeostasis by an organelle-specific Hsp90 chaperone network. *Cell* **131,** 257–270 (2007).
19. Siegelin, M. D. *et al.* Exploiting the mitochondrial unfolded protein response for cancer therapy in mice and human cells. *J. Clin. Invest* **121,** 1349–1360 (2011).
20. Kang, B. H. *et al.* Combinatorial drug design targeting multiple cancer signaling networks controlled by mitochondrial Hsp90. *J. Clin. Invest.* **119,** 454–464 (2009).
21. Chae, Y. C. *et al.* Control of tumor bioenergetics and survival stress signaling by mitochondrial HSP90s. *Cancer Cell* **22,** 331–344 (2012).
22. Litonin, D. *et al.* Human mitochondrial transcription revisited: only TFAM and TFB2M are required for transcription of the mitochondrial genes in vitro. *J. Biol. Chem* **285,** 18129–18133 (2010).
23. Koeck, T. *et al.* A common variant in TFB1M is associated with reduced insulin secretion and increased future risk of type 2 diabetes. *Cell. Metab.* **13,** 80–91 (2011).
24. Barrientos, A. *et al.* MTG1 codes for a conserved protein required for mitochondrial translation. *Mol. Biol. Cell* **14,** 2292–2302 (2003).
25. Christian, B. E. & Spremulli, L. L. Mechanism of protein biosynthesis in mammalian mitochondria. *Biochim. Biophys. Acta* **1819,** 1035–1054 (2012).
26. Uchiumi, T. *et al.* ERAL1 is associated with mitochondrial ribosome and elimination of ERAL1 leads to mitochondrial dysfunction and growth retardation. *Nucleic Acids Res.* **38,** 5554–5568 (2010).
27. Pike, S. T., Rajendra, R., Artzt, K. & Appling, D. R. Mitochondrial C1-tetrahydrofolate synthase (MTHFD1L) supports the flow of mitochondrial one-carbon units into the methyl cycle in embryos. *J. Biol. Chem.* **285,** 4612–4620 (2010).
28. Wallace, D. C. Mitochondria and cancer. *Nat. Rev. Cancer.* **12,** 685–698 (2012).
29. Eismann, T. *et al.* Peroxiredoxin-6 protects against mitochondrial dysfunction and liver injury during ischemia-reperfusion in mice. *Am. J. Physiol. Gastrointest. Liver Physiol.* **296,** G266–G274 (2009).
30. Lyle, A. N. *et al.* Poldip2, a novel regulator of Nox4 and cytoskeletal integrity in vascular smooth muscle cells. *Circ. Res* **105,** 249–259 (2009).
31. Tiranti, V. *et al.* Loss of ETHE1, a mitochondrial dioxygenase, causes fatal sulfide toxicity in ethylmalonic encephalopathy. *Nat. Med* **15,** 200–205 (2009).
32. Yankovskaya, V. *et al.* Architecture of succinate dehydrogenase and reactive oxygen species generation. *Science* **299,** 700–704 (2003).
33. Taipale, M. *et al.* Quantitative analysis of HSP90-client interactions reveals principles of substrate recognition. *Cell* **150,** 987–1001 (2012).
34. Shay, J. E. & Celeste Simon, M. Hypoxia-inducible factors: crosstalk between inflammation and metabolism. *Semin. Cell Dev. Biol.* **23,** 389–394 (2012).
35. Neumann, H. P. *et al.* Germ-line mutations in nonsyndromic pheochromocytoma. *N. Engl. J. Med.* **346,** 1459–1466 (2002).
36. King, A., Selak, M. A. & Gottlieb, E. Succinate dehydrogenase and fumarate hydratase: linking mitochondrial dysfunction and cancer. *Oncogene* **25,** 4675–4682 (2006).
37. Astuti, D. *et al.* Gene mutations in the succinate dehydrogenase subunit SDHB cause susceptibility to familial pheochromocytoma and to familial paraganglioma. *Am. J. Hum. Genet.* **69,** 49–54 (2001).
38. Gimenez-Roqueplo, A. P. & Tischler, A. S. Pheochromocytoma and paraganglioma: progress on all fronts. *Endocr. Pathol.* **23,** 1–3 (2012).
39. Selak, M. A. *et al.* Succinate links TCA cycle dysfunction to oncogenesis by inhibiting HIF-alpha prolyl hydroxylase. *Cancer Cell* **7,** 77–85 (2005).
40. Ward, P. S. & Thompson, C. B. Metabolic reprogramming: a cancer hallmark even Warburg did not anticipate. *Cancer Cell* **21,** 297–308 (2012).
41. Laderoute, K. R. *et al.* 5′-AMP-activated protein kinase (AMPK) is induced by low-oxygen and glucose deprivation conditions found in solid-tumor microenvironments. *Mol. Cell. Biol.* **26,** 5336–5347 (2006).
42. Mihaylova, M. M. & Shaw, R. J. The AMPK signalling pathway coordinates cell growth, autophagy and metabolism. *Nat. Cell. Biol.* **13,** 1016–1023 (2011).
43. Cheong, H., Lu, C., Lindsten, T. & Thompson, C. B. Therapeutic targets in cancer cell metabolism and autophagy. *Nat. Biotechnol.* **30,** 671–678 (2012).
44. Wu, M. *et al.* Multiparameter metabolic analysis reveals a close link between attenuated mitochondrial bioenergetic function and enhanced glycolysis dependency in human tumor cells. *Am. J. Physiol. Cell Physiol.* **292,** C125–C136 (2007).


## Acknowledgements

We gratefully acknowledge the assistance of The Wistar Institute Proteomics Core for performing LC-MS/MS analyses, Tony Chang-Wong for assistance in computational processing of proteomics data, and Sira Sriswasdi for preparing heat maps. This work was supported by the PheoPara Alliance, National Institutes of Health (NIH) Grants CA140043, CA78810, HL54131 and CA118005 to DCA, NS021328 to DCW and Department of Defense grant PR100171 to AST. Support for Core Facilities utilized in this study was provided by Cancer Center Support Grant (CCSG) CA010815 to The Wistar Institute.

## Author contributions

Y.C.C., A.A., A.S.T., R.D.M., D.C.W., L.R.L., D.W.S. and D.C.A. designed research; Y.C.C., A.A., K.D.S., H.W., J.F.P. and E.D.K. performed research; S.L., K.P., S.F. and R.D.M. contributed new reagents/analytical tools; Y.C.C., A.A., A.S.T., R.D.M., D.C.W., L.R.L., D.W.S. and D.C.A. analysed data, and Y.C.C., A.A., A.S.T., D.C.W., D.W.S. and D.C.A. wrote the paper.

## Additional information

**Supplementary Information** accompanies this paper at http://www.nature.com/naturecommunications

**Competing financial interests:** The authors declare no competing financial interests.

**Reprints and permission** information is available online at http://npg.nature.com/reprintsandpermissions/

**How to cite this article:** Chae, Y. C. *et al.* Landscape of the mitochondrial Hsp90 metabolome in tumours. *Nat. Commun.* 4:2139 doi: 10.1038/ncomms3139 (2013).

Cancer Letters 316 (2012) 46–52

Contents lists available at SciVerse ScienceDirect

Cancer Letters

journal homepage: www.elsevier.com/locate/canlet

# Characterization of two mouse models of metastatic pheochromocytoma using bioluminescence imaging

Alessio Giubellino [a,*], Girma M. Woldemichael [b], Carole Sourbier [c], Martin J. Lizak [d], James F. Powers [e], Arthur S. Tischler [e], Karel Pacak [a]

[a] Program in Reproductive and Adult Endocrinology, Eunice Kennedy Shriver National Institute of Child Health and Human Development, NIH, Bethesda, MD 20892-1109, USA
[b] Molecular Targets Laboratory, SAIC-Frederick, Inc., National Cancer Institute, NIH, Frederick, MD 21702, USA
[c] Urologic Oncology Branch, National Cancer Institute, NIH, Bethesda, MD 20892, USA
[d] Mouse Imaging Facility, National Institute of Neurological Disorders and Stroke, NIH, Bethesda, MD 20892, USA
[e] Tufts Medical Center, Department of Pathology, Boston, MA 02111, USA

ARTICLE INFO

*Article history:*
Received 26 July 2011
Received in revised form 13 October 2011
Accepted 14 October 2011

*Keywords:*
Pheochromocytoma
Metastasis
Luminescence
BLI
Animal model

ABSTRACT

Pheochromocytoma is the most common tumor of the adrenal medulla in adults. The lack of sensitive animal models of pheochromocytoma has hindered the study of this tumor and *in vivo* evaluation of antitumor agents. In this study we generated two sensitive luciferase models using bioluminescent pheochromocytoma cells: an experimental metastasis model to monitor tumor spreading and a subcutaneous model to monitor tumor growth and spontaneous metastasis. These models offer a platform for sensitive, non-invasive and real-time monitoring of pheochromocytoma primary growth and metastatic burden to follow the course of tumor progression and for testing relevant antitumor treatments in metastatic pheochromocytoma.

Published by Elsevier Ireland Ltd.

## 1. Introduction

Pheochromocytoma is a rare neuroendocrine tumor that develops in the adrenal medulla and represents the most common tumor in this location in adults [1]. Closely related tumors in other locations are classified as paragangliomas. Although often sporadic, pheochromocytoma/paraganglioma may present in several familial syndromes, and certain subtypes are particularly prone to malignancy [2]. The risk of developing metastases can be 30%, or higher, depending on the genetic background and location of the primary tumor [3,4]. In particular, metastatic lesions in the liver and lungs are associated with shorter (usually less than 5 years) survival rate [5,6].

Currently there is no curative treatment for this disease. Several therapeutic options can relieve patient symptoms, but relapses occur [7,8]. The lack of novel therapies, especially novel targeted therapies, is in part due to the lack of suitable animal models. All efforts to establish cell lines from primary human pheochromocytomas and paragangliomas have been unsuccessful because the cells survive but do not proliferate *in vitro* [9]. It is therefore important to develop reliable animal models for sensitive screening and pre-clinical testing of novel antitumor compounds [10–12].

Successful treatment of any metastatic cancer depends on early detection and localization [13,14]. Despite excellent improvements in various imaging techniques, small metastatic lesions are often not detected because of suboptimal spatial resolution of current anatomical and functional imaging modalities. The same applies to animal models of metastatic cancer. Optimal use of animal models for the development of new therapeutic approaches should therefore employ optimal imaging techniques.

In recent years, several non-invasive imaging techniques, including magnetic resonance imaging (MRI) and computed tomography (CT), have been adapted to imaging studies in small laboratory animals [15]. One of the methods used recently for non-invasive tracking of tumor cells in experimental animals is the use of luciferase bioluminescence [16]. Bioluminescence refers to the enzymatic generation of visible light by living organisms. Currently, the most common luminescence reporter used is the firefly luciferase [17], which in the presence of oxygen ($O_2$) and ATP, catalyses the cleavage of the substrate luciferin and results in the emission of a photon of light [18]. *In vivo* implantation of tumor cells transfected or transduced with the luciferase gene

* Corresponding author. Address: Program in Reproductive and Adult Endocrinology, NICHD, NIH, Building 10-CRC, 1E-3140, 10 Center Dr., Bethesda, MD 20892-1109, USA.
*E-mail address:* giubella@mail.nih.gov (A. Giubellino).

0304-3835/$ - see front matter Published by Elsevier Ireland Ltd.
doi:10.1016/j.canlet.2011.10.019

allows sequential monitoring of tumor growth within the viscera by measuring these photon signals. This technology is reshaping efficacy evaluations and drug-target algorithms in drug animal testing for several tumor types [19,20]. No reports to date have evaluated the use of this technology in pheochromocytoma cell models of tumor growth and metastasis *in vivo*. For these reasons we generated a bioluminescent pheochromocytoma cell line and we injected these cells into immunocompromised nude mice for the real time monitoring of tumor and metastatic burden. Here we report the development and characterization of two animal models of pheochromocytoma using bioluminescence for rapid and quantifiable tumor measurement and identification of tumor metastasis in real time *in vivo* and *ex vivo*. We examined the animals using serial magnetic resonance imaging in parallel for comparison with the bioluminescence imaging, which allows for sensitive and quantitative detection of early tumor development.

## 2. Material and methods

### 2.1. Cell line and reagents

The mouse pheochromocytoma cell line MTT was maintained in DMEM supplemented with 10% FBS, 5% Horse Serum (Gibco), and antibiotic/antimycotic. Cells were grown until 80% confluence, then detached using 0.05% Trypsin/EDTA, incubated for 3 min at 37 °C and resuspended and counted to obtain a concentration of $5 \times 10^5$ cells/200 μl before injection. D-luciferin potassium salt (Caliper LifeSciences) was diluted in PBS at a concentration of 15 mg/ml, filter-sterilized using a 0.22 μm filter, aliquoted and stored at −20 °C until use.

### 2.2. pLLuc construct and retroviral transduction

The EGFP gene in the retroviral vector pLEGFP-N1 (Clontech) was replaced with the firefly luciferase gene generated via PCR from the pGL3-Basic (Promega) vector and inserted between the BamH-1 and Not-1 sites resulting in the pLLuc retroviral vector. The retrovirus packaging cell line Amphopak-293 (Clontech) was transfected with the pLLuc retroviral vector to generate 293pLLuc cells. Selection with G418 enabled the generation of stably transfected 293pLLuc cells. Target cells were transduced by incubating them overnight with conditioned medium obtained from 293 pLLuc cells containing retroviral particles filtered through a 0.45 μm filter to remove any cellular debris. Transduced cells were selected with G418 to generate stable cell lines expressing luciferase.

### 2.3. Animal experiment and bioluminescence imaging (BLI)

All animal studies were conducted in accordance with principles and procedures outlined in the NIH Guide for the Care and use of Animals and approved by the NIH ACUC Committee. Five hundred thousand MTT-luc cells were injected into the tail vein of female athymic nude mice (Taconic, Germantown, MD). Experimental groups consisted of 10-weeks-old mice ($n = 6$) housed in a pathogen-free facility. The animals were imaged weekly by both bioluminescence imaging (BLI) and magnetic resonance imaging (MRI) (described below). Mice were anesthetized with isofluorane for imaging, and euthanized using $CO_2$ inhalation and cervical dislocation. Several organs from the mice were dissected and preserved in 10% formalin.

### 2.4. MRI

For MRI, anesthesia was induced in a chamber with 5% isoflurane in an 80%/20% medical air/oxygen mixture. Mice were then transferred to a cradle with a built in mask and anesthesia was maintained at 30–45 breaths per minute with 1–2% isoflurane. Temperature was maintained by blowing heated air through the bore of the scanner (Bair-Hugger/Arizant, Eden Prarie, MN). All scans were performed using a 7 Tesla Bruker Biospec system (Bruker-Biospin, Billerica, MA) and a 35 mm linear bird cage coil. Each data set consisted of an initial locator scan, followed by a $T_2$-weighted scan, and a proton density weighted scan. To reduce motion artifacts, the acquisition was gated so that acquisition occurred between breaths (Small Animal Instruments, Inc. Stony Brook, NY).

$T_2$-weighted images consisted of twelve 1 mm slices over a $6 \times 3$ cm FOV acquired using a RARE (Rapid Acquisition Relaxation Enhanced) sequence. The image matrix was $256 \times 256$ and four echoes were acquired per excitation. The effective echo time was 20.6 ms.

Proton density weighted images consisted of twelve 1.5 mm slices over a $3 \times 3$ cm FOV acquired using a FLASH (Fast Low Angle Snapshot) sequence. The image matrix was $256 \times 256$, TE was 3 ms, and the excitation flip angle was 30°.

### 2.5. Bioluminescence imaging

All bioluminescent data were collected and analyzed with a Xenogen IVIS system.

*In vitro* imaging, MTT-luc bioluminescent cells were serially diluted from 4000 to 8 cell in DMEM media in a 96 well plate, and D-luciferin at a concentration of 150 μg/ml was added directly to the media 10 min before imaging. Imaging was performed at 20 s/plate.

For *in vivo* imaging luciferase activity was assessed in anesthetized animals (1–2% isoflurane) 15 min following i.p. administration of 150 mg/kg luciferin in phosphate buffered saline. The mice were then placed inside the camera box under continuous exposure to 1–2% isofluorane. The experiments were performed in the NIH Mouse Image Facility in accordance to ACUC regulations.

All imaging variables were equalized and photographic and bioluminescent images at different time points were collected for each sample. The bioluminescence data are presented visually as a color overlay on the photographic image. Using the Living Image software (Xenogen), a region of interest (ROI) was drawn around tumor sites of interest and total photons count or photons/s was quantified. For *ex vivo* imaging, Luciferin was injected into the animal i.p. before necropsy. Tissues of interest were then resected and placed in a culture plate with 300 μg/ml D-luciferin in PBS.

### 2.6. Histopathology

In order to confirm the presence of pheochromocytoma tumor cells, selected tissues were removed from the mice and preserved in 10% formalin immediately after *ex vivo* imaging. Tissues were paraffin embedded, sectioned, stained with hematoxylin and eosin, and examined by microscopy using a Leica microscope.

### 2.7. Statistical analysis

Tumor volume and mean bioluminescence was determined for each experiment together with the standard errors of the mean. To illustrate the relationship between bioluminescent signal, tumor volume and cell number a regression plot was used.

## 3. Results

### 3.1. Generation of stably transduced luciferase expressing MTT cells

We have previously described the generation of the aggressive, rapidly growing mouse pheochromocytoma cell line MTT from liver metastasis of the slower-growing MPC cells [21,22]. For retroviral delivery and expression of luciferase in MTT cells, we first generated the construct pLLuc via replacement of EGFP with a luciferase gene between the BamH-1 and Not-1 sites of the retroviral vector pLEGFP. This construct employs the human cytomegalovirus (CMV) immediate early promoter to drive firefly luciferase expression while the expression of the neomycin resistance gene is driven by a separate constitutively active viral promoter contained within the 5′ LTR. After transfection with the pLLuc and selection with G418 of the packaging cell line Amphopak-293, filtered conditioned medium from the stably transfected 293-LLuc cells containing retroviral particles was used to transduce MTT cells. The infected MTT cells were then selected with G418 for 4 weeks to obtain stably transduced MTT-Luc cells. Quantitation of firefly luciferase expression in MTT-Luc cells was done by directly adding a luciferin substrate into the culture medium of plated cells. Luminescence was imaged to obtain photon/s per cell 15 min after addition of the substrate. As shown in Fig. 1 (panel A), serial dilutions of these cells showed a proportional decrease in mean photon emission, with an average of 200 photons/s per cell, indicating a stable and sustained intensity of the bioluminescence signal. We named this new cell line MTT-luc. Analysis of covariation between number of cells plated and light intensity (total photon flux) showed a highly significant correlation ($R^2 = 0.995$) as illustrated in Fig. 1B.

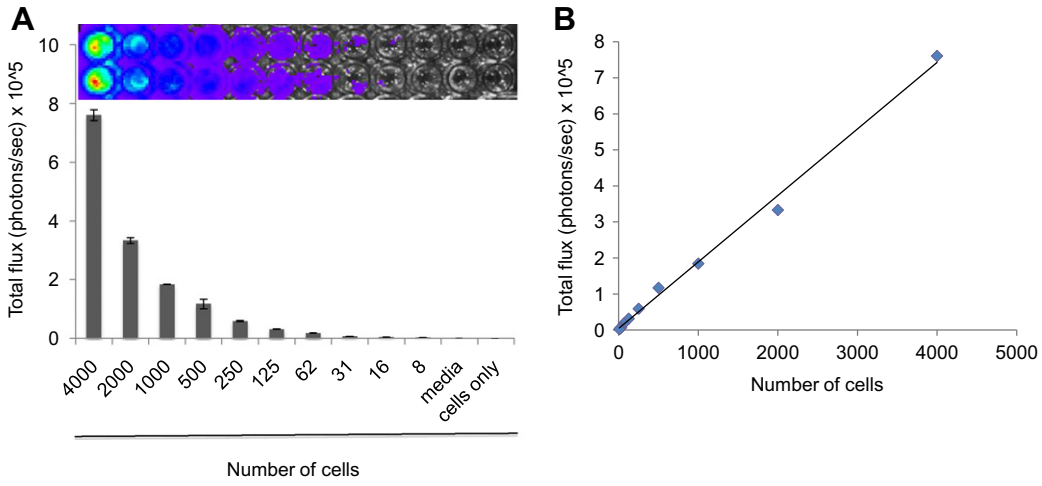


**Fig. 1.** (A) Bioluminescence signal of the murine pheochromocytoma MTT-luc cells *in vitro*. MTT-luc cells were diluted from 4000 to 8 cells, plated in duplicate in a 96 well plate and imaged for 20 s after addition of luciferin to the media. Media alone (Media; luciferin added) and 4000 cells (Cells only; no luciferin) were used as negative controls. (B) Correlation plot of photon counts vs. number of plated cells ($R^2$ = 0.99).

### 3.2. Detection and non-invasive BLI monitoring of MTT-luc cells in an experimental metastasis model

We then used a tail vein (experimental metastasis) injection of MTT-luc cells to evaluate the sensitivity of BLI to detect experimental metastasis after systemic circulation of the tumor cells. Mice were imaged immediately after injection to verify the success of the procedure (data not shown) and subsequently imaged over time by BLI over a 7-weeks period. Images of a representative nude mouse are shown in Fig. 2A (upper sequence). In parallel, animals were subjected to serial MRI. Shown in Fig. 2A (lower sequence) are images of the same mouse over the same time period.

The results show that tumor signals increased significantly over the seven weeks of the study with exponential growth seen especially localized in the upper abdominal cavity. As expected, localized bioluminescent signals indicating metastasis began to appear in the area of the liver and were detectable at an early stage of development, starting at the second week post-injection. By the third week, several areas of tumor growth were evident by both BLI and MRI. Total photon flux from tumors seen in BLI was found to correlate well with the number of lesions observed by MRI (Fig. 2B). An analysis of covariation between number of metastatic lesion as counted on the MRI image and bioluminescent light intensity (total photon flux) shows a highly significant correlation ($R^2$ = 0.992) as illustrated in Fig. 2C. By the 4th week the tumor masses were clearly identifiable by MRI. Fig. 2D illustrates the progression of tumor size over time from the 4th week represented as a sphere from averaged tumor diameters calculated by MRI analysis. The survival curve representation for this model is shown in Fig. 2E. At necropsy, several organs were excised, imaged *ex vivo* and preserved for histological evaluation. *Ex vivo* bioluminescence confirmed the presence of MTT-luc metastasis in the liver and in several other organs, including lungs, spleen, ovaries, kidney and brain (Fig. 3 and Table 1). The total photons/sec of the organs were quantified for each animals ($n$ = 6) and mean values are displayed in Fig. 3.

### 3.3. Tumorigenicity and spontaneous metastasis of subcutaneously implanted MTT-luc cells

To assess the tumorigenicity and tumor growth modality of MTT-luc cells into immunocompromised animals, we injected $1 \times 10^6$ cells s.c. into the left flank of 6-week-old nude mice. The use of luciferase-reporter cells allowed for the immediate detection of tumor cells at the time of injection (data not shown) and enabled the detection of cells implanted at various sites. The growth of the MTT-luc tumors in the nude mice was monitored over time *in vivo* by bioluminescent imaging. Images at key time points from a representative animal are shown in Fig. 4A, illustrating the progressive increase in the bioluminescence signal over time. Mean photons emitted from the tumors over time and tumor volume as assessed by caliper dimensions when the tumors became measurable (by week 4) are illustrated in Fig. 4B. Notably, the tumor cells were visible by bioluminescence imaging much earlier than the tumor became measurable or palpable.

Analysis of covariation between BMI light intensity (total photon flux) and measured tumor volume showed a high degree of correlation ($R^2$ = 0.99) as shown in Fig. 4C.

Only a few aggressive cell lines have been reported to spontaneously metastasize from subcutaneous implantation in the literature. For this reason, at the end of the 7-week experiment we wanted to verify if any metastatic MTT-luc tumor cells were detectable by bioluminescence analysis in several organs. Fifteen minutes after luciferin injections, the mice were euthanized and several internal organs, including liver, lungs, spleen, ovaries and brain, were analyzed for bioluminescence signals (Fig. 5 and Table 1). Indeed, we were able to detect MTT-luc cells in several of these organs. The lungs, which represented the organ most consistently seeded by subcutaneously implanted MTT-luc cells, are also a favored site of metastasis of human pheochromocytomas [6].

### 3.4. Bioluminescence signals correlate with metastatic lesions identified by histopathology

To confirm the presence of metastatic tumor cells in the main organs targeted in the two metastatic models we described, we performed histopathological examination of formalin-fixed tissues collected after *ex vivo* imaging. For the experimental metastasis model in which tumor cells were injected in the mouse tail vein, the most intense and reproducible signals were derived from the liver; indeed, histopathological analysis of livers from these animals revealed macro and micrometastasis (Fig. 6, left panel).

In the second models (subcutaneous injection of tumor cells), histopathological analysis confirmed the presence of micrometastasis in the lungs (Fig. 6, right panel), consistent with the *ex vivo* bioluminescence signal.

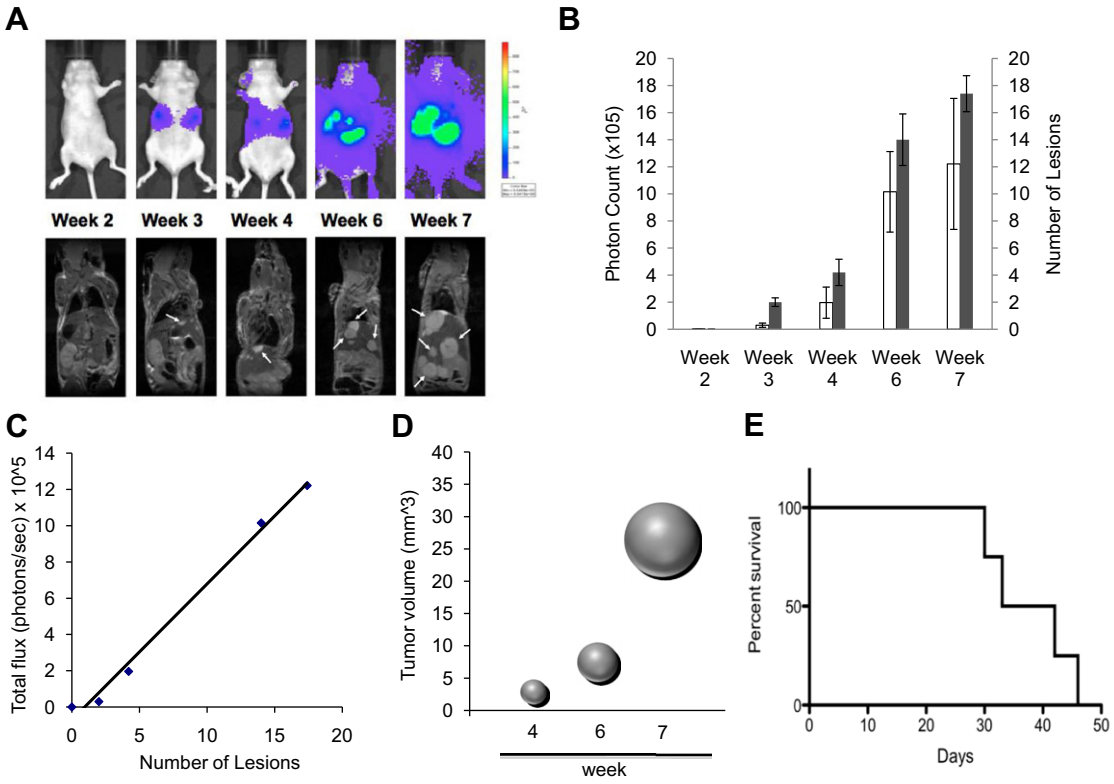


**Fig. 2.** Kinetics of tumor cell growth by Bioluminescence and MRI signals *in vivo* in an experimental metastasis model. MTT-cells ($5 \times 10^5$) were injected via tail vein into nude mice ($n = 6$). Images were taken weekly for 7 weeks. (A) Representative images are shown of the same mouse by bioluminescence detection (upper row) and MRI scanning (lower row). Arrows indicate some of the tumor lesions as evidenced by MRI imaging. (B) Quantification of tumor signal over time is represented as mean photon counts (total flux) compared with quantification of number of lesions counted on the MRI images s represented as mean; error bars represent standard error of the mean. In MRI the lesions were counted and measured using OsiriX software. (C) Correlation plot of photon counts vs. number of lesions ($R^2 = 0.99$). (D) Bubble plot representation of metastatic tumor progression as spheres calculated from averaged tumor mass diameters measured by MRI imaging. (E) Kaplan-Meier plot illustrating animal survival following intravenous injection of tumor cells.

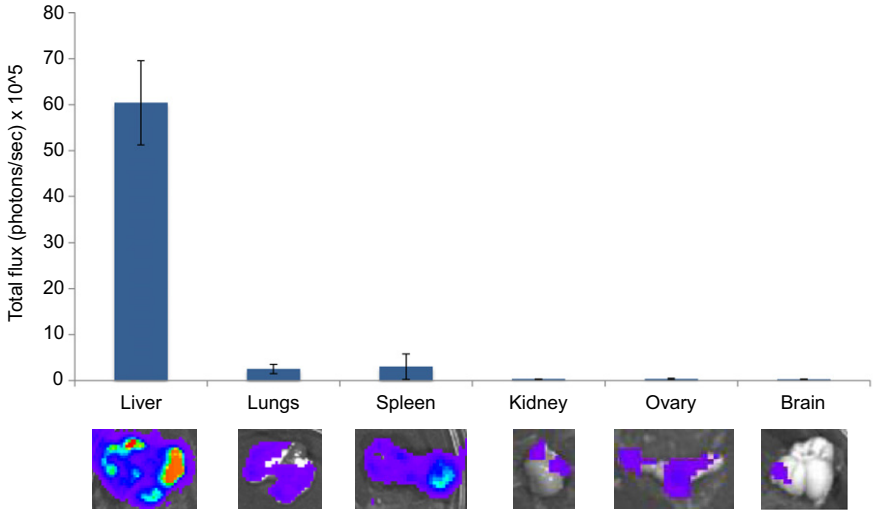


**Fig. 3.** *Ex vivo* analysis of organ metastasis by bioluminescence in the experimental metastasis model. Fifteen minutes after luciferin injection, the animals were euthanized and internal organs analyzed for bioluminescence signals. Representative images of internal organs are shown (lower panel); photons/s emitted by each organ were averaged and are represented in the upper panel, including standard deviations.

## 4. Discussion

Bioluminescence has been used for the detection of primary tumor growth and tumor metastasis in animal models of several tumors, but, to our knowledge, this is the first report on the use of bioluminescence in animal models of pheochromocytoma. The use of this technology allows for the non-invasive and real-time assessment of tumor burden in the same group of animals over time [19]. This type of model is particularly well suited for evaluating the efficacy of novel therapy and has been developed with the intent to create a platform for pre-clinical evaluation of new targeted therapy for pheochromocytoma.

Previous studies in our group have established a metastatic model of pheochromocytoma by mouse passages of the murine

**Table 1**
Comparison of number of metastatic lesions in the two animal models (metastatic-take).

| | Experimental metastasis model (tail vein injection) | Spontaneous metastasis model (subcutaneous injection) |
|---|---|---|
| Liver | 6/6 (100%) | 6/6 (100%) |
| Lungs | 6/6 (100%) | 6/6 (100%) |
| Brain | 4/6 (66%) | 5/6 (83%) |
| Spleen | 6/6 (100%) | 2/6 (33%) |
| Ovary | 4/6 (66%) | 4/6 (66%) |
| Kidney | 1/6 (16%) | 3/6 (50%) |

pheochromocytoma cell line MPC [21]. Through disaggregation and culturing of liver tumor metastasis, we established the MTT cell line, which displays a reproducible metastatic phenotype when injected intravenously. In order to follow the localization of these cells in the intact animal longitudinally, we generated a bioluminescent MTT cell line and compared the bioluminescent signal with serial MRI imaging.

In our study we demonstrated a strong correlation between the detection of photons and the radiologic examination. BLI offers several advantages over more traditional radiologic techniques, such as MRI and CT scanning, which require long scan times and expensive instrumentation. Bioluminescence offers a signal with practically no background, as other source of significant bioluminescence are absent in mammals, and the light generated easily penetrates mammalian tissues and can be detected by sensitive charge-coupled device (CCD) cameras and quantified more precisely by the conversion of the luminescence signal into a digital value. This is in contrast with the use of fluorescent tags, that require an excitation signal (which penetrate tissue layers with difficulty), and are limited by the presence of tissue autofluorescence and photobleaching. Moreover, the luciferase gene can be stably integrated into the chromosomes of target cells, and so carries over subsequent cell divisions and is not lost over time.

Luciferase-transduced cells can be easily monitored in virtually any location in the body, including sanctuary sites, where only a few cells are sufficient to generate a detectable signal that would be undetectable by MRI or CT scanning; thus, it is by far the most sensitive of the non-invasive techniques. Consequently, among the several imaging techniques available for *in vivo* studies, bioluminescence is the more sensitive to detect minimal residual disease, which is one of the more daunting and elusive entities in clinical oncology.

Moreover, BLI can represent quantitatively the amount of viable tumor cells in the body, allowing comparison not only within the same experiment but also across several experiments. The ability to non-invasively track the growth of tumors and metastases *in vivo* also permits a better understanding of the mechanisms of cancer development and intervention. Several investigations in other types of cancers have already demonstrated the power of BLI in longitudinal therapy intervention studies for the follow-up of tumor growth after treatment with experimental drugs [23]. In these types of studies the BLI signal in the animal injected with tumor cells is determined prior to intervention with the drug of interest to establish a reference/starting measurement. Subsequent scans are then normalized relative to the reference signal in the same animal and differences are calculated between the control group (receiving vehicle alone) vs. the group receiving the tested drug.

We have also established a spontaneous metastasis model of pheochromocytoma, in which cells from a subcutaneous implant send micrometastasis to the lungs. These models are rare in the lit-

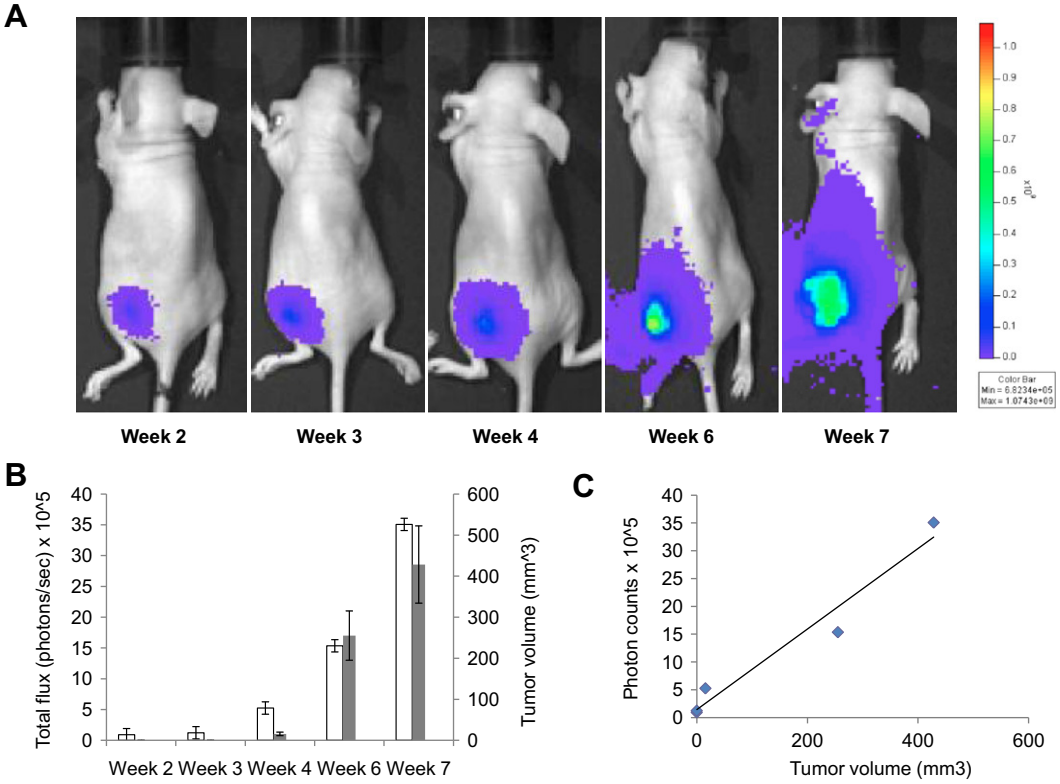


**Fig. 4.** Longitudinal subcutaneous tumor monitoring. MTT-luc ($1 \times 10^6$ tcells) cells were injected subcutaneously in the left flank of Nude mice ($n = 6$). (A). Representative images from the same mouse and taken weekly after implantation, are presented. (B) Tumor growth was monitored and quantified (as photon/s) weekly by BLI, together with tumor volume here represented as average per week; error bars indicate standard error of the mean. (C) Correlation plot of photon counts vs. tumor volume ($R^2 = 0.99$).

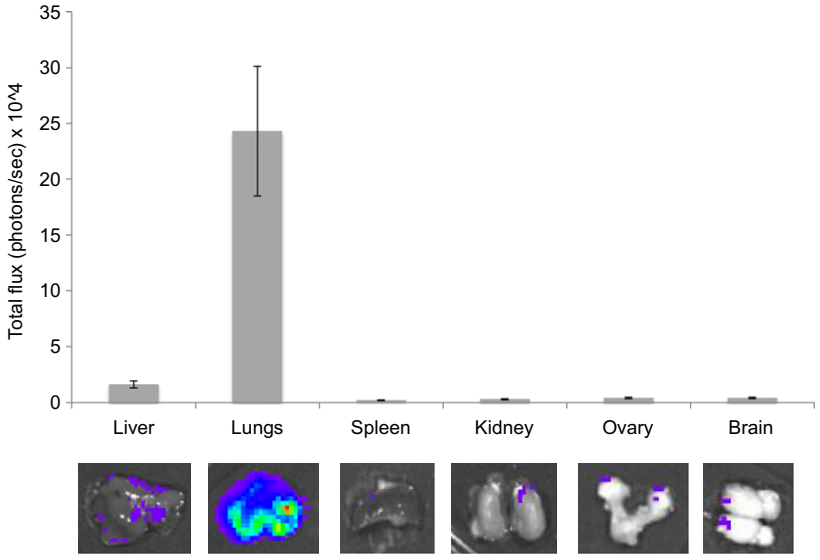


**Fig. 5.** *Ex vivo* analysis of organ metastasis by bioluminescence in the spontaneous metastasis model. Fifteen minutes after luciferin injection, the animals were euthanized and internal organs analyzed for bioluminescence signals. Representative images of internal organs are shown (lower panel); photons/s emitted by each organ were averaged and are represented in the upper panel, including standard deviations.

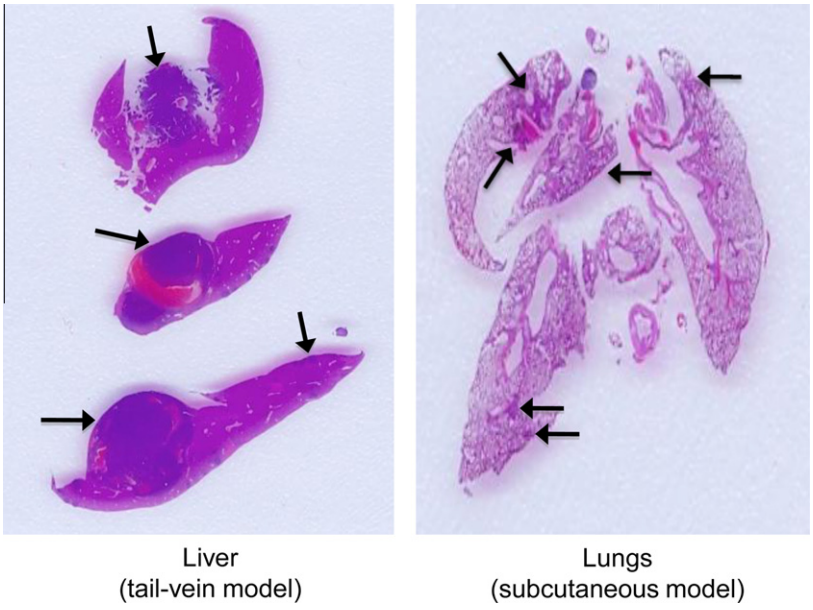


**Fig. 6.** Histopathological analysis in metastatic sites. Representative histological sections of liver and lung metastasis from MTT-luc cells. The presence of metastatic tumor cells initially detected *in vivo* and *ex vivo* by BLI imaging was confirmed by histopathological analysis. Metastatic sites are indicated by the arrows.

erature, and represent a unique opportunity to explore steps of the metastatic cascade that are not testable in an experimental metastasis model [24]. Indeed, spontaneous metastases spread following a natural mechanism of invasion of the surrounding tissue, and allow the examination of all steps of the metastatic cascade. This model could in particular be more clinically relevant, when testing for drugs that target more advanced disease stages. For example other groups using a spontaneous metastasis model of the breast cancer cell line MDA-MB-435 [25] was able to demonstrate the responsiveness of metastasis to therapies that were initially found to be ineffective in the treatment of the primary tumor. On the same line other groups have successfully used these animal models for testing novel molecular targeted therapies [26].

Besides the study of intact animals along the course of the study, *ex vivo* analysis at the end of experiments allows for additional important information to be collected from the same animal. Namely, *ex vivo* bioluminescence can help to identify very small metastatic lesions that are not easily detectable by *in vivo* imaging, more accurately assessing metastatic burden. For example, while it was relatively easy to detect signals from the abdominal cavity, brain lesions were undetectable by both MRI imaging and *in vivo* BLI. In contrast, *ex vivo* BLI was able to promptly detect a small number of tumor cells that crossed the blood-brain barrier causing micrometastatic brain disease.

A technical point of interest was that we were able to use G418 to exert selective pressure on transduced MTT cells. This was somewhat unexpected because the primary tumor from which MPC and MTT are derived arose in a *Nf1* knockout mouse generated by insertion of a neomycin resistance gene in reverse orientation into the *Nf1* gene [27] and the original MPC line was intrinsically

G418-resistant (JF Powers, unpublished). The apparent loss of intrinsic resistance might have resulted from somatic recombination, a possibility that itself has implications for design of targeted cancer therapy.

In summary, these experiments demonstrate the ability of bioluminescent imaging to follow the progression of pheochromocytoma cells in live animals in order to study the course of tumor progression and to test clinically relevant antitumor treatments in a mouse model of metastatic pheochromocytoma. The sites of metastasis in this model are also favored for metastases of human pheochromocytomas [6]. No comparable human cell-based model currently exists.

## Acknowledgments

This work was supported by the Intramural Research funding of the Eunice Kennedy Shriver National Institute of Child Health and Human Development of the National Institutes of Health and by grant 10665589 from the Department of Defense (to AST). This work was also funded in part with federal funds from the National Cancer Institute (NCI), National Institutes of Health (NIH), under contract N01-CO-12400 as well as by the Intramural Research Program of the NIH/NCI Center for Cancer Research.

## References

[1] A. Jemal, F. Bray, M.M. Center, J. Ferlay, E. Ward, D. Forman, Global cancer statistics, CA Cancer J. Clin. 61 (2011) 69–90.
[2] V. Kantorovich, K.S. King, K. Pacak, SDH-related pheochromocytoma and paraganglioma, Best Pract. Res. Clin. Endocrinol. Metab. 24 (2010) 415–424.
[3] R.E. Goldstein, J.A. O'Neill Jr., G.W. Holcomb 3rd, W.M. Morgan 3rd, W.W. Neblett 3rd, J.A. Oates, N. Brown, J. Nadeau, B. Smith, D.L. Page, N.N. Abumrad, H.W. Scott Jr., Clinical experience over 48 years with pheochromocytoma, Ann. Surg. 229 (1999) 755–764 (discussion 764-756).
[4] H. John, W.H. Ziegler, D. Hauri, P. Jaeger, Pheochromocytomas: can malignant potential be predicted?, Urology 53 (1999) 679–683
[5] H. Lehnert, J. Mundschenk, K. Hahn, Malignant pheochromocytoma, Front Horm. Res. 31 (2004) 155–162.
[6] L. Amar, E. Baudin, N. Burnichon, S. Peyrard, S. Silvera, J. Bertherat, X. Bertagna, M. Schlumberger, X. Jeunemaitre, A.P. Gimenez-Roqueplo, P.F. Plouin, Succinate dehydrogenase B gene mutations predict survival in patients with malignant pheochromocytomas or paragangliomas, J. Clin. Endocrinol. Metab. 92 (2007) 3822–3828.
[7] R. Adjalle, P.F. Plouin, K. Pacak, H. Lehnert, Treatment of malignant pheochromocytoma, Horm. Metab. Res. 41 (2009) 687–696.
[8] J.T. Adler, G.Y. Meyer-Rochow, H. Chen, D.E. Benn, B.G. Robinson, R.S. Sippel, S.B. Sidhu, Pheochromocytoma: current approaches and future directions, Oncologist 13 (2008) 779–793.
[9] A.S. Tischler, J.F. Powers, J. Alroy, Animal models of pheochromocytoma, Histol. Histopathol. 19 (2004) 883–895.
[10] J.E. Talmadge, R.K. Singh, I.J. Fidler, A. Raz, Murine models to evaluate novel and conventional therapeutic strategies for cancer, Am. J. Pathol. 170 (2007) 793–804.
[11] P.S. Steeg, Tumor metastasis: mechanistic insights and clinical challenges, Nat. Med. 12 (2006) 895–904.
[12] J. Sleeman, P.S. Steeg, Cancer metastasis as a therapeutic target, Eur. J. Cancer 46 (2010) 1177–1180.
[13] K. Pantel, C. Alix-Panabieres, S. Riethdorf, Cancer micrometastases, Nat. Rev. Clin. Oncol. 6 (2009) 339–351.
[14] T. Shibue, R.A. Weinberg, Metastatic colonization: settlement, adaptation and propagation of tumor cells in a foreign tissue environment, Semin. Cancer Biol. 21 (2011) 99–106.
[15] V. Koo, P.W. Hamilton, K. Williamson, Non-invasive in vivo imaging in small animal research, Cell Oncol. 28 (2006) 127–139.
[16] K. O'Neill, S.K. Lyons, W.M. Gallagher, K.M. Curran, A.T. Byrne, Bioluminescent imaging: a critical tool in pre-clinical oncology research, J. Pathol. 220 (2010) 317–327.
[17] N. Thorne, J. Inglese, D.S. Auld, Illuminating insights into firefly luciferase and other bioluminescent reporters used in chemical biology, Chem. Biol. 17 (2010) 646–657.
[18] S. Inouye, Firefly luciferase: an adenylate-forming enzyme for multicatalytic functions, Cell Mol. Life Sci. 67 (2010) 387–404.
[19] C.P. Klerk, R.M. Overmeer, T.M. Niers, H.H. Versteeg, D.J. Richel, T. Buckle, C.J. Van Noorden, O. van Tellingen, Validity of bioluminescence measurements for noninvasive in vivo imaging of tumor load in small animals, Biotechniques 43 (2007) 7–13, 30.
[20] S. Gross, D. Piwnica-Worms, Spying on cancer: molecular imaging in vivo with genetically encoded reporters, Cancer Cell 7 (2005) 5–15.
[21] L. Martiniova, E.W. Lai, A.G. Elkahloun, M. Abu-Asab, A. Wickremasinghe, D.C. Solis, S.M. Perera, T.T. Huynh, I.A. Lubensky, A.S. Tischler, R. Kvetnansky, S. Alesci, J.C. Morris, K. Pacak, Characterization of an animal model of aggressive metastatic pheochromocytoma linked to a specific gene signature, Clin. Exp. Metastasis 26 (2009) 239–250.
[22] J.F. Powers, M.J. Evinger, P. Tsokas, S. Bedri, J. Alroy, M. Shahsavari, A.S. Tischler, Pheochromocytoma cell lines from heterozygous neurofibromatosis knockout mice, Cell Tissue Res. 302 (2000) 309–320.
[23] H. Hong, Y. Yang, Y. Zhang, W. Cai, Non-invasive cell tracking in cancer and cancer therapy, Curr. Top Med. Chem. 10 (2010) 1237–1248.
[24] C. Khanna, K. Hunter, Modeling metastasis in vivo, Carcinogenesis 26 (2005) 513–523.
[25] S.A. Vantyghem, S.M. Wilson, C.O. Postenka, W. Al-Katib, A.B. Tuck, A.F. Chambers, Dietary genistein reduces metastasis in a postsurgical orthotopic breast cancer model, Cancer Res. 65 (2005) 3396–3403.
[26] G. Francia, W. Cruz-Munoz, S. Man, P. Xu, R.S. Kerbel, Mouse models of advanced spontaneous metastasis for experimental therapeutics, Nat. Rev. Cancer 11 (2011) 135–141.
[27] T. Jacks, T.S. Shih, E.M. Schmitt, R.T. Bronson, A. Bernards, R.A. Weinberg, Tumour predisposition in mice heterozygous for a targeted mutation in Nf1, Nat. Genet. 7 (1994) 353–361.

# Combined Inhibition of mTORC1 and mTORC2 Signaling Pathways Is a Promising Therapeutic Option in Inhibiting Pheochromocytoma Tumor Growth: In Vitro and In Vivo Studies in Female Athymic Nude Mice

Alessio Giubellino, Petra Bullova, Svenja Nölting, Hana Turkova, James F. Powers, Qingsong Liu, Sylvie Guichard, Arthur S. Tischler, Ashley B. Grossman, and Karel Pacak

Program in Reproductive and Adult Endocrinology (A.G., P.B., H.T., K.P.), *Eunice Kennedy Shriver* National Institute of Child Health and Human Development, National Institutes of Health, Bethesda, Maryland 20892; Department of Endocrinology (S.N., A.B.G.), William Harvey Research Institute, Barts and the London School of Medicine, Queen Mary University of London, London EC1M 6BQ, United Kingdom; Department of Pathology (J.F.P., A.S.T.), Tufts Medical Center, Boston, Massachusetts 02111; Dana-Farber Cancer Institute (Q.L.), Biological Chemistry and Molecular Pharmacology, Harvard Medical School, Boston, Massachusetts 02215; AstraZeneca (S.G.), Oncology iMed, Mereside, Alderley Park, Macclesfield, Cheshire, SK10 4TG, United Kingdom; and Oxford Centre for Diabetes, Endocrinology, and Metabolism (A.B.G.), Churchill Hospital, University of Oxford, Headington, Oxford OX3 7LE, United Kingdom

Several lines of evidence, including the recent discovery of novel susceptibility genes, point out an important role for the mammalian target of rapamycin (mTOR) signaling pathway in the development of pheochromocytoma. Analyzing a set of pheochromocytomas from patients with different genetic backgrounds, we observed and confirmed a significant overexpression of key mTOR complex (mTORC) signaling mediators. Using selective ATP-competitive inhibitors targeting both mTORC1 and mTORC2, we significantly arrested the in vitro cell proliferation and blocked migration of pheochromocytoma cells as a result of the pharmacological suppression of the Akt/mTOR signaling pathway. Moreover, AZD8055, a selective ATP-competitive dual mTORC1/2 small molecular inhibitor, significantly reduced the tumor burden in a model of metastatic pheochromocytoma using female athymic nude mice. This study suggests that targeting both mTORC1 and mTORC2 is a potentially rewarding strategy and supports the application of selective inhibitors in combinatorial drug regimens for metastatic pheochromocytoma. **(*Endocrinology* 154: 646–655, 2013)**

Pheochromocytoma is a neuroendocrine tumor arising from the chromaffin cells of the adrenal medulla; extra-adrenal pheochromocytomas are related to the sympathetic and parasympathetic ganglia and are usually referred to as paragangliomas (1). Most are benign and surgically curable, but when malignant, there are few effective therapies (2, 3). After pharmacological treatment for hypertension and other catecholamine-dependent symptoms (using $\alpha$- and $\beta$-adrenergic receptor antagonists), surgery is the main therapeutic option. For persisting disease, radiolabeled meta-iodobenzylguanidine therapy, peptide receptor radionucleotide therapy with radiolabeled somatostatin analogs (4), and certain types of chemotherapy may be helpful, but in advanced disease, in particular in patients carrying succinate dehydrogenase subunit B (SDH-B) mutations, surgical resection is frequently ineffective and recurrence is frequent and eventually lethal (2).

ISSN Print 0013-7227 ISSN Online 1945-7170
Printed in U.S.A.

doi: 10.1210/en.2012-1854 Received August 15, 2012. Accepted December 10, 2012.
First Published Online January 10, 2013

Abbreviations: DMSO, dimethylsulfoxide; eIF4B, eukaryotic translation initiation factor 4B; IRB, Institutional Review Board; mTOR, mammalian target of rapamycin; mTORC, mTOR complex; MTT, 3-(4,5-dimethylthiazol-2-yl)-2,5-diphenyltetrazolium bromide; NF1, neurofibromatosis type 1; PI3K, phosphoinositide 3-kinase; SDH-B, succinate dehydrogenase subunit B; S6K1, S6 kinase 1; VHL, von Hippel-Lindau.

**Table 1.** Patient Information Relative to the Samples Used for the Gene Expression Study

| Patient | Sex | Age, y | Type | Location | Genetic Background | Biochemistry |
|---|---|---|---|---|---|---|
| 1 | M | 26 | Met | Retroperitoneal | SDHB | NE, NMN |
| 2 | F | 36 | Met | Peri-iliac | SDHB | NE |
| 3 | M | 31 | P | Left peri-aortic mass | SDHB | DA |
| 4 | M | 53 | Mlt | Nasopharyngeal | SDHB | NE, DA |
| 5 | F | 9 | Mlt | Left iliac bifurcation | SDHB | Epi, NE, DA |
| 6 | M | 31 | Mlt | Left adrenal | SDHD | NE, DA |
| 7 | M | 62 | P | Left adrenal | SDHD | |
| 8 | F | 37 | P | Adrenal | SDHD | |
| 9 | F | 26 | Mlt | Right carotid body | SDHD HNP | NE |
| 10 | M | 67 | Bi | Carotid body | SDHD HNP | |
| 11 | F | 47 | Mlt | Carotid body | SDHD HNP | |
| 12 | F | 64 | P | Right glomus jugular tumor | SDHD HNP | |
| 13 | M | 33 | Bi and Mlt | Bilateral adrenal | VHL | |
| 14 | F | 42 | Bi | Right adrenal | VHL | |
| 15 | M | 25 | P | Right adrenal | VHL | |
| 16 | M | 7 | P | Left adrenal | VHL | NE, Epi |
| 17 | M | 45 | Met | Liver | SDHB Met | NE, NMN, DA |
| 18 | M | 39 | Met | Right lung | SDHB Met | NE |
| 19 | M | 48 | Met | Liver | SDHB Met | NE, DA |
| 20 | F | 37 | Met | Parietal bone mass | SDHB Met | Epi, NE |

Abbreviations: Bi, bilateral; DA, dopamine; Epi, epinephrine; F, female; HNP, head and neck paragangliomas; M, male; Met, metastatic; Mlt, multiple; NE, norepinephrine; NMN, normetanephrine; P, primary.

As a part of larger clinical trials for the evaluation of novel targeted therapies in neuroendocrine tumors or as single case reports, a small number of patients with malignant pheochromocytomas and paragangliomas have shown at least temporary responses to the multiple tyrosine kinase inhibitor sunitinib (5). Other specific targeted therapies, including the tyrosine kinase inhibitor imatinib, were not found to be of significant benefit for these patients (6). Thus, there is an ongoing and urgent need for specific targeted therapies for such patients.

The mammalian target of rapamycin (mTOR) is a serine/threonine protein kinase that is a master regulator of cell proliferation and survival (7), integrating complex upstream pathways and signals, including insulin, growth factors, and nutrient sensing, from the surrounding environment. The role of mTOR in cancer is well established (8), and it represents a rational molecular target in oncology (9). Two major mTOR complexes (mTORCs) regulate its activity: mTORC1, which is allosterically inhibited by the macrolide antibiotic rapamycin (sirolimus) and contains the regulatory-associated protein raptor, and mTORC2 including the rapamycin-insensitive mTOR companion protein rictor (10). mTORC1 is mostly involved in growth factor-stimulated cellular proliferation and cellular homeostasis through phosphorylation of the ribosomal protein S6 kinase 1 (S6K1) and the eukaryotic translation initiation factor 4E-binding protein 1. It is allosterically inhibited by rapamycin, but the downstream substrate 4E-binding protein 1 is only partially dephosphorylated by rapamycin. This explains the limited effect of rapalogs on protein synthesis. Rapamycin-resistant mTORC2 plays a prominent role in the regulation of the actin cytoskeleton and cellular motility. mTORC2 directly phosphorylates the serine/threonine protein kinase Akt/protein kinase B at S473, linking this complex to the activation of the mTORC1 pathway. Activation of mTORC2 leads to Akt phosphorylation and thus feeds forward in a positive fashion (11).

Accumulating evidence has supported that the phosphoinositide 3-kinase (PI3K)/AKT/mTOR signaling pathway plays an important role in the pathogenesis of several

**TABLE 2.** Patient Information of the Samples Used for Primary Cell Cultures and Treatments[a]

| Patient | Sex | Age, y | Type | Location | Genetic Background | Biochemistry | Inhibition at 1$\mu$M AZD8055, % | Inhibition at 3$\mu$M AZD8055, % |
|---|---|---|---|---|---|---|---|---|
| 1 | F | 44 | P | Right adrenal | Sporadic | NE, DA, NMN | 27.1 | 48.5 (Torin-1, 48.2) |
| 2 | F | 28 | P | Right adrenal | SDHB | NE, DA, NMN, CgA | 22.6 | 68.9 |
| 3 | F | 47 | P | Right carotid body | Sporadic | CgA | 23.2 | |
| 4 | M | 5 | P | Left adrenal | VHL | MN, NMN | 17.1 | 51.9 (Torin-1, 52.4) |

Abbreviations: CgA, chromogranin A; DA, dopamine; F, female; M, male; MN, metanephrine; NE, norepinephrine; NMN, normetanephrine; P, primary.

[a] Included are the percent inhibition with 1 $\mu$M and 3 $\mu$M AZD8055 and 3 $\mu$M Torin-1.

neuroendocrine tumors, including pheochromocytoma (3, 12). For instance, S6K1, as a downstream target of the pathway, has been shown to be overexpressed in human pheochromocytoma, suggesting the potential use of inhibitors of this pathway in this disease (13). Recent reports also link the mTOR pathway to mutations in the *TMEM127* gene, which predisposes to the development of pheochromocytoma (14), emphasizing the importance of studying familial syndromes of pheochromocytoma to understand the pathogenic mechanisms involved in both sporadic and familial forms of the disease.

Unfortunately, studies using mTOR inhibitors in patients with pheochromocytoma have not clearly shown any therapeutic benefit. The mTOR inhibitor everolimus (RAD001; Novartis, Basel, Switzerland) failed to demonstrate a major clinical benefit in a small group of patients with pheochromocytoma (15). However, the inhibitors used in this study target only partially mTORC1, and in some solid tumors, treatment with these drugs has been associated with elevated Akt phosphorylation (16). These unpromising clinical studies were consistent with early experimental work showing that rapamycin inhibited proliferation of normal rat chromaffin cells stimulated by exogenous mitogens but was relatively ineffective against spontaneously proliferating PC12 rat pheochromocytoma cells (17).

Recent data have identified mTORC2 as the major kinase that phosphorylates Akt on Ser-473 (18, 19), and we have previously reported that levels of phospho-Akt are increased in pheochromocytoma compared with normal adrenal tissue (20). Moreover, there are several lines of evidence emphasizing a prominent role for mTORC2 in development of pheochromocytoma. For example, hypoxia-inducible factor 2$\alpha$, which is downstream of the mTORC2 pathway (21), is particularly overexpressed in some subtypes of pheochromocytoma (22–25). This suggests that drugs that would target both mTORC1 and mTORC2 might be of a greater benefit and demonstrate antitumor activity where agents targeting only the mTORC1 have failed.

Novel inhibitors targeting both mTORC1 and mTORC2 have been recently developed, including AZD8055 and Torin-1 (26–28). Compared with rapamycin and everolimus, they have high activity against both mTORC1 and mTORC2. In addition to their antiproliferative effects, these drugs can potentially inhibit tumor cell invasion and metastatic spread (specifically through inhibition of mTORC2) (29), which is the most lethal complication, especially in patients with SDH-B mutations (30). In the current study, using mTORC1- and mTORC2-selective dual inhibitors, we now report inhibition of both cell proliferation and migration of pheochromocytoma cells in vitro; the inhibitory effect was associated with a potent inhibition of the Akt/mTOR signaling pathway. Moreover, we have demonstrated the ability of AZD8055 to significantly reduce tumor burden in an animal model of metastatic pheochromocytoma. These results argue in favor of the importance of pursuing selective targeting of mTORC1 and mTORC2 as a potential novel approach for patients with malignant pheochromocytoma.

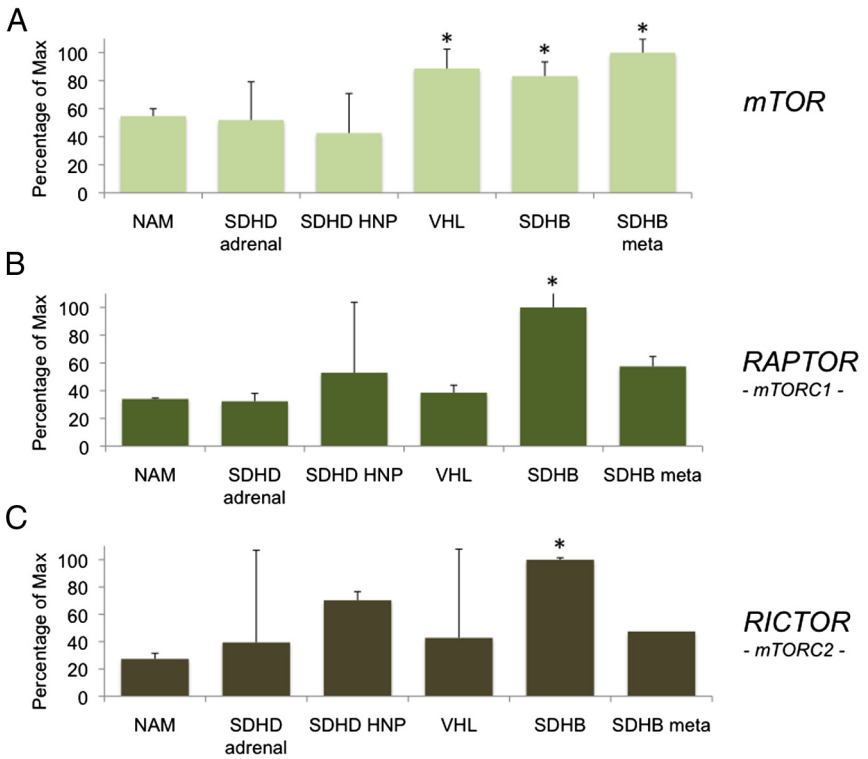


**Figure 1.** Levels of mTOR, raptor, and rictor are elevated in tumors with SDHB gene mutations. Pheochromocytoma/paraganglioma tumor samples from patients with different genetic backgrounds were analyzed by real-time PCR. SDH-B, metastatic SDH-B, and VHL-related pheochromocytoma exhibit a significant increase in expression of mTOR (*$P < .05$) than in normal adrenal when compared with samples of other genetic background tumors. Raptor and rictor expression is significantly increased in SDH-B pheochromocytoma patients when compared with normal adrenal medulla. Results are presented as percentage of the maximal value. Abbreviations: HNP, head and neck paraganglioma; NAM, normal adrenal medulla; SDHB meta, SDH-B metastatic.

## Materials and Methods

### Cell lines and reagents

The mouse pheochromocytoma cell line MTT was maintained in DMEM supplemented with 10% fetal bovine serum, 5% horse serum, and antibiotic/an-

timycotic (Gibco-Life Technologies, Grand Island, New York). Cells were grown until 80% confluence and then detached using 0.05% trypsin/EDTA, incubated for 3 minutes at 37°C, resuspended, and counted to obtain the desired concentration. AZD8055 was provided by AstraZeneca (London, United Kingdom). Torin-1 was developed by the Dana-Farber Cancer Institute, Biological Chemistry and Molecular Pharmacology Section, Harvard Medical School (Boston, Massachusetts). All of the compounds were dissolved in dimethylsulfoxide (DMSO); stock solutions were stored at −20°C and thawed prior to use. Controls were treated with the highest concentration of DMSO in the panel.

## Human samples

Pheochromocytoma tumor tissue for the real-time PCR and for drug testing was obtained from patients visiting our clinic (Institutional Review Board [IRB] protocol 00-CH-0093); the study was approved by the IRB of the *Eunice Kennedy Shriver* National Institute of Child Health and Human Development, National Institutes of Health (NIH), and patients gave written informed consent. Tables 1 and Table 2 summarize patient clinical information. Guidelines for genetic testing were previously described (31). Normal human adrenal medullas (n = 4) were obtained from anonymous organ donors with absent adrenal tumor or dysfunction and collected within 2 to 5 hours after confirmed brain death at the Department of Urology, School of Medicine, Comenius University, Bratislava, Slovakia. Separation of cortex from adrenal medulla was ascertained as previously described (32).

## Cell proliferation assays

Cell proliferation was determined by 3-(4,5-dimethylthiazol-2-yl)-2,5-diphenyltetrazolium bromide (MTT) assay. MTT cells ($15 \times 10^3$) were incubated in 96-well plates for 24 hours before serum deprivation and treatment with the indicated concentrations of rapamycin, AZD8055, or Torin-1 in the presence of serum (10%) for 24 hours. An MTT solution (1 mg/mL; Sigma Chemical Co, St. Louis, Missouri) was added and plates were incubated at 37°C for 3 hours before measuring absorbance at 562 nm (Bio-TEK Instruments, Winooski, Vermont).

## Cell migration assay

Cell migration was measured using modified Boyden chambers (Transwell assay). MTT cells were seeded at 150 000 cells per chamber, and cell migration was stimulated with serum (10%) in presence of the drugs (AZD8055 and Torin-1) or vehicle alone (control). At the end of the experiment, nonmigrating MTT cells were removed from the upper chamber with cotton swabs, and migrated MTT cells were fixed and stained with Diff-Quick reagents. Bright light images were digitally acquired. Mean values from four fields (1 × 1.4 mm) were calculated for each of triplicate wells per condition. $IC_{50}$ values were determined using GraphPad Prism software.

## Real-time PCR

Real-time PCR was performed on a 7500 real-time PCR system (Applied Biosystems, Foster City, California) using detector TaqMan, reporter FAM (6-carboxyfluorescein) and quencher TAMRA (tetramethylrhodamine) for the genes and detector VIC (4,7,2′-trichloro-7′-phenyl-6-carboxyfluorescein) for *18S* rRNA. Primer sequence TaqMan gene expression assays were from Applied Biosystems as recommended for the genes. Primers were premixed to a concentration of 18 $\mu$M for each primer and 5 $\mu$M for the probe, which represented a 20× mix. Final reaction volume was 25 $\mu$l; amounts of templates for *18S* rRNA and for other genes were 5 and 25 ng, respectively. PCR was performed as follows: 50°C for 2 minutes, 95°C for 10 minutes, and 50 cycles of two-step PCR

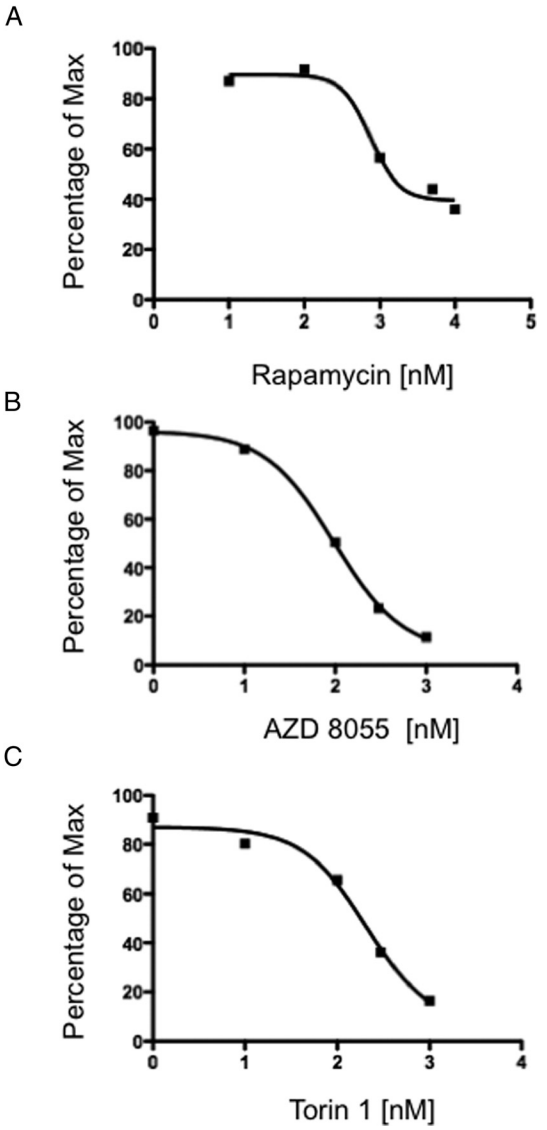


**Figure 2.** Rapamycin, AZD8055, and Torin-1 inhibit proliferation of MTT cells in vitro. The MTT proliferation assay was performed using MTT cells, and 15 000 cells per well were plated on a 96-well plate. The next day, MTT cells were treated for 48 hours with rapamycin (A), AZD8055 (B), or Torin-1 (C). Drug concentrations used were as follows: rapamycin, 10 nM, 100 nM, 1000 nM, 5000 nM, and 10 000 nM; AZD8055 and Torin-1, 1 nM, 10 nM, 100 nM, 300 nM, and 1000 nM. The graph represents the dose response of $\log_{10}$ concentrations of rapamycin, AZD8055, or Torin-1 vs signal intensity in a thiazolyl blue formazan (MTT)-based assay. $IC_{50}$ for each compound was calculated using GraphPad Prism.

(95°C for 15 seconds and 60°C for 1 minute). The results were analyzed by 7500 system software, version 1.3 (Applied Biosystems), calculated based on the Δ−Δ Ct (threshold cycle) method and then by Microsoft Excel. Each result was correlated to the housekeeping gene *18S* rRNA.

## Drug treatment and Western blotting

MTT cells were grown to log phase (~70% confluent) before treatment with the indicated concentrations of rapamycin, AZD8055, or Torin-1 for 6 hours at 37°C and 5% $CO_2$. Control cells were incubated with the vehicle for the same period of time. The cells were washed twice with ice-cold PBS and lysed in cell lysis buffer (Cell Signaling Technology, Danvers, Massachusetts) supplemented with Complete protease inhibitor cocktail (Roche, Indianapolis, Indiana) and 1mM phenylmethylsulfonyl fluoride. Protein lysates were denatured by boiling with 4× sodium dodecyl sulfate sample buffer for 5 minutes. Proteins were separated by 4%–20% SDS-PAGE and transferred to polyvinylidene difluoride membrane. The membrane was incubated with total Akt, phospho-Akt (Ser473), phospho-S6 (Ser235/236), phospho-S6 (Ser240/244), phospho-eukaryotic elongation factor-2 kinase (Ser366), phospho-eukaryotic translation initiation factor 4B (eIF4B) (Ser422), and actin primary antibodies (Cell Signaling) overnight at 4°C, which was followed by washing and incubation with the horseradish peroxidase-conjugated secondary antibody at room temperature for 1 hour. The blots were visualized using Amersham ECL Plus Western blotting reagents.

## Animal experiments and bioluminescence imaging

All animal studies were conducted in accordance to the principles and procedures outlined in the NIH Guide for the Care and Use of Animals and approved by the NIH Animal Care and Use Committee. For the spontaneous metastasis model, $1.5 \times 10^6$ MTT-luc cells were injected sc in the right flank of female athymic nude mice (Taconic, Germantown, Maryland). The experimental group consisted of 10-week-old mice (n = 7) housed in a pathogen-free facility. After 10 days, allowing for tumor cells to engraft, we started a treatment with 20 mg/kg AZD8055 in one group of animals (n = 7). Animals in the control group (n = 7) were treated with the same volume of vehicle instead, on a daily, 7 days a week schedule. The animals were imaged weekly by Bioluminescence (described below). All bioluminescent data were collected and analyzed with a Xenogen IVIS system. For in vivo imaging, luciferase activity was performed on anesthetized animals (1%–2% isoflurane) 15 minutes after ip administration of 150 mg/kg luciferin in PBS. The mice were then placed inside a camera box under continuous exposure to 1%–2% isoflurane. The experiments were performed in the NIH Mouse Image Facility in accordance to ACUC regulations.

All imaging variables were equal, and photographic and bioluminescent images at different time points were collected for each sample. The bioluminescence data are presented visually as a color overlay on the photographic image. Using the Living Image software (Xenogen), a region of interest was drawn around tumor sites of interest and the total photon count or photons per second was quantified.

## Tumor dissociation and tyrosine hydroxylase immunocytochemistry in primary cell culture

Pheochromocytoma tumor tissue was obtained from patients visiting our clinic (IRB protocol 00-CH-0093); the study was approved by the IRB of the *Eunice Kennedy Shriver* National Institute of Child Health and Human Development, NIH, and patients gave written informed consent. Dissociated cells were plated at low density (~$5 \times 10^3$ cells/35-mm dish) in RPMI 1640 medium with 15% fetal bovine serum plus penicillin/streptomycin. Cultures in control medium or dosed with 1 $\mu$M or 3 $\mu$M AZD8055 or 3 $\mu$M Torin-1 were maintained for 1 week with media replaced twice. Cultures were then fixed and stained for tyrosine hydroxylase (TH), a marker of catecholamine-synthesizing ability, to discriminate tumor cells from non-neoplastic fibroblasts and other cell types in primary cultures (33). To measure drug-induced cytotoxicity, surviving TH-positive cells were counted in an area of the culture dish defined by a randomly placed 22 × 22-$mm^2$ coverslip.

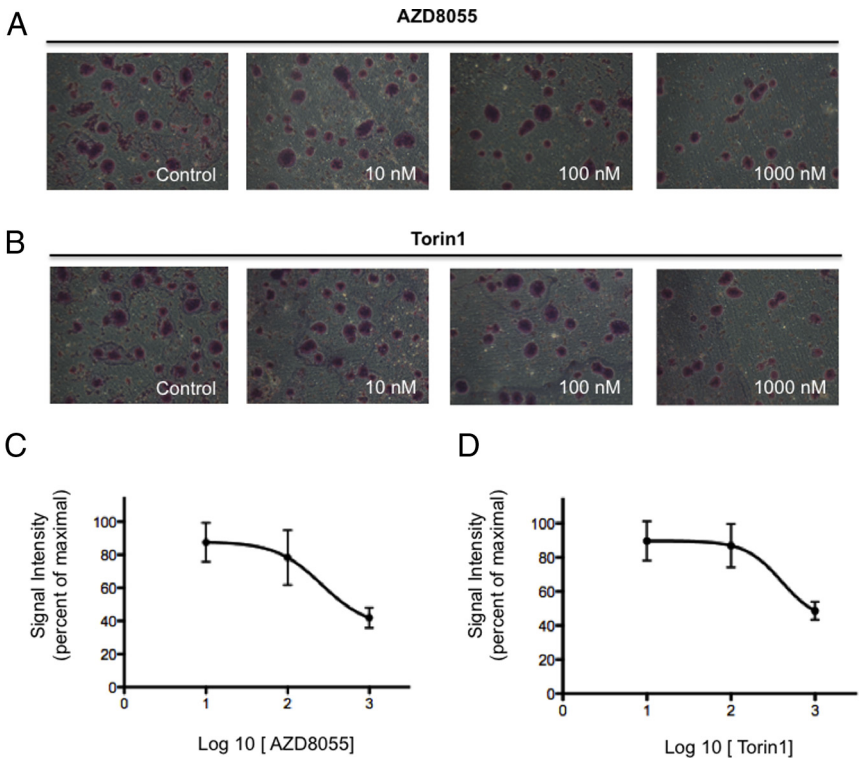


**Figure 3.** Incubation with AZD8055 or Torin-1 inhibits cell migration of pheochromocytoma MTT cells. MTT cells plated in a Transwell chamber treated with different concentrations (10 nM, 100 nM, and 1000 nM) of AZD8055 (A) or Torin-1 (B) in the presence of serum for 24 hours show a decreased ability to migrate when compared with the control cells. Inhibition of migration caused by the drugs is accompanied by a lowered ability of the cells to form clusters. Mean numbers of migrated cells per microscopic field (at ×10 magnification) were counted and are represented in the graph: AZD8055 (C) and Torin-1 (D) dose-response curves; error bars represent SDs.

### Statistical analysis

Tumor volume and mean bioluminescence were determined for each experiment together with the SEM. Statistical analyses were performed using GraphPad Prism software, including unpaired *t* test and nonparametric Mann-Whitney *U* test (GraphPad Software, San Diego, California).

## Results

### mTOR, raptor, and rictor are overexpressed in subsets of pheochromocytomas

First, we wanted to verify the expression of mTOR, raptor, and rictor in several tumors from our collection of pheochromocytomas/paragangliomas from patients with different genetic backgrounds. Expression analysis was performed with 20 tumor samples from patients with von Hippel-Lindau (VHL), SDH-B, SDH-B metastases, SDH-D adrenal, SDH-D head and neck paraganglioma mutations, and 4 normal adrenal medulla. Table 1 summarizes the clinical information of the patients used for these studies. Expression of the three genes in these groups was analyzed by real-time PCR (Figure 1). As shown in Figure 1, patients with SDH-B and VHL mutations showed a significant increase (compared with normal adrenal medulla) in mTOR expression when compared with the other samples analyzed in this panel. Interestingly, both SDH-B and metastatic SDH-B pheochromocytoma showed a significant increase in expression of mTOR compared with normal adrenal medulla ($P < .05$). Analysis of both raptor and rictor expression demonstrated a significant increase in SDH-B pheochromocytoma tissue when compared with patients in other groups as well as the normal adrenal medulla.

### mTORC1/2 inhibitors inhibit pheochromocytoma cell proliferation and migration

Based on the importance of the mTOR pathway in pheochromocytomas and paragangliomas, we tested mTOR inhibitors in a proliferation assay using the metastatic mouse pheochromocytoma-derived MTT cell line (34). As shown in Figure 2, the original mTOR inhibitor rapamycin was able to inhibit MTT cell proliferation with an $IC_{50}$ of 756nM (Figure 2A). In comparison, the novel mTORC1/2 inhibitors AZD-8055 and Torin-1 were able to significantly inhibit cellular proliferation in a dose-dependent manner in MTT cells over a range of concentrations (1nM to 1$\mu$M) with an $IC_{50}$ of 96nM (Figure 2B) and 207nM (Figure 2C), respectively. These data show that rapamycin induces only partial growth inhibition, whereas the dual inhibitors have a much greater suppression of proliferation.

The effect of mTORC1/2 inhibitors treatment on cell migration was tested in the metastatic pheochromocytoma cell line MTT; we found that AZD8055 reduced serum-stimulated migration (Figure 3, A and C), with an $IC_{50}$ of 260nM. Torin-1 was also able to significantly inhibit MTT cell migration, with an $IC_{50}$ of 400 nM (Figure 3, B and D). Interestingly, MTT cells tended to become confluent in clusters, reminiscent of the zellballen nested arrangement characteristic of pheochromocytoma histopathology. As shown in the micrograph images in Figure 3, inhibition with either mTOR inhibitors reduced the formation of such clusters.

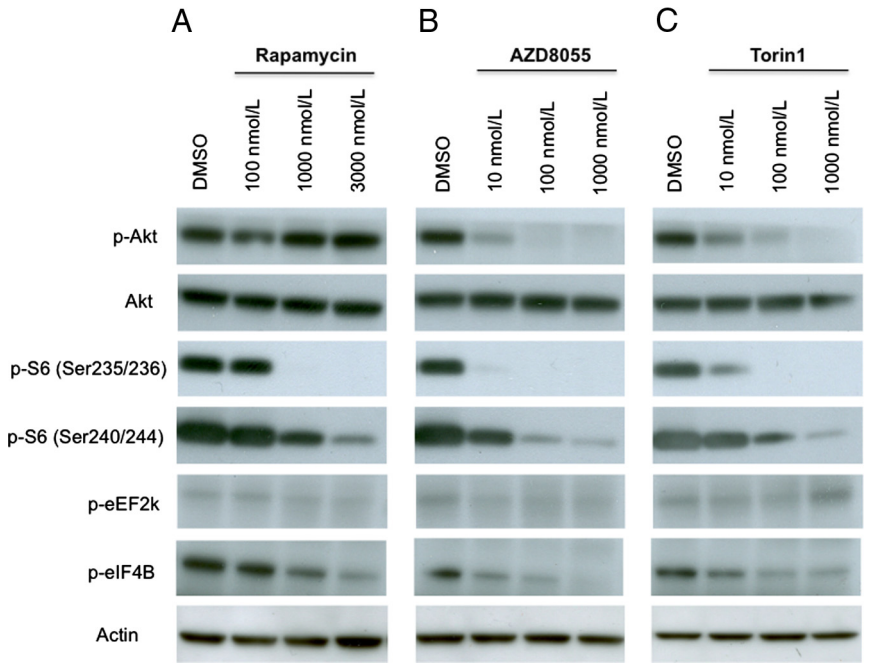


**Figure 4.** mTOR inhibition by rapamycin, AZD8055, and Torin-1 influences several protein in the mTOR pathway. MTT cells were treated with rapamycin (A), AZD8055 (B), or Torin-1 (C) at different concentrations (100 nM, 1000 nM, and 3000 nM for rapamycin; 10 nM, 100 nM, and 1000 nM for AZD8055 and Torin-1). The cells were incubated in the presence of the drugs for 6 hours. Total cell lysates were prepared and analyzed by Western blotting. Control cells were treated with DMSO alone for the same period of time. The levels of phosphorylated forms of proteins (phospho [p]-Akt[Ser473], p-S6[Ser235/236], p-S6[Ser240/244], p-eEF2k, and p-eIF4B) decrease with increasing concentrations of the drugs. Actin was used as a loading control.

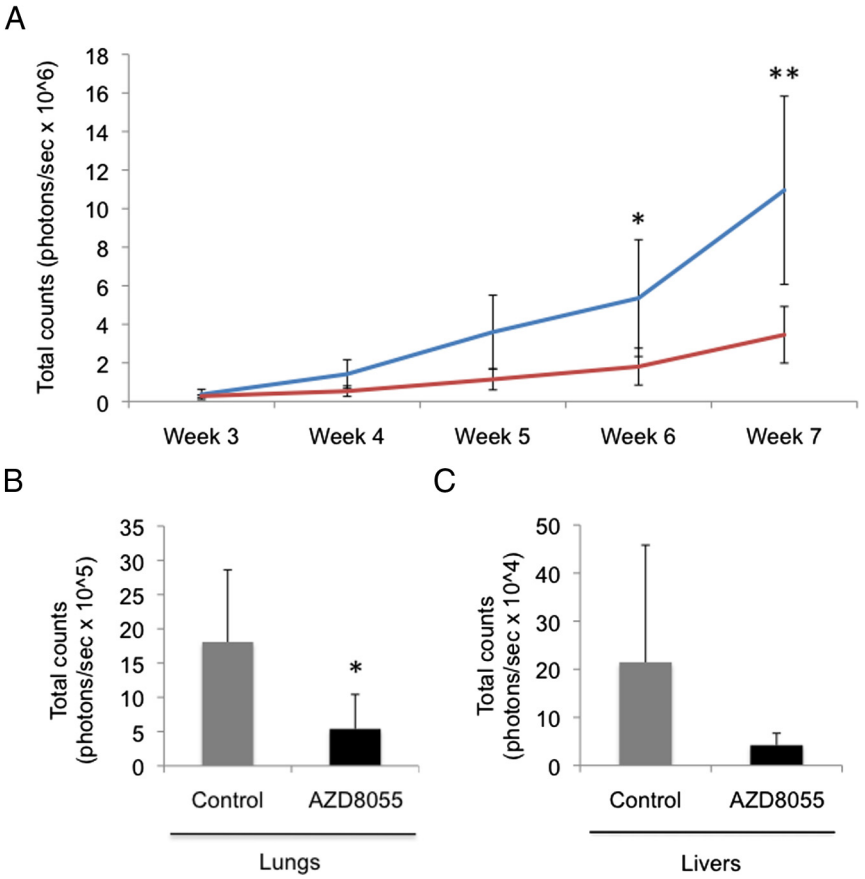


**Figure 5.** AZD8055 reduces pheochromocytoma tumor and metastatic burden in mice. MTT-luc cells ($1.5 \times 10^6$) were injected sc in the flank of nude mice. After 7 weeks of treatment with 20 mg/kg AZD8055, or the same volume of vehicle in the control group, the animals were euthanized and lungs and livers were excised for comparison. A, Tumor burden as a function of tumor cell bioluminescence signal is graphed: AZD8055-treated animals (red line) is compared with the control animals (blue line). $^{**}P = .0021$; $^{*}P = .012$ (*t* test). B and C, Sizes of metastatic tumors in lungs (B) ($^{*}P < .05$, Mann-Whitney *U* test) and livers (C) were compared in treated mice compared with animals treated with vehicle (control).

### AZD8055 and Torin-1 treatment affects mTOR downstream signaling

As part of the assessment of mTORC1/2 inhibitor activity in pheochromocytoma cells, MTT cells were exposed to different concentrations of rapamycin, AZD8055, and Torin-1 for 6 hours to assess downstream markers of mTOR kinase activity. Both AZD8055 and Torin-1 decreased phosphorylation of S6 ribosomal protein on Ser235/236 and Ser240/244 as well as phosphorylation of eukaryotic translation initiation factor 4B on Ser422. Unlike the allosteric mTOR inhibitor rapamycin, the dual inhibitors were also able to significantly decrease phosphorylation of Akt on Ser473. Moreover, lower concentrations of AZD8055 and Torin-1 (Figure 4, B and C) were necessary to obtain the same degree of biomarker modulation compared with rapamycin (Figure 4A).

### AZD8055 reduces pheochromocytoma tumor and metastatic burden in vivo

The antitumor effect of AZD8055 was assessed in vivo in a recently developed spontaneous metastasis model of pheochromocytoma (35). From week 3 through week 7, a significant reduction of tumor burden was observed in the AZD8055-treated animals (n = 7) compared with vehicle-treated animals (n = 7; Figure 5A). As previously described (35) in the MTT pheochromocytoma model, the two main organs where spontaneous metastases develop are the lungs and liver. On day 49, after in vivo bioluminescence measurements had been taken, the animals were euthanized and both lungs and livers were excised and luciferase activity was measured by Xenogen imaging. A trend of reduced metastatic burden was observed in lungs (Figure 5B) and livers (Figure 5C) of the treated animals compared with the control group, although only differences in lung metastasis were statistically significant using nonparametric statistics in the time frame of our experiment.

### AZD8055 and Torin-1 inhibits proliferation of primary cells from patients with pheochromocytoma

The growth-inhibitory effect of AZD8055 and Torin-1 was evaluated in human primary cells derived from donated tumor tissue collected from patients suffering from pheochromocytoma, including one SDH-B tumor. Immunohistochemical staining for TH, the rate-limiting step in the biosynthesis of catecholamines, was used as a marker of pheochromocytoma cells to discriminate them from other cell types that are inevitably present in primary cultures. As shown in Figure 6, AZD8055 (Figure 6A) as well as Torin-1 (Figure 6B) decreased the number of TH-positive cells to 50% of control cells, confirming their cytotoxic effect also on human pheochromocytoma cells. Table 2 summarizes the clinical information on the patients used for these studies.

## Discussion

The treatment of rare tumors represents a major challenge in oncology. In particular, neuroendocrine tumors, such as pheochromocytomas and paragangliomas, are rare tumors for which there are very limited therapeutic options

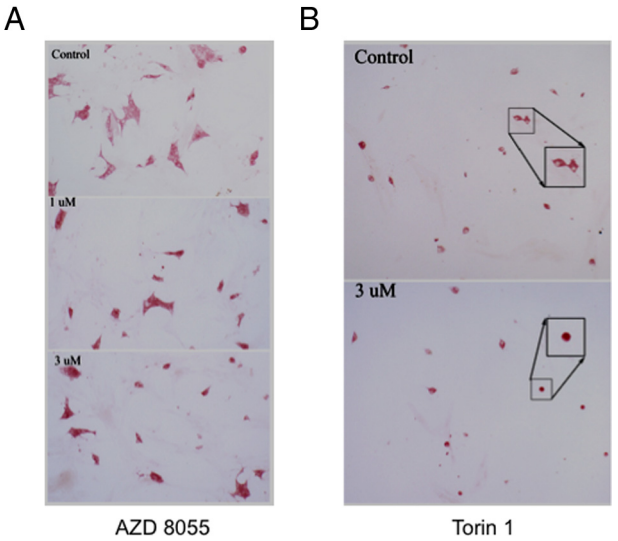


**Figure 6.** AZD8055 and Torin-1 show an inhibitory effect on survival of primary human pheochromocytoma cells. Dissociated cells from human tumor samples were plated at low density and treated with 1$\mu$M and 3$\mu$M AZD8055 (A) or 1$\mu$M Torin-1 (B) for 1 week. Control cells were incubated with DMSO for the same period of time. The cells were then fixed and stained for TH to discriminate tumor cells from other cell types in primary cultures. TH-positive cells were then counted to compare the number of treated cells with control cells. In the drug-containing culture, neoplastic chromaffin cells (red cytoplasm) are decreased in number and some are rounded (inset). Original magnification, ×20; expanded boxes show selected cells at higher magnification.

(36, 37). Malignant pheochromocytomas have been historically very difficult to treat, because traditional chemotherapy has been mostly unsuccessful and data from clinical trials are difficult to interpret due to the low prevalence of the disease and the inability to recruit in the same trial an adequate number of patients (38).

However, the study of the molecular determinants of pheochromocytoma tumorigenesis has suggested a handful of potential targets to explore with novel targeted therapies, which have already demonstrated successful treatment for other forms of cancer (39). Currently, there is increasing interest in the pheochromocytoma research community to seek novel targeted therapies that have predominantly a cytostatic effect by interfering with a specific molecular target needed for carcinogenesis and sustained tumor growth (3, 38, 40).

A significant number of tumors is associated with familial etiology and can be included in familial syndromes such as VHL, multiple endocrine neoplasia type 2, neurofibromatosis type 1 (NF1), and SDH mutation-related tumors (4). VHL and SDH-related tumors in these cases seem to share the same tumorigenic pseudohypoxia/angiogenesis pathways. There are currently no human cell lines available for these tumors, hindering the testing of novel drugs in vitro.

Hereditary pheochromocytomas and paragangliomas can be divided into two clusters based on the transcription profile revealed by microarray analysis. Cluster 1 includes the tumors with VHL and SDHx mutant genes, cluster 2 involves tumors with mutations in *RET* and *NF1* genes (25, 41). Sporadic tumors were surprisingly represented in both clusters (42). As further genes were discovered, additional microarray studies were performed to classify them into these two clusters. Mutations in *KIF1Bb*, *TMEM127*, and *MAX* genes were clustered with *RET/NF1* (43). *RET* and *NF1* mutations lead to activation of the rat sarcoma/rapidly accelerated fibrosarcoma/MAPK and the PI3K/Akt/mTOR signaling pathways. *TMEM127* mutant tumors cluster with the *RET/NF1* group, and they enhance mTOR activity independent of the above two kinase pathways. Microarray expression analysis of *KIF1Bb* mutant tumors also groups them with tumors associated with *RET/NF1* mutations, although a potential role of the mutation in kinase pathways is not yet known (43). On the other hand, a recently discovered *MAX* gene mutation, which leads to dysregulation of the myelocytomatosis–myc-associated factor X–MAX dimerization protein 1 network, is grouped with this cluster for its connection with mTOR pathway (44). Conversely, *SDHAF2* and *SDHA* mutations, recently described, can be clustered with *SDHx/VHL* (43).

Identification of a unifying player in tumor cells with deregulated energy metabolism and altered redox balance is required to elucidate molecular mechanisms associated with these discrepancies. Several pieces of experimental evidence indicate a potential role for the PI3K/Akt/mTOR pathway. Recently identified mutations in the *TMEM127* gene have confirmed the importance of this pathway in the pathogenesis of pheochromocytoma (45) and further stress the importance of studying the molecular pathways downstream of susceptibility genes in expanding our understanding of the disease (37, 46). Elevated levels of the phosphorylated form of S6K1 were observed in both cluster 1 and cluster 2 tumor samples with more significant increases in cluster 2 tumors. Such results further support an important role for the mTOR pathway in pheochromocytomas/paragangliomas (47).

The present work has shown that the dual mTORC1 and mTORC2 inhibitors AZD8055 and Torin-1 were able to block proliferation in our mouse pheochromocytoma cell line and were more effective than the pure mTORC1 inhibitor rapamycin. The Western blotting studies confirmed inhibition of the targets downstream to mTOR, but additionally, the dual inhibitors decrease Akt phosphorylation. We have previously demonstrated increased levels of activated Akt in a model of pheochromocytoma induced by ectopic expression of ErbB-2 (20), in conjunction with reduction of the phosphatase and tensin homolog protein, consistent with other experimental work (48).

These experimental studies reinforce the importance of the pathway.

The dual inhibitors also blocked cell migration. These results translated to the in vivo situation in our transplanted athymic mice. Finally, we were able to use a small number of human tumors to show cell loss induced by the inhibitors. Thus, it would appear that the dual TORC1/2 inhibitors may offer a novel and effective therapy for pheochromocytomas and paragangliomas with invasive and/or malignant characteristics, and it is worth considering their use in the clinical situation.

Of note, all efforts to establish cell lines from human pheochromocytomas and paragangliomas have been unsuccessful because the cells survive but do not proliferate in vitro (49). For this reason, we used first-passage primary cell cultures from patients with pheochromocytoma to access the effect of AZD8055 on human samples. TH, a marker of catecholamine-producing cells, was used to distinguish pheochromocytoma cells from non-neoplastic fibroblast and other cell types in the primary cell culture.

Our results suggest that dual inhibition of mTORC1 and mTORC2 (29) is a potential novel therapeutic approach for patients with pheochromocytoma and may overcome the problem encountered with the use of mTORC1 inhibitors alone (15, 50). Future efforts will be directed toward using these compounds in combinations with other chemotherapeutic drugs or novel targeted therapies.

## Acknowledgments

Address all correspondence and requests for reprints to: Alessio Giubellino, MD, Reproductive and Adult Endocrinology Program, *Eunice Kennedy Shriver* National Institute of Child Health and Human Development, National Institutes of Health, Building 10-CRC, 1E-3140, 10 Center Drive, Bethesda, Maryland, 20892-1109. E-mail: giubella@mail.nih.gov; or Karel Pacak, MD, PhD, DSc, Senior Investigator, Chief, Section on Medical Neuroendocrinology, Professor of Medicine, *Eunice Kennedy Shriver* National Institute of Child Health and Human Development, National Institutes of Health, National Institutes of Health, Bethesda, Maryland, 20892-1109. E-mail: karel@mail.nih.gov.

This work was supported by the Intramural Research Program of the *Eunice Kennedy Shriver* National Institute of Child Health and Human Development, National Institutes of Health. J.F.P. and A.S.T. were supported by Grant W81XWH-11-1-0670 from the Department of Defense.

Disclosure Summary: S.G. is a current employee and shareholder of AstraZeneca. All other authors declare no competing financial interests.

## References

1. **Tischler AS.** Pheochromocytoma and extra-adrenal paraganglioma: updates. *Arch Pathol Lab Med*. 2008;132:1272–1284.
2. **Adjalle R, Plouin PF, Pacak K, Lehnert H.** Treatment of malignant pheochromocytoma. *Horm Metab Res*. 2009;41:687–696.
3. **Nolting S, Grossman AB.** Signaling pathways in pheochromocytomas and paragangliomas: prospects for future therapies. *Endocr Pathol*. 2012;23:21–33.
4. **Kaltsas GA, Papadogias D, Makras P, Grossman AB.** Treatment of advanced neuroendocrine tumours with radiolabelled somatostatin analogues. *Endocr Relat Cancer*. 2005;12:683–699.
5. **Jimenez C, Cabanillas ME, Santarpia L, et al.** Use of the tyrosine kinase inhibitor sunitinib in a patient with von Hippel-Lindau disease: targeting angiogenic factors in pheochromocytoma and other von Hippel-Lindau disease-related tumors. *J Clin Endocrinol Metab*. 2009;94:386–391.
6. **Gross DJ, Munter G, Bitan M, et al.** The role of imatinib mesylate (Glivec) for treatment of patients with malignant endocrine tumors positive for c-kit or PDGF-R. *Endocr Relat Cancer*. 2006;13:535–540.
7. **Wullschleger S, Loewith R, Hall MN.** TOR signaling in growth and metabolism. *Cell*. 2006;124:471–484.
8. **Sabatini DM.** mTOR and cancer: insights into a complex relationship. *Nat Rev Cancer*. 2006;6:729–734.
9. **Wander SA, Hennessy BT, Slingerland JM.** Next-generation mTOR inhibitors in clinical oncology: how pathway complexity informs therapeutic strategy. *J Clin Invest*. 2011;121:1231–1241.
10. **Guertin DA, Sabatini DM.** Defining the role of mTOR in cancer. *Cancer Cell*. 2007;12:9–22.
11. **Laplante M, Sabatini DM.** mTOR signaling in growth control and disease. *Cell*. 2012;149:274–293.
12. **Horsch D, Grabowski P, Schneider CP, et al.** Current treatment options for neuroendocrine tumors. *Drugs Today (Barc)*. 2011;47:773–786.
13. **Nardella C, Lunardi A, Fedele G, et al.** Differential expression of S6K2 dictates tissue-specific requirement for S6K1 in mediating aberrant mTORC1 signaling and tumorigenesis. *Cancer Res*. 2011;71:3669–3675.
14. **Qin Y, Yao L, King EE, et al.** Germline mutations in TMEM127 confer susceptibility to pheochromocytoma. *Nat Genet*. 2010;42:229–233.
15. **Druce MR, Kaltsas GA, Fraenkel M, Gross DJ, Grossman AB.** Novel and evolving therapies in the treatment of malignant phaeochromocytoma: experience with the mTOR inhibitor everolimus (RAD001). *Horm Metab Res*. 2009;41:697–702.
16. **Dancey J.** mTOR signaling and drug development in cancer. *Nat Rev Clin Oncol*. 2010;7:209–219.
17. **Powers JF, Tischler AS, Cherington V.** Discordant effects of rapamycin on proliferation and p70S6 kinase phosphorylation in normal and neoplastic rat chromaffin cells. *Neurosci Lett*. 1999;259:137–140.
18. **Sarbassov DD, Ali SM, Sengupta S, et al.** Prolonged rapamycin treatment inhibits mTORC2 assembly and Akt/PKB. *Mol Cell*. 2006;22:159–168.
19. **Hresko RC, Mueckler M.** mTOR.RICTOR is the Ser473 kinase for Akt/protein kinase B in 3T3-L1 adipocytes. *J Biol Chem*. 2005;280:40406–40416.
20. **Lai EW, Rodriguez OC, Aventian M, et al.** ErbB-2 induces bilateral adrenal pheochromocytoma formation in mice. *Cell Cycle*. 2007;6:1946–1950.
21. **Toschi A, Lee E, Gadir N, Ohh M, Foster DA.** Differential dependence of hypoxia-inducible factors 1$\alpha$ and 2$\alpha$ on mTORC1 and mTORC2. *J Biol Chem*. 2008;283:34495–34499.
22. **Pollard PJ, El-Bahrawy M, Poulsom R, et al.** Expression of HIF-1$\alpha$, HIF-2$\alpha$ (EPAS1), and their target genes in paraganglioma and pheo-

chromocytoma with VHL and SDH mutations. *J Clin Endocrinol Metab*. 2006;91:4593–4598.
23. **Cervera AM, Apostolova N, Crespo FL, Mata M, McCreath KJ.** Cells silenced for SDHB expression display characteristic features of the tumor phenotype. *Cancer Res*. 2008;68:4058–4067.
24. **Lopez-Jimenez E, Gomez-Lopez G, Leandro-Garcia LJ, et al.** Research resource: transcriptional profiling reveals different pseudohypoxic signatures in SDHB and VHL-related pheochromocytomas. *Mol Endocrinol*. 2010;24:2382–2391.
25. **Favier J, Briere JJ, Burnichon N, et al.** The Warburg effect is genetically determined in inherited pheochromocytomas. *PLoS One*. 2009;4:e7094.
26. **Thoreen CC, Kang SA, Chang JW, et al.** An ATP-competitive mammalian target of rapamycin inhibitor reveals rapamycin-resistant functions of mTORC1. *J Biol Chem*. 2009;284:8023–8032.
27. **Liu Q, Chang JW, Wang J, et al.** Discovery of 1-(4-(4-propionylpiperazin-1-yl)-3-(trifluoromethyl)phenyl)-9-(quinolin-3-yl)benz o[h][1,6]naphthyridin-2(1H)-one as a highly potent, selective mammalian target of rapamycin (mTOR) inhibitor for the treatment of cancer. *J Med Chem*. 2010;53:7146–7155.
28. **Chresta CM, Davies BR, Hickson I, et al.** AZD8055 is a potent, selective, and orally bioavailable ATP-competitive mammalian target of rapamycin kinase inhibitor with in vitro and in vivo antitumor activity. *Cancer Res*. 2010;70:288–298.
29. **Sparks CA, Guertin DA.** Targeting mTOR: prospects for mTOR complex 2 inhibitors in cancer therapy. *Oncogene*. 2010;29:3733–3744.
30. **Kantorovich V, King KS, Pacak K.** SDH-related pheochromocytoma and paraganglioma. *Best Pract Res Clin Endocrinol Metab*. 2010;24:415–424.
31. **Erlic Z, Rybicki L, Peczkowska M, et al.** Clinical predictors and algorithm for the genetic diagnosis of pheochromocytoma patients. *Clin Cancer Res*. 2009;15:6378–6385.
32. **Fliedner SM, Breza J, Kvetnansky R, et al.** Tyrosine hydroxylase, chromogranin A, and steroidogenic acute regulator as markers for successful separation of human adrenal medulla. *Cell Tissue Res*. 2010;340:607–612.
33. **Tischler AS, Ruzicka LA, Riseberg JC.** Immunocytochemical analysis of chromaffin cell proliferation in vitro. *J Histochem Cytochem*. 1992;40:1043–1045.
34. **Martiniova L, Lai EW, Elkahloun AG, et al.** Characterization of an animal model of aggressive metastatic pheochromocytoma linked to a specific gene signature. *Clin Exp Metastasis*. 2009;26:239–250.
35. **Giubellino A, Woldemichael GM, Sourbier C, et al.** Characterization of two mouse models of metastatic pheochromocytoma using bioluminescence imaging. *Cancer Lett*. 2012;316:46–52.
36. **Grogan RH, Mitmaker EJ, Duh QY.** Changing paradigms in the treatment of malignant pheochromocytoma. *Cancer Control*. 2011;18:104–112.
37. **Pacak K.** Phaeochromocytoma: a catecholamine and oxidative stress disorder. *Endocr Regul*. 2011;45:65–90.
38. **Santarpia L, Habra MA, Jimenez C.** Malignant pheochromocytomas and paragangliomas: molecular signaling pathways and emerging therapies. *Horm Metab Res*. 2009;41:680–686.
39. **Schilsky RL.** Personalized medicine in oncology: the future is now. *Nat Rev Drug Discov*. 2010;9:363–366.
40. **Ye L, Santarpia L, Gagel RF.** The evolving field of tyrosine kinase inhibitors in the treatment of endocrine tumors. *Endocr Rev*. 2010;31:578–599.
41. **Waldmann J, Fendrich V, Holler J, et al.** Microarray analysis reveals differential expression of benign and malignant pheochromocytoma. *Endocr Relat Cancer*. 2010;17:743–756.
42. **Dahia PL, Ross KN, Wright ME, et al.** A HIF1$\alpha$ regulatory loop links hypoxia and mitochondrial signals in pheochromocytomas. *PLoS Genet*. 2005;1:72–80.
43. **Welander J, Soderkvist P, Gimm O.** Genetics and clinical characteristics of hereditary pheochromocytomas and paragangliomas. *Endocr Relat Cancer*. 2011;18:R253–R276.
44. **Jafri M, Maher ER.** The genetics of phaeochromocytoma: using clinical features to guide genetic testing. *Eur J Endocrinol*. 2012;166:151–158.
45. **Jiang S, Dahia PL.** The busy road to pheochromocytomas and paragangliomas has a new member, TMEM127. *Endocrinology*. 2011;152:2133–2140.
46. **Qin Y, Buddavarapu K, Dahia PL.** Pheochromocytomas: from genetic diversity to new paradigms. *Horm Metab Res*. 2009;41:664–671.
47. **Favier J, Igaz P, Burnichon N, et al.** Rationale for anti-angiogenic therapy in pheochromocytoma and paraganglioma. *Endocr Pathol*. 2012;23:34–42.
48. **Di Cristofano A, De Acetis M, Koff A, Cordon-Cardo C, Pandolfi PP.** Pten and p27KIP1 cooperate in prostate cancer tumor suppression in the mouse. *Nat Genet*. 2001;27:222–224.
49. **Tischler AS, Powers JF, Alroy J.** Animal models of pheochromocytoma. *Histol Histopathol*. 2004;19:883–895.
50. **Chrisoulidou A, Kaltsas G, Ilias I, Grossman AB.** The diagnosis and management of malignant phaeochromocytoma and paraganglioma. *Endocr Relat Cancer*. 2007;14:569–585.